# ASSESSING THE EFFICACY OF PHYSICS-INFORMED NEURAL NETWORKS FOR ENHANCED FLOOD ROUTING SIMULATION

Jayawardane Mudiyanselage Paboda Mayangi Jayawardane

248077T

Master of Science (Major Component of Research)

Department of Civil Engineering
Faculty of Engineering

University of Moratuwa
Sri Lanka

October 2025

# ASSESSING THE EFFICACY OF PHYSICS-INFORMED NEURAL NETWORKS FOR ENHANCED FLOOD ROUTING SIMULATION

Jayawardane Mudiyanselage Paboda Mayangi Jayawardane

248077T

Thesis submitted in partial fulfillment of the requirements for the degree

Master of Science (Major Component of Research)

Department of Civil Engineering

Faculty of Engineering

University of Moratuwa

Sri Lanka

October 2025

# DECLARATION

I declare that this is my own work and this thesis/dissertation does not incorporate without acknowledgement any material previously submitted for a degree or diploma in any other University or Institute of higher learning and to the best of my knowledge and belief it does not contain any material previously published or written by another person except where the acknowledgement is made in the text. I retain the right to use this content in whole or part in future works (such as articles or books).

Signature: Date: 2025/10/29

The above candidate has carried out research for the ~~PhD/MPhil/~~Masters thesis~~/dissertation~~ under my supervision. I confirm that the declaration made above by the student is true and correct.

Name of Supervisor: Prof. R. L. H. L. Rajapakse

Signature of the Supervisor: Date: 2025/10/30

# DEDICATION

This thesis is dedicated to all those who offered unwavering support and encouragement throughout my academic journey. This achievement is not mine alone; it is also a reflection of the compassion, guidance, and solidarity of the remarkable individuals who stood by me during this transformative period.

To my supervisor, Prof. Lalith Rajapakse, I express my heartfelt gratitude. Your insightful guidance, generous mentorship, and encouragement have been instrumental in shaping this research.

I lovingly dedicate this work to my family, whose constant encouragement and patience have been my greatest strength. To my parents and brother, thank you for your unconditional support and belief in me. A special tribute goes to my late mother, whose dream for my academic success continues to inspire and guide me every day.

I also dedicate this thesis to my friends and research colleagues for their motivation, support, and positivity throughout this endeavor. Finally, this work is for anyone passionate about learning and committed to the pursuit of knowledge through research.

# ACKNOWLEDGEMENT

First and foremost, I extend my heartfelt gratitude to my supervisor, Prof. Lalith Rajapakse, from the Department of Civil Engineering at the University of Moratuwa, for his steadfast guidance, encouragement, and insightful mentorship throughout this research. His expertise, patience, and unwavering support have been pivotal in shaping the direction and quality of this thesis.

I also wish to sincerely thank the Progress Review Committee, especially Dr. Kasun De Silva, for their critical feedback, thoughtful suggestions, and consistent support, which helped enhance the depth and clarity of this work.

Special thanks are due to the Urban Water Management Division of the Sri Lanka Land Development Corporation (SLLDC). I am especially grateful to the General Manager (Planning and Design), Eng. (Mrs.) A.H. Thushari and all the staff members for their kind cooperation and timely provision of the necessary datasets. Their support was instrumental in the successful execution of this study.

I am also thankful to the academic staff of the Department of Civil Engineering, University of Moratuwa, including Prof. H.R. Pasindu, the Research Coordinator, and the lecturers and professors of the Hydraulics Division, for their continued academic guidance and encouragement throughout the MSc program.

My sincere appreciation also goes to the administrative staff of the Department of Civil Engineering, the University of Moratuwa, and the UNESCO Madanjeet Singh Centre for South Asia Water Management (UMCSAWM), including Ms. Vinu Kalanika and Ms. Janani Nisansala, for their support, which created a positive and enabling research environment.

To my fellow researchers and colleagues, thank you for your collaboration, encouragement, and knowledge-sharing that enriched this journey and made it a truly collective effort. Finally, I am deeply grateful to my family and friends for their constant motivation, patience, and unwavering belief in me. Their love and emotional strength carried me through every challenge I faced along this path.

# ABSTRACT


**Assessing the Efficacy of Physics-Informed Neural Networks or Enhanced Flood Routing Simulation**

Flooding has emerged as one of the most destructive natural hazards, causing extensive damage to infrastructure, livelihoods, and ecosystems. The intensifying impacts of climate change, particularly altered rainfall patterns and increased frequency of extreme precipitation events, have further amplified the severity and recurrence of both riverine and localized urban flooding. These conditions often overwhelm existing channel capacities, highlighting the need for accurate flood modeling to support critical decisions related to urban resilience and disaster preparedness. While traditional hydrodynamic models such as HEC-RAS remain widely used for flood simulation, the recent advancement of data-driven methods, particularly Machine Learning (ML), offers promising alternatives. This study explores the application of Physics-Informed Neural Networks (PINNs) as a novel approach for 1D flood routing and peak flow prediction within urban canal networks, especially in data-scarce environments. The PINN framework integrates physical laws, as partial differential equations (PDEs), directly into the model, enhancing the ability to address data scarcities. The 1D Saint-Venant equations were used as the guiding PDE within this particular model. Observed water level data, canal cross sections and rainfall data from the Urban Water Management Division of the Sri Lanka Land Development Corporation (SLLDC) were used as model inputs. The methodology was implemented on three major canal systems in Colombo, Sri Lanka: Madiwela East Diversion, Dehiwala-Wellawatta-Kirulapone Canal System, and Parliament Lake-Kiththampahuwa-Kinda-Dematagoda Canal System. The performance of the PINN model was evaluated by comparing its predicted water levels against observed data at multiple water level monitoring stations along the mentioned canals, using Nash-Sutcliffe-Efficiency (NSE) and Root Mean Square Error (RMSE) as evaluation metrics. In parallel, HEC-RAS 1D hydraulic models were developed for each canal system using the same boundary and terrain data. These models served as a benchmark for comparison with the PINN approach. The results revealed that the PINN model consistently achieved higher accuracy, outperforming HEC-RAS at intermediate water level validation locations. PINN model predictions exhibited NSE values exceeding 0.98 at training locations and above 0.95 at validation points, with corresponding RMSE values below 0.10 m (10 cm). In comparison, while HEC-RAS also demonstrated acceptable performance with NSE values above 0.90 in most cases, its RMSE values were comparatively higher, ranging from 0.10-0.17 m in some locations. These findings highlight higher accuracy of the PINN model, particularly in predicting flood peaks and spatial water level profiles. The integration of physics-based constraints with machine learning allows PINNs to outperform traditional models like HEC-RAS, especially in urban flood scenarios with sparse data availability.



**Keywords**: Climate variability, data-scarce regions, flood peaks, flood modelling, HEC-RAS, PINN

# TABLE OF CONTENTS

# LIST OF FIGURES

# LIST OF TABLES

# LIST OF ABBREVIATIONS

| Abbreviation | Description |
|---|---|
| ANN | Artificial Neural Network |
| BC | Boundary Condition |
| CNN | Convolutional Neural Network |
| DP | Deep Learning |
| GNN | Graph Neural Network |
| HEC-RAS | Hydrologic Engineering Center - River Analysis System |
| IC | Initial Condition |
| LSTM | Long Short-Term Memory |
| ML | Machine Learning |
| NSE | Nash–Sutcliffe Efficiency |
| PDE | Partial Differential Equation |
| PINN | Physics-Informed Neural Network |
| RMSE | Root Mean Square Error |
| R-R | Rainfall–Runoff |
| SLLDC | Sri Lanka Land Development Corporation |
| SRM | Short-Term Runoff Modelling |
| CRM | Continuous Runoff Modelling |
| GS | Gaussian Software |

# CHAPTER 1

# INTRODUCTION

## 1.1 Background of the Study

Flooding continues to be a global hydrological challenge, exacerbated by the growing impacts of climate change, rapid urbanization, and land-use changes (Monfared et al., 2024). In both developed and developing regions, the rising frequency and intensity of extreme precipitation events have led to increased runoff volumes, overwhelming existing drainage systems and amplifying the risk of pluvial and riverine flooding (Idrees et al., 2022). Accurate and reliable rainfall-runoff (R-R) modeling is therefore critical not only for predicting flood events but also for ensuring sustainable water resource planning, early warning systems, and disaster risk reduction (Shekar et al., 2023).

Further, precise R-R modelling is mandatory for water resource engineers to define the path of water resource management. It includes a diverse area benchmarking from assessing the quality and quantity of water resources, up to areas of forecasting hydraulic extremes (Shekar et al., 2023). These R-R models are further important to predict the discharge and to estimate hydrological balances, in making decisions related to early warnings and incident mitigations under droughts or floods. Most common ways of modeling R-R can be divided into two main classes as: physically based, conceptual models, and mathematically based, data-driven models. But R-R modeling keeps challenging in aspects of precision, due to the uncertainty and randomness of available data (Shekar et al., 2024), even though R-R modeling is considerably important.

Deep learning (DP) techniques are data-driven, mathematical models that were commonly applied recently, for accurate R-R modelling compared to physics-based modelling techniques (S. Yang et al., 2020). Support Vector Machine (SVM), Regression Trees (RT), Artificial Neural Network (ANN) (Nifa et al., 2023), Convolutional Neural Network (CNN), and Long Short-Term Memory (LSTM) (Waqas et al., 2021) are some common DP techniques applied for R-R modeling. Each of these DP models has positive and negative comparisons against each other, such as ANN is more favorable in performance compared to SVM, but both are inefficient in capturing series information in input data (Nifa et al., 2023). Further, these DP models heavily rely on input data, while the quality and quantity of data influence the performance of the trained DP model significantly. Depending on the type of data, R-R modeling can be divided into short-term runoff modeling (SRM), for hourly or daily basis, and continuous runoff modeling (CRM) for weekly, monthly, or yearly basis (Sudheer et al., 2002). CRM can be utilized in monitoring sediment transportation and water management, while SRM is utilized in flood forecasting.

Under SRM, satisfying data requirements might be challenging, including modelling event-based scenarios like floods (Bai et al., 2024). Thus, there exists a predominant barrier in the implementation of usually practiced DP techniques like ANN, CNN, and LSTM in such scenarios. This gap can be addressed by applying Physics Informed Neural Network (PINN), where physics laws are integrated with the Neural Network (NN) model to achieve accurate and generalized results (Raissi et al., 2017). Within the PINN model, governing non-linear partial differential equations are solved and transferred to models as a loss function to be utilized as the training set of data (Bai et al., 2024). This novel DP technique can be applied to any study area having relations with physics or equations (Bai et al., 2024).

Hence, this approach can be adhered to stimulate flood wave propagations in an open channel system using limited data resources and boundary conditions, described by kinematic wave propagation in the loss function. Precisely modelled flood wave heights or stage hydrographs can be generated at different collocation points using received rainfalls, and more accurate flood forecasting and predictions can be generated (Markidis, 2021a). These modelled stage hydrographs can be compared with stage hydrographs generated through observed water heights, and deviations can be identified to assess the efficacy of using PINN in flood routing.

## 1.2 Research Gap Identification

Downstream of the Kelani River basin, there are major issues due to urban flooding. To face the effects of urban flooding, means of reducing the inundation depths, inundation extents, and mitigating floods, several structural flood mitigation measures have been implemented by the Urban Water Center (UWC), Sri Lanka Land Development Authority (SLLDC), such as new canal developments, existing canal improvements, or the establishment of pumping stations. North Lock Widening and Pumping Station, New Mutwal Tunnel, Kolonnawa Canal Diversion, Madiwela East Diversion, and South Diversions are some such mitigation measures. Even though these measures are implemented, they are insufficient to account for the generated flood volumes, thus, monitoring and predicting flood extents with inundation depths are mandatory to take emergency decisions about early warnings regarding urban floods in the downstream of the Kelani River basin. But, in the developed canal systems by UWC, the stimulated stage hydrographs using physically-based hydrological models show deviations compared to observed stage hydrographs, which lead to a troubled understanding of the flood peaks. Thus, in this research, the deviation of stimulated flood peaks from observed flood peaks will be addressed using PINN, leading the path to generate more precise flood peak predictions and flood routing.

## 1.3 Aims and Objectives

The main objective of the study is to check the applicability of utilizing PINN in improving the performance in flood wave predictions compared to traditional hydrological models in urban environments.

The specific objectives are as follows:

i). To develop a numerical model (HEC-RAS or similar) to stimulate 1D flood wave propagation along the selected canal(s).

ii). To develop and utilize PINN models to stimulate flood wave propagation along the selected canals, generating stage hydrographs at different collocation points along the selected canal(s).

iii). To compare the performance of the numerical model (HEC-RAS) and PINN models with observed flood depths to validate the generated results and to check the efficacy.

iv). To analyze the effect of the performance of selected hyperparameters on the prediction accuracy in the PINN model.

## 1.4 Methodology

This study was commenced through five key phases to evaluate the performance of PINN against traditional HEC-RAS models for 1D flood simulation in urban canal networks within the Colombo Metropolitan Area, Sri Lanka.

i). Data Collection and Case Study Selection

Primary hydrometeorological data, including rainfall and water levels, were collected from the UWC of SLLDC. Cross-sectional data of canals and DEMs were used for hydraulic modeling. Based on data completeness, connectivity, and spatial distribution of monitoring stations, three canal systems were selected as follows:

a). Madiwela East Diversion

b). Dehiwala-Wellawatta-Kirillapone Canal System

c). Parliament Lake-Dematagoda Canal System

ii). Flood Event Selection and Data Preprocessing

Representative flood events were identified by analyzing time series of rainfall and water levels, focusing on events evident across all three systems. The flood event from November 13$^{th}$ to 17$^{th}$, 2022, was selected based on peak magnitude and data availability. Missing data were gap-filled using linear interpolation to ensure model continuity based on missing data percentage values.

iii). Development of the PINN Model

A PINN model was developed using the kinematic wave equation derived from Saint-Venant Equations. A dual-head DNN architecture was used to predict water levels at upstream and downstream stations. The model incorporated spatial-temporal rainfall input and was trained with a composite loss function that includes data loss, physics residuals, initial and boundary condition losses. Hyperparameter tuning was performed using both manual and Bayesian methods. Model evaluation was done using NSE and RMSE, with spatial generalization tested through collocation points.

iv). HEC-RAS Model Setup and Simulation

HEC-RAS 1D unsteady models were constructed for the same three canal systems using DEM-based canal digitization. The models were calibrated using observed water level data, with inflow hydrographs at the upstream and stage hydrographs at the downstream. Manning's roughness value of 0.04 was used depending on the canal conditions. Simulations were run at 5-minute intervals, with a warm-up period, and the outputs were validated against both observed and PINN-predicted values.

v). Comparative Evaluation and Validation

Both modeling approaches were compared under the selected flood event. PINN predictions were validated against observed water levels and HEC-RAS outputs at monitoring and intermediate points. Evaluation used NSE, RMSE, residual plots, and physical law compliance to assess predictive accuracy and generalization. Visualization tools supported the interpretability of results.

## 1.5 Main Findings

The principal findings derived from this study on the application of PINN for 1D flood routing in urban canal networks are summarized as follows:

i). PINN models showed high predictive accuracy across all canal systems in both training and validation phases. They achieved exceptionally high NSE (> 0.98) and RMSE (< 3 cm) during training at both upstream and downstream monitoring stations across all three canal systems. Further, validation at intermediate stations and ungauged locations showed strong performance (NSE > 0.95, RMSE mostly < 5 cm), confirming the PINN model's ability to generalize 1D spatiotemporal flood behavior, including effective flood peak simulation under real rainfall forcing.

ii). The PINN Models outperformed HEC-RAS in all validation scenarios. While HEC-RAS models also showed strong agreement (NSE > 0.87), they often overestimated peak water levels (RMSE up to 13 cm at Yakbedda Bridge). But, PINN models produced lower RMSEs (often < 5 cm), indicating better alignment with observed hydrographs under both peak and low flow conditions.

iii). The PINN models provided faster, more efficient modeling for real-time applications. It effectively simulated continuous water level profiles along canal systems at different collocation points with fewer inputs and less computational time compared to HEC-RAS, highlighting its potential for rapid flood forecasting in data-scarce urban environments. Thus, this approach can be applied to a new urban environment quickly. The accurate prediction of water levels along the canals can give chances to announce flood level variations along the canals and provide real-time warnings.

iv). The sensitivity analysis revealed that PINN performance was most sensitive to neural architecture (neurons, layers), followed by physics-based loss weights in hydrodynamically complex networks. This underscores the importance of balancing physical law enforcement with neural expressivity during model training.

v). The study demonstrates that PINN models can serve as a reliable and computationally efficient alternative to conventional hydraulic models like HEC-RAS, particularly in data-limited or real-time applications where rapid decision-making is required.

## 1.6 Dissertation Structure

Chapter 1 outlines the introduction to the study, delineates the research gap, defines the research aims and objectives, summarizes the methodological approach, presents the key findings, and describes the overall structure of the thesis.

Chapter 2 delivers the literature relevant to the study. It provides literature regarding the application of ML techniques in hydrology, limitations in the application of ML techniques, an introduction to PINN modelling, and HEC-RAS modelling, and lists the advantages of PINN modelling in different fields of hydrology.

Chapter 3 illustrates the methodology of the study for the PINN code development, HEC-RAS model development, data collection, and data processing. Further, the physics theories behind the PINN code development are explained, which are the basis of the code.

Chapter 4 shows the results and discussions obtained through two modelling approaches, the PINN and the HEC-RAS model. Initially, this section explains the hyperparameter optimization results for three models and moves to the results comparison section. The last section of this chapter presents a sensitivity analysis conducted for the PINN model to identify the most influential parameters.

Chapter 5 consists of the conclusion, recommendations, and Future works of the study for further extensive development based on these findings.

# CHAPTER 2

# LITERATURE REVIEW

## 2.1 Chapter Introduction

This chapter presents a comprehensive review of the existing literature to justify the identified research gap and to establish an initial understanding related to two modelling approaches, PINN and HEC-RAS, required to achieve the main research aim and specific objectives. Relevant literature was extracted regarding the importance of Rainfall-Runoff models, the application of ML models in hydrology, traditional hydraulic modelling techniques used, and their fields of application, and the application of PINN models in hydrology fields.

## 2.2 General

Sustainable water resource management cannot be established without a proper understanding of the hydraulic aspects that are unique to the considered basin or the case study area (Reddy et al., 2021). This highlights the importance of having a broad perception of the engaging hydrological processes. The best approach for establishing the needed understanding is to go for more accurate and reliable modeling. Most of these hydrological processes are complex and dynamically varying phenomena, hence more accurate modeling is mandatory to establish a correct perception about the scenarios, which will lead to accurate decision making (Nourani et al., 2014). Effects of climate changes, and spatial changes leading to non-linear variability of watershed characteristics and precipitation patterns make the modeling process more complex, while highlighting the need for innovative modeling strategies that are capable of making accurate predictions to manage the hydrological processes (Reddy et al., 2021).

These complex phenomena lead R-R modeling using physically based software to be more conflicting, deviating the simulated results from the observed values, hence, AI techniques have been introduced to address this gap. R-R modeling using AI techniques like Support Vector Regression (SVR), Artificial Neural Network (ANN), Convolutional Neural Network (CNN), and Long Short Term Memory (LSTM) has been popular in the past decade or two, and they have shown more precise results for stimulated scenarios compared to physically based models like HEC-RAS, MIKE-FLOOD (Nifa et al., 2023). Thus, the popularity of applying AI technologies in R-R modeling has increased (Ghobadi & Kang, 2023). Literature discusses different advantages and disadvantages of applying each of these AI tools in the field of hydrology, Nifa et al.(2023) points out that, ANN is more favorable in performance compared to SVM, but both inefficient under capturing series information in input data, Xiang et al. (2020) discusses that LSTM as the best AI model to identify time series patterns and to predict continuous stimulations, in the same time Nifa et al. (2023) mention that LSTM is more accurate in stimulating daily streamflow but not for monthly basis. The issue Nifa et al. (2023) raise as the reason for having reduced accuracy in LSTM compared to ANN is the unavailability of an extensive amount of monthly rainfall data to train the model. This highlights one major need that guides the model accuracy, as the availability of an extensive amount of data to train the model.

## 2.3 Hydrological Models

Hydrology has become an important aspect of human lives and the environment, with its solid connection with livable physical attributes. Hence, modelling hydrological conditions is very important to build up a broad understanding of environmental processes that affect humans (Singh, 2018). Hydrological modeling can be applied to the occurrence, circulation, and distribution of water, where it can range from simple river flow modeling to complex flood predictions. With climate change, urbanization, land-use changes, and other irrigation requirements, the modeling processes have become further complex, stressing the need for hydrological modeling (Peel & Blöschl, 2011). Empirical, conceptual, and physically-based models are the three main (3) types of models that are commonly in use, where all these models constitute unique characteristics that will help to understand different hydrological processes (Devia et al., 2015). Along with these models, catchment characteristics such as soil properties, land cover, catchment topography, soil moisture levels, groundwater aquifer characteristics, and soil-water interactions are also considered to have an accurate representation of the study areas, and to have reliable and speedy outputs from hydrological models (Wagener et al., 2001). The simplified, complex hydrological processes are generated using hydrological models, where hydrologists can take more accurate decisions, understanding the true behavioral pattern of linked parameters.

## 2.4 Types of Hydrologic Models

Rainfall-runoff models can be categorized into subdivisions depending on several key considerations. Considering the spatial distribution, lumped and distributed models are classified, where lump models consider the whole catchment as a single unit, and in distributed models, they divide one single catchment into several smaller parts (Sorooshian, 2008). Considering the time parameter, models are classified as static and dynamic, where static models exclude the time factor while dynamic models include the time factor. These models are named as event-based or continuous models as well (Wheater et al., 2007). All these model subclasses can be summarized under three main types as empirical, conceptual, and physically-based models, and with the advancement of these models with novel aspects, they perform very important and complex phenomena accurately (Devia et al., 2015).

### 2.4.1 Empirical Models

Empirical models are data-driven. These black-box models completely rely on observation-oriented data sets, without integrating with hydrological systems or physical processes. These models build mathematical equations between the respective input and output values to match the input data domain. It highlights the importance of having a considerably large data set to train them, as they focus on the statistical relationship between rather than building a connection with hydrological processes. AI-integrated applications such as ANN, CNN, and LSTM are most commonly applied black-box models in the recent decade or two, and they were also applied in enhancing sustainable water resource management with their ability to establish more accurate and speedy results. However, these models have a low explanatory ability and cannot be directly applied to another catchment without training using the data unique to that catchment.

### 2.4.2 Conceptual Models

These models are named as parametric models or grey-box models, which use semi-empirical formulas to interconnect the input parameters like rainfall, infiltration, percolation, and other catchment characteristics, with outputs like evaporation and runoff. By combining these semi-empirical formulas and input field data, semi-physical basis models are developed, which rely on an extensive amount of hydrological data under the calibration process. The accuracy of these models can be increased by increasing the curve-fitting ability. Stanford Watershed Model IV (SWM-IV) and Sacramento Soil Moisture Accounting Model (SAC-SMA) are some examples that can be listed under this category.

### 2.4.3 Physically-based Models

Physically based models are white-box models, where they are mathematically idealized models that are more accurate representations of real hydrological phenomena. These models are also addressed as mechanistic models, where they represent the model parameters as variables of both time and space. Processes related to water are modeled using finite difference models, with detailed inputs such as soil moisture content, initial water depth, topography, river network dimensions, and other physical catchment characteristics. In these models, the amount of data does not determine the accuracy of the output, rather, the accuracy of the input data determines the accuracy of the output. Thus, an accurate representation of catchment properties is more important. HEC-HMS, HEC-RAS, and SWAT models are the most commonly used physically based models used by hydrologists.

## 2.5 Need for Artificial Intelligence Techniques in Hydrology

The changes in environmental conditions, due to changes in climate and urbanization, create more complex hydrological processes. These complex phenomena lead to hydrological modeling using physically based software being more conflicting. Due to the complicated and nonlinear nature of flow production processes, a deviation of stimulated results from the observed values is experienced. Hence, AI techniques have been introduced to address this gap to increase the accuracy of the results (S. Yang et al., 2020). In physically based models, input parameters like catchment properties, soil-moisture levels, groundwater levels, infiltration and etc., keep dynamically varying; thus, these variations affect model predictions, highlighting the need to provide more accurate data as input parameters. But in data-driven AI models, a mathematical relationship is built in between inputs and outputs, and these output values are generated despite the physical relationship between the parameters, leading to more accurate and reliable scenario generation addressing the boundaries of noisy, non-linear, non-stationary, complex, and dynamic data sets (Chang et al., 2023). AI has been applied in sections like forecasting groundwater levels, modeling R-R, stream flow time series forecasting, coastal water quality predictions, reservoir water level modeling, etc. In recent decades, the need for the application of AI in hydrology to face the consequences of climate and urbanization-induced global changes (Alagha et al., 2021) has been clearly highlighted.

## 2.6 Applications of AI Techniques in Hydrology

High computational costs, time-consuming, and accuracy issues were the main drawbacks under physically based models, but by applying AI into hydrology modeling, most of these issues can be addressed. SVM, RT, ANN (Nifa et al., 2023), CNN, and LSTM (Waqas et al., 2021) are some common DP techniques applied for hydrological modeling. The main advantage in application of AI in hydrology is the ability to generate applications in hydro-meteorological forecasting and classification. Based on them, future predictions can be conducted to account for extreme hydrological events to mitigate hazards. With climate change, precipitation patterns are changing, leading to extreme precipitation events, highlighting the need for the availability of quantitative precipitation projections. Nagahamulla et al. (2011) developed an ANN model to predict monsoon rainfall in Sri Lanka, Ranjan et al. (2013) found significant results using a backpropagation network for rainfall prediction, and Pakdaman et al. (2022) used ANN and Random Forest (RF) algorithms for multi-model ensemble forecasting of monthly precipitation in Southwest Asia, providing evidence to ML application in precipitation forecasting. These have been applied in water level prediction and temperature predictions, also, where Rathnayake et al. (2023) applied Boosting Algorithms and Adaptive Network-based Fuzzy Inference Systems (ANFIS) to predict water levels in Malwathu Oya River Basin and suggested the efficacy of applying the gradient boosting approach rather than generic black box algorithms. Chang et al. (2023) and Hernández-Bedolla et al. (2022) mentioned about application of ML techniques in their studies for identifying the variations of precipitation and temperature. Further application of ML and AI techniques in streamflow predictions and flood routing has also gained significant attention, as highlighted in Section 2.8.

## 2.7 Physical-based Models for Flood-Modelling

A significant amount of research work has been conducted on flood modelling, where flood modelling is essential to understand the flood risk and simulate the flood conditions (Agonafir et al., 2023) under changing topographical and hydrological conditions. Modelling plays an important role in efforts to reduce both infrastructure damage and loss of life, which are occurring due to flooding by identifying flood-prone locations and their vulnerability (Batica, 2016), and to improve mitigation plans. With proper flood simulations, systematic structural and nonstructural flood mitigation strategies can be formulated to establish effective flood management (Hdeib & Aouad, 2023) within the flood-prone areas. For modelling floods, hydrologic-hydraulic models, numerical models, statistical models, and machine learning models have been used. Table 1 shows the characteristics of such models, advantages, limitations, and input data types for the analysis. As a summary from Table 1, hydrological and hydraulic modeling techniques by Hydraulic Engineering Center (HEC) were frequently used for modeling flood conditions with its versatile applications, but the need for a broad range of input data is a major limitation for the analysis due to data shortages (Agonafir et al., 2023).

*Table 1: Hydrological models used in flood simulations*

| Model used in the Analysis | Characteristics of the Model | Applications of the Model | Input Data |
|---|---|---|---|
| **SWMM (Storm Water Management Model) [1,5,7,34]** | A multi-objective genetic algorithm [1]<br>Urban drainage model and a management model [7] | Attenuating the flood hydrograph peak at the urban catchment outlets [1]<br>Urban floods simulations under drain pipe enlargement and low impact development [5,7]<br>Calculate surface runoff from each catchment area, flow depth, discharge, and water quality in each drainage channel and pipeline [34] | Number of outlet parameters in detention ponds, location of the ponds [1]<br>Bias-corrected meteorological data [7]<br>Maps of land use, rain data, and drainage channel dimensions [34] |
| **HEC HMS model, hydrological modelling [2,26, 29]** | Rainfall runoff modelling [2, 26,29] | Evaluate the performance of satellite rainfall estimates (SREs) through hydrologic and flash flood modelling [26]<br>Assess sources of precipitation through hydrological modelling for the catastrophic floods [29] | Imagery from Landsat for land use and land cover (LULC) [2]<br>Satellite rainfall estimates (SREs) [26] |
| **HEC RAS 2-D hydrodynamic model [3,6,21, 25,27, 30]** | A 2D mathematical hydrologic model | Determine flood-prone areas and strengthen the robustness of your mitigation strategies [3]<br>To create a flash flood inundation danger rating map, compute and simulate the water surface heights, flow velocities, flow depths, and spread [21] | Soil map data, LULC maps, DEM data [3]<br>Water demand and rainfall patterns, and daily water balance [6]<br>Geological, metrological, and hydrological groups of the drainage basins [21] |
| **Urban Flood Risk Mitigation models [4]** | Integrated Evaluation of Ecosystem Services in an integrated GIS environment [4] | Providing instances of natural water retention measures (NWRM) for each kind of land use as resilient solutions by addressing site-specific runoff reduction, and estimating the quantity of runoff due to extreme rainfall events for each watershed, is taken into consideration [4] | |

| Model used in the Analysis | Characteristics of the Model | Applications of the Model | Input Data |
|---|---|---|---|
| **Info-works Integrated Catchment Modelling (ICM) [5]** | Risk mitigation and management [5] | To provide nonstructural measures for the mitigation and management of urban flood-prone areas [5] | |
| **1D/2D hydrodynamic models [8,32,33]** | 1D1/1D and 1D1/2D urban flood models [33] | Recognize the mechanisms behind flash floods in metropolitan settings. [8]<br>Compare the simulation results of a 1D1/1D model and a 1D1/2D model for urban flood simulation<br>developed and improved existing urban flood models [32, 33] | Hydrological and hydrodynamic data[8]<br>Instantaneous flow propagation and overestimation of the flood depths within surface ponds [33] |
| **Analytic hierarchy process (AHP) [9,20]** | Comprehensive flood risk assessment model [9] | Identify high-risk areas, prioritize mitigation measures, and aid in effective urban planning and disaster management [9]<br>To evaluate and generate potential flash flood hazard maps [20] | Topographic maps, LULC maps, rainfall data, and infrastructure data [9]<br>DEM data and the GIS tools [20] |
| **Statistical estimation model for disaster impacts [13]** | Multi-Criteria Analysis, Pearson Correlation test | present a scientific answer to the question of how to quickly and effectively determine the impact of a catastrophic occurrence. | Characteristics of floods, and contains details relevant to mitigative measures |
| **Rainfall Runoff Inundation (RRI) model [14,16,22, 24]** | Use of remote sensing (RS) data [16] | To efficiently simulate the extreme flash flood events [14]<br>Simulate flash flood events with the use of remote sensing data [16,22] | Rainfall and runoff data [14,22]<br>DEM data and satellite imagery [24] |
| **GIS-based Hydrological analysis [15]** | Land-use prediction, hydrological analysis/calculation | Calculate the amount of rainfall that will fall in the natural and artificial feasible outfalls of each watershed in order to analyze the runoff rainwater volume to prevent urban flooding in 2030 (predicted land use). | Hydrological data |
| **Physically based distributed hydrologic model [19]** | | Improvements in flood warning and forecasting in urban watersheds, even for short-lived events on small catchments | High-resolution weather radar data and precipitation forecasts made by a convective storm nowcast system |

## 2.8 Application of AI models in Flood Routing

Drawbacks in physically based models encouraged the application of AI models in flood routing, with advantages like increased accuracy, low computational costs, addressing complexities, and robustness in the method. Major ML algorithms like ANN, neuro-fuzzy (NF), adaptive neuro-fuzzy inference systems (ANFIS), support vector machines (SVM), and multilayer perception (MLP) were applied within the recent past, both in flood routing and flood predictions (Mosavi et al., 2018). The ANNs are one of the most popular ML approaches, which are versatile and efficient in modeling complex flood processes with high tolerance levels and accurate approximations (Abbot & Marohasy, 2014). Initial application of ANNs in flood modeling was in the 1990s, where complex and non-linear relationships between rainfall and floods, as well as river flow and discharge, could be generated despite the catchment characteristics. But still, ANNs constitute the main drawbacks related to relatively low accuracy, iterative parameter tuning, and slow response to gradient-based learning processes, with these drawbacks, ANNs show very limited accuracy in peak-flow predictions and precipitation prediction (Wu & Chau, 2010). In ANNs, backpropagation is utilized to increase the accuracy of weights, and it was identified as the most suitable and powerful prediction tool in flood time-series prediction. MLP is another ML approach that has been used for flood routing, which is an advanced representation of ANN (Senthil Kumar et al., 2005). It utilized supervised backpropagation, with a high number of layers and activating non-linear behavior.

Even though MLPs become more popular among hydrologists compared to other ANN models, the main drawback was found as the difficulty in optimizing the model (Mosavi et al., 2018). This is one of the most advanced systems that has the capability of giving the most reliable estimators to complex scenarios like flooding, which is formed through a combination of ANN and fuzzy logics, providing the capability of modeling nonlinear functions. Fuzzy logic is a simplified mathematical model that works by incorporating expert knowledge into fuzzy interface systems, which will incorporate an approximator function with less complexity, and provide great potential for nonlinear modeling of hydraulic extremes (Choubin et al., 2016). Further, ANFIS utilizes ANN in identifying and tuning parameters, acting as a hybrid ML model. The model constitutes advantages like fast and easy implementation, high accuracy, and strong generalizing ability, and due to these advantages, ANFIS became more popular among hydrologists under flood modeling (Shu & Ouarda, 2008).

The SVM is another approach that was applied under flood modeling. Support vector is classified as a non-linear search algorithm that will reduce overfitting, working based on a statistical learning theory. SVM was applied as a robust and efficient ML algorithm that can act as an alternative to ANNs (Vapnik & Mukherjee,1999). SVM is suitable for both linear and non-linear classification, and efficient in mapping of inputs into feature spaces can be ensured. Advantages of SVM can be listed as accurate results, excellent generalizing ability, and better performance compared to ANNs, but drawbacks like high computational cost and unrealistic outputs can result (Dehghani et al., 2014).

Decision Tree (DT) is another approach that is commonly applied in flood modeling. It utilizes trees of decisions where the expected variable values will appear in leaves of the tree (Mosavi et al., 2018). Random forest method, classification and regression trees are some popular DT models that are applied in flood routing and prediction, and they can be applied as a better alternative to ANN and SVM models, where DTs will provide the best performance out of the three (3) ML approaches (Yu et al., 2017). Similarly, a trend was improved to use EPSs, where several alternative models were ensembled together to increase the flood prediction ability and accuracy, and several studies have also shown the ability of EPS models to improve the model accuracy (Sajedi-Hosseini et al., 2018). They use multiple fast learning or statistical algorithms like ANNs, MLP, DTs, rotation forest (RF), bootstrap, and boosting, allowing higher accuracy and robustness in models (Yu et al., 2017). But all these models' accuracy relies on the quality and the quantity of input data, where the model performances are affected severely by the input data. Thus, there is a limitation in applying these models in data-scarce situations. To address the gap, a novel AI technique was introduced as PINN, where related physics-informed partial differential equations are utilized for generating a residual value in modifying the values generated through the approximator network (Bai et al., 2024). Where governing equations and empirical knowledge can be utilized as training data to address the data scarcity issue.

## 2.9 Application of PINN in Hydrology

Application of PINN in hydrology emerged as a promising approach to address problems associated with hydrological aspects, mainly due to data scarcity. Integration of physical laws with neural networks, unlike in usual, completely black box AI models, made the PINN approach more promising to apply in solving hydrology-related issues. To identify the application of PINN in field of hydrology a search query was conducted using databases of “Web of Science”, “Research Gate” and “Scopus”, incorporating key terms of ("Physics-Informed " OR "PINN") AND ("Hydrology" OR "Flood" OR "Streamflow " OR "Hydrodynamic" OR "Rainfall-Runoff " OR "Deep Learning in Hydrology" OR "Groundwater" OR "Stream Flow" OR "Numerical Methods in Hydrology" OR "Watershed" OR "Water Resource" OR "Precipitation" OR "Climate"). From the search query, out of 345 papers, 201 papers were screened utilizing the topic and keywords, and then using the abstract, 63 papers were sorted, that are matching with the purpose of the study, connecting PINN and the field of hydrology. Figure 01 shows a network map for keywords included in the literature, which were utilized to identify closely related fields of study with PINN in hydrology.

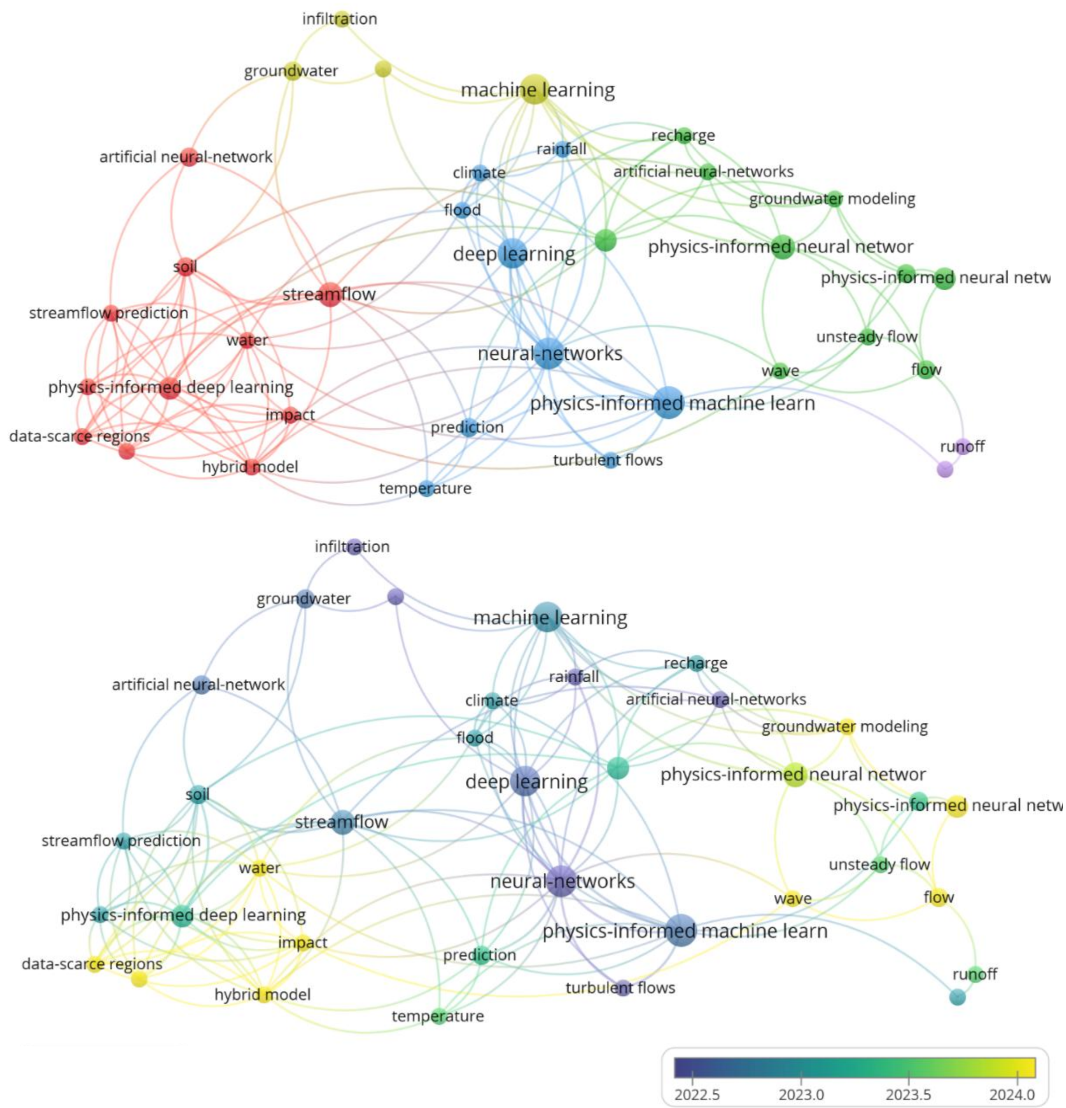


*Figure 1: Network visualization and overlay visualization using VOSviewer*

From the network visualization of key words, “physics-informed machine learning”, “physics-informed neural network”, “physics-informed deep learning”, and “machine learning” were identified as central key words of the four main clusters. These central keywords related to PINN showed links with hydrology related keywords as, “streamflow”, “groundwater modeling”, “climate”, “climate change”, “flood”, “rainfall” and “runoff, presenting the application of PINN in those fields. Similarly, the link connections with key terms, “data scare regions” and “ungauged basins” with “physics informed deep learning”, shows the ability of applying PINN in such scenarios where usual black box AI models are struggling with data unavailability.

Further, the overlay visualization shows the time domain in which most of the key terms appeared in the literature. It highlights that the application of PINN in hydrology aspects started within the recent past, within a time duration of 2 years. Moreover, the application of physics-based guiding equations in data-scarce occasions was identified in late 2023, highlighting the novel ability to address prevailing issues of data scarcity and uncertainty in the field of hydrology.

### 2.9.1 Application of PINN in Streamflow Modelling

Rainfall-Runoff modeling involves translating precipitation data to streamflow predictions. A limited number of case study applications were found in the literature, regarding the application of PINN in RR modeling for open channel systems with or without uniform cross sections. Luo et al. (2024) had conducted a study for both straight channel steady flow systems and for looped network unsteady flow systems utilizing PINN, and had calculated the error due to the deviation of results compared to observed streamflow. The study utilized Saint-Venant equations as the guiding partial differential equations (PDEs), relating to the principle of mass conservation and momentum conservation, to generate the residual value that will be used to train the model. Under the pre-training of the model, cross-sectional hydraulic parameters like slope and Manning's coefficient were provided with approximate values, and they were optimized utilizing the L-BFGS-B optimizer for each cross section. Additionally, the study had checked for the impact of the number of cross sections on changing the accuracy of the PINN model, and had discovered that with the reduction of the cross-section points, there is a deterioration in model accuracy. And Luo et al. (2024) had further shown that in both the cases studied, the PINN model showed highly accurate results compared to traditional models like the HEC-RAS model, showing low Root Mean Square Error (RMSE) and Mean Absolute Percentage Error (MAPE) values. Zhong et al. (2023) also conducted a study integrating a differentiable parameter learning algorithm and the EXP-HYDRO conceptual model in RR modeling in data-scarce regions. Niu et al. (2023) also applied the kinematic wave equation, which is a simplification of SVE equations, where lateral inflow, wind shear, and eddy losses were neglected, as the PDE in the PINN model to stimulate 1D surface flow. Other than SVE, the Advection-dispersion equation (ADE) was also used in PINN as a guiding partial differential equation. Using the SVE, ADE, and SVE-ADE approach, the residual values in the PINN model are calculated to have a minimized mean squared error (MSE) loss function, and all three (3) PINN models were utilized to stimulate 1D streamflow. And Niu et al. (2023) suggested that the accuracy of PINN models is related to the number of network layers and neurons, and also has a high tolerance level to noisy data.

### 2.9.2 Application of PINN in Groundwater Modelling

Groundwater modeling incorporating PINN is an emerging trend that was applied to address the issues of sparse observational data and irregular boundary conditions. Chen et al. (2023) modelled water flow in unsaturated soils integrating with Richardson Richards equation (RRE) as the guiding PDE. Within this study, a comparison was built up between GN-PINN, PLF-PINN, and the base model PINN using RRE to check the accuracy of these models. It was conducted by solving three (3) main problems related to groundwater flow as: (1) 1D infiltration problem, (2) 1D cyclic wetting-drying problem, and (3) 2D infiltration problem. Cuomo et al. (2023) and Schiano Di Cola et al. (2024) used the groundwater flow equation in an unconfined aquifer as the guiding PDE in utilized PINN model. This equation describes the flow of groundwater through a porous medium based on Darcy's Law. Cuomo et al. (2023) applied the

PINN model in stimulating three (3) groundwater flow situations: (1) 1D case of a single pumping well, (2) 2D case of a single pumping well, and (3) 1D case of multiple pumping wells in an infinite aquifer. And finally, the results from the PINN model for these three scenarios were compared with a Finite Difference Method (FDM) to emphasize the advantages of the application of PINN in groundwater modeling, such as the ability to handle high-dimensional problems, complexities in boundary conditions, and data scarcity.

### 2.9.3 Application of PINN in Flood Modelling

Flood modeling requires accurate simulation of the flow dynamics in rivers or flood plains to make important decisions related to evacuation. PINN has been applied in finding the flood inundation depths, in uncertainty quantification, and inundation forecasting using a smaller number of data points. The studies have been conducted for both channel and non-channel systems to stimulate the inundation depths from floods utilizing SVEs for mass and momentum conservation, and stage hydrographs were generated based on the scenario. Studies by Markidis (2021b), Yang et al. (2024), and Kohanpur et al. (2023) showed the application of PINN for both flood routing and predictions. But there is very limited or no research work that has been conducted to predict the flood peak depths in channel systems, which is required with high accuracy as an indicator of the severity of flooding.

## 2.9 Objective Functions

To evaluate the model performance in hydrological models, a list of objective functions is used in the calibration and validation processes as an indicator of model accuracy. Model calibration and validation are conducted to check the fitness of the simulated results from inputs and observed outputs from the catchment, and these objective functions can also determine the need for model optimization (Abdulla and Al-Badranih, 2000). Nash Sutcliffe Efficiency (NASH) (Equation 01) is one of the objective functions that is very good in evaluating peak flows, and the NASH value ranges between ∞ and 1.0, where 1.0 shows the best fit (Xiong and Guo, 1999).

$$NASH = 1 - \frac{\sum_{i=1}^{n}(Si - Oi)^2}{\sum_{i=1}^{n}(Oi - \bar{O}i)^2} \tag{1}$$

Mean Absolute Percentage Error (MAPE) is another objective function that evaluates prediction accuracy by expressing the error as a percentage of the observed values, providing a scale-independent metric as in Equation 02. Lower MAPE values show better model performance (Jackson et al., 2019).

$$MAPE = \frac{1}{n}\sum_{i=1}^{n}\left|\frac{Oi - Si}{Si}\right| \times 100 \tag{2}$$

Root Mean Square Error (RMSE) measures the average magnitude of error between predicted and observed values, with a stronger emphasis on larger errors due to the squaring of residuals. Shows poor results in low flow evaluations and varies from 0 to ∞, where 0 indicates the best results (Chu & Shirmohammadi, 2004).

$$RMSE = \sqrt{\frac{\sum_{i=1}^{n}(Oi - Si)^2}{n}} \tag{3}$$

Where $n$ is the number of data points, $O_i$ is the observed discharge, $S_i$ is the simulated discharge, and $\bar{O}$ is the mean of the observed discharge, respectively.

## 2.10 Summary

Hydrological modeling is very important for hydrologists to make important decisions regarding water resource management. Among those, flood modeling and predictions are crucial to establish proper protection, mitigation, or evacuation measures. These models can be developed under three main categories: black-box, grey-box, and white-box models, depending on the level of influence or involvement of physically-based characteristics in model generation.

Most ML approaches are black-box models, where they build up a statistical relationship between the inputs and outputs. Models like HEC-HMS, HEC-RAS, and RRI are physically based white box models, where catchment characteristics, physical laws guide the model performance. But application of ML and AI approaches in hydrology became very convenient and versatile with the abilities of ML approaches, such as modeling complex hydrological phenomena, low computational cost, and high accuracy compared to traditional physically based models. Even though these ML models are versatile, the model accuracy depends on the quality and quantity of input data. This issue sets boundaries in the application of ML approaches in data-scarce scenarios in hydrology as groundwater flow modeling, stream flow modeling in ungauged basins, and flood inundation depth predictions, etc.

To address this gap, PINN was applied, where PDEs were used as guiding equations to train the neural network, surpassing the limitations of data scarcity. Hence, within this study efficacy of the application of PINN in stimulating peak flood depths will be investigated in the channel network in the Colombo Metropolitan area, Sri Lanka. The area was undergoing severe urban flood events within the recent past, highlighting the need of having accurate flood predictions to reduce the tangible and intangible damage. A similar flood peak stimulation will be conducted using HEC-RAS software, and the accuracy of these models will be evaluated using objective functions such as NASH, RMSE, and MAPE, comparing with the observed flood peak depths at previous occurrences. Furthermore, the ability to use the accurately predicted flood peak depths in improving city resilience will be analyzed.

# CHAPTER 3

# METHODOLOGY

## 3.1 General

This chapter presents the research processes that were adhered to within the study. The methodology flow chart of the study is as in Figure 2, which compares the temporal and spatial variation of 1D flood routing results between the traditional HEC-RAS model and PINN models. The methodology starts with identifying suitable canal systems in the Colombo Metropolitan Area, Sri Lanka, to apply PINN and HEC-RAS approaches, which frequently face issues due to flooding.

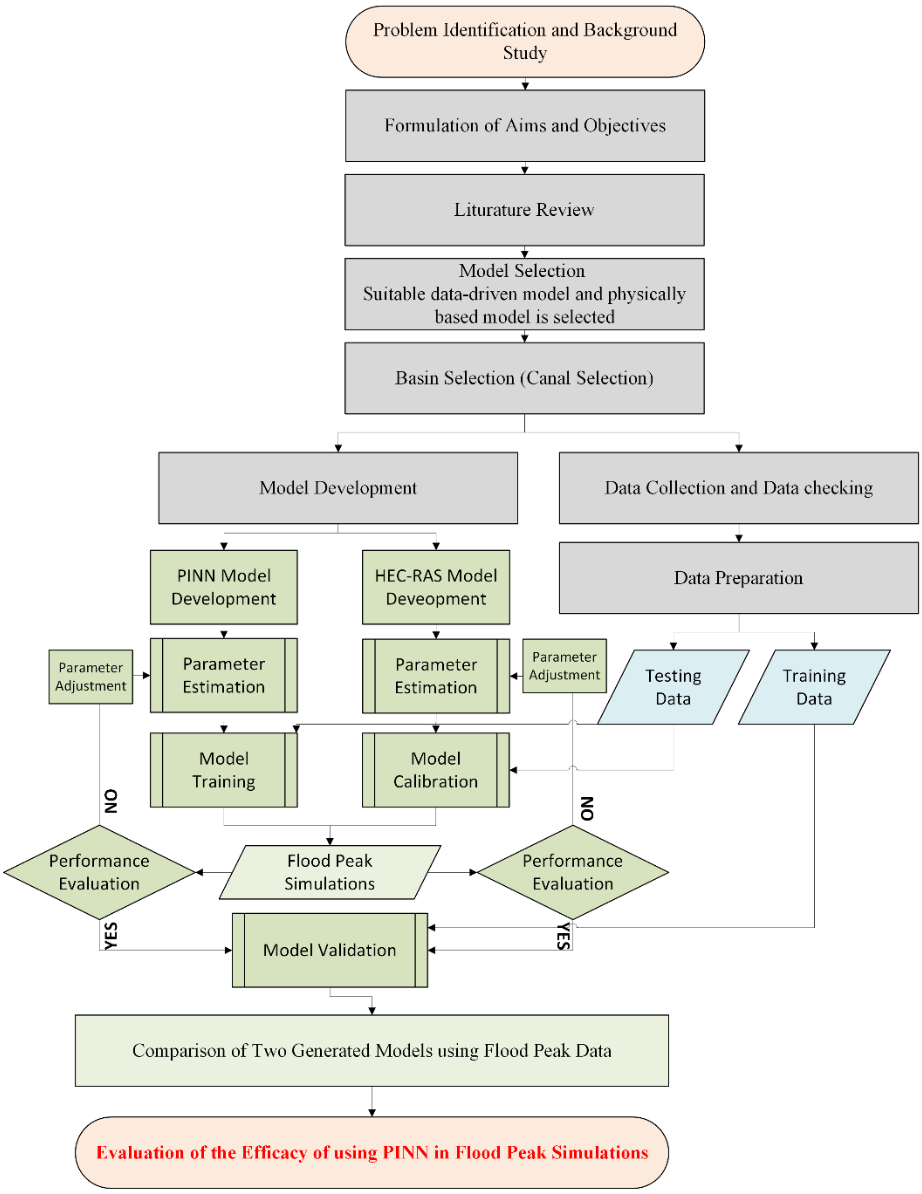


*Figure 2: Methodology Flowchart*

## 3.2 Case Study Area

The selected Case study area is the Colombo Metropolitan Area, Sri Lanka, from latitude 6° 43' 00" N to 6° 58' 00" N and longitude 79° 50' 00" E to 80° 00' 00" E. The research area spans 27.165 $km^2$ and encompasses several Divisional Secretarial Divisions (DSDs), including Colombo, Thimbirigasyaya, Dehiwala, Moratuwa, Kesbawa, Rathmalana, Maharagama, Kaduwela, and Kotte, as shown in Figure 03.

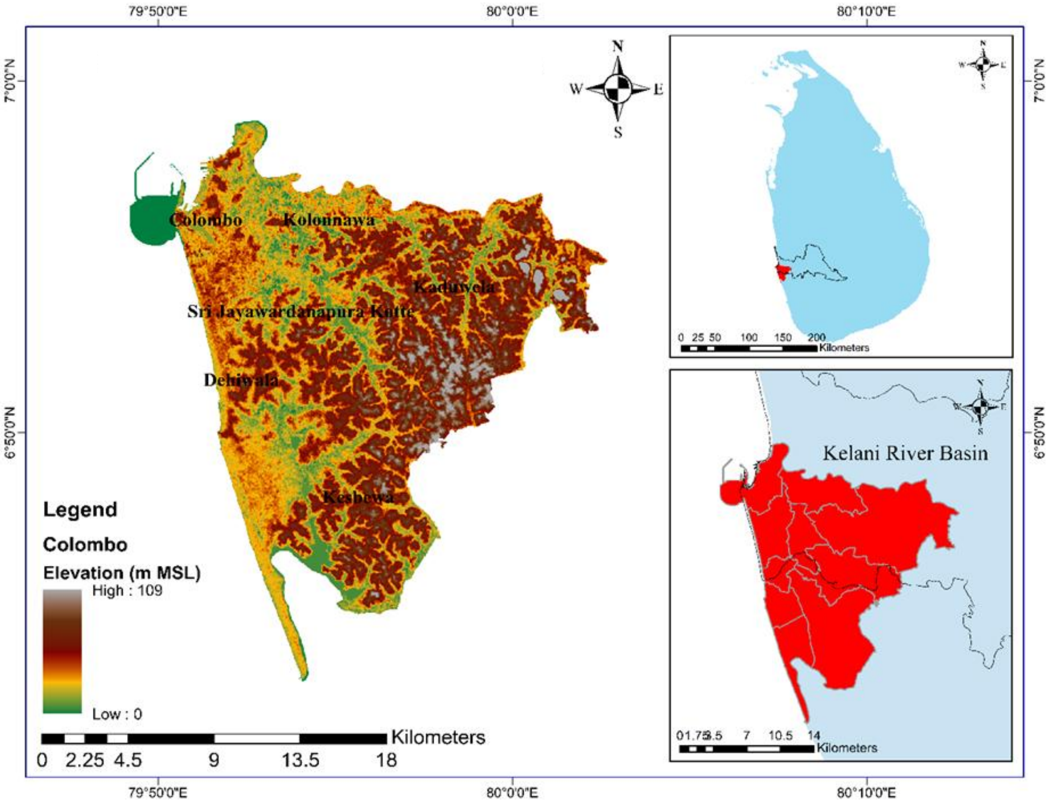


*Figure 3: Colombo Metropolitan Area, Sri Lanka*

The study area predominantly experiences South-Western monsoon rains from May to September, as well as inter-monsoon rains from March to April and October to November. This region receives an annual average rainfall of approximately 2,400 mm, with inter-monsoonal rainfall accounting for almost half of the total annual precipitation. According to the Urban Water Management Division of the Sri Lanka Land Development Co-operation (SLLDC), the area is experiencing flooding in three main forms: the Kelani River flooding, capacity exceedance in the existing canal system, and localized flooding. The heavy rainfall, flat terrain, and low slope are the key drivers that make the study area further vulnerable (Wagenaar et al., 2019). Due to its high vulnerability, a well-regulated canal network was constructed and maintained by SLLDC to carry flood volumes, as in Figures 4 and 5. This canal network includes Madiwela East Diversion, Wellawatta canal, Dehiwala canal, Kirulapone canal, Torington canal, St. Sebestain canal, Kolonnawa canal, Dematagoda canal, and Main Drain connected to regulate flood volumes. The carried flood volumes through those canals are pumped to the nearby sea or the Kelani River. In facilitating pumping, established pumping stations, including St. Sebastian North pumping station, St. Sebastian South pumping station, and Ambathale stormwater pumping station, are used. The canal system, along with pumping stations, plays a major role in urban flood management in the Colombo Metropolitan Area, Sri Lanka.

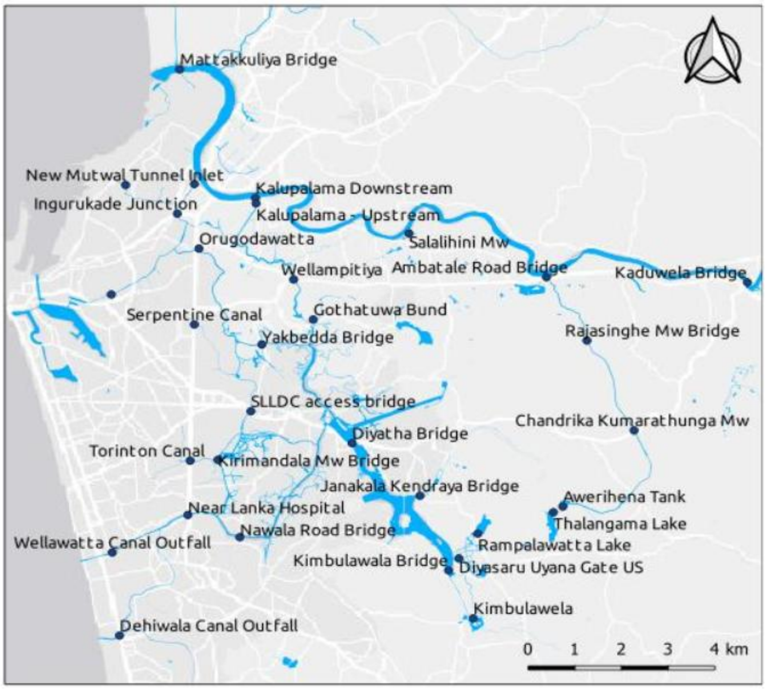


*Figure 5: Canal system and water level monitoring stations proposed by SLLDC in Colombo Metropolitan Area (Source: https://pub.curwsl.org/ )*

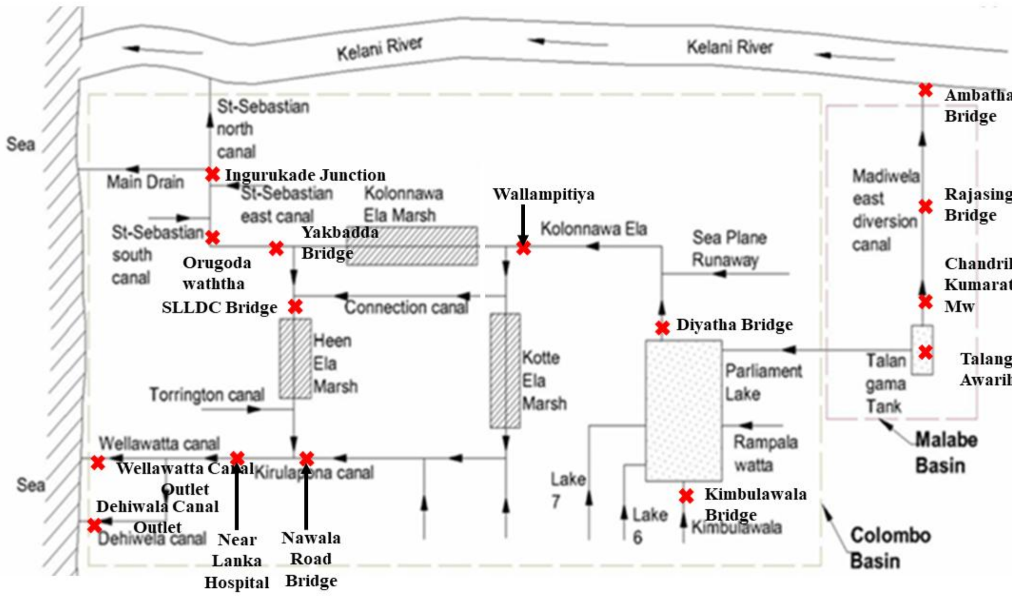


*Figure 5: Schematic diagram for canals and water level monitoring locations (Wagenaar et al., 2019)*

Out of the whole canal network, three main canal systems were selected for modelling purposes to compare flood peak stimulating ability and 1D flood routing ability along the canal network using PINN and HEC-RAS approaches. This selection was conducted based on the data availability and locations of water level monitoring stations and is discussed in Section 3.5.

## 3.3 Physics-Informed Neutral Network Code Development

The PINN code was developed to facilitate 1D unsteady flow modelling through the selected canals in the Colombo Metropolitan Area, Sri Lanka. PINN is a promising technique to incorporate field observations and theoretical partial differential equations (PDEs). Based on the PDE, the residual loss is calculated as a part of the loss function, and it is used in training the model. This approach is efficient in states with low data availability. Thus, within this study, the PINN code is used both in flood peak modelling and 1D flood routing with a limited amount of data. Within this section, a description of the developed PINN code will be provided, incorporating the physical background of the flow of water in open channels, the development of deep neural networks, loss calculation, and parameter optimizations.

### 3.3.1 Physical Law - Partial Differential Equation (PDE)

The kinematic wave equation is applied as the PDE within the code, which is a simplified version of the dynamic Saint-Venant equations (SVE) for open channel flows. The SVEs are derived based on mass and momentum conservation as follows, considering two cross-sections within the same reach.

For mass conservation:

$$\frac{\partial A}{\partial t} + \frac{\partial Q}{\partial x} = 0 \tag{4}$$

For momentum conservation:

$$\frac{\partial Q}{\partial t} + \frac{\partial}{\partial x}\left(\frac{Q^2}{A}\right) + gA\left(\frac{\partial h}{\partial x}\right) = -gAS_f + S_x \tag{5}$$

where Q ($m^3/s$) is the discharge, A ($m^2$) cross-sectional area, t (s) is the time, x (m) is the length along the channel, h (m) channel water level, $S_f$ is the frictional force, $S_x$ is other forces like wind, $\partial h/\partial x$ is the bed slope and g = 9.81 $m/s^2$ is the gravitational acceleration.

Equation 5 can be further simplified, omitting lateral inflows, wind shear, and eddy losses as follows, equalizing the channel bed slope to the friction slope.

$$S_o = S_f \tag{6}$$

Based on the derived Equation 6, the boundary conditions and initial conditions for the model are derived using Manning's Equation as in Equation 7.

$$Q(x,t) = \frac{1}{\eta} A \times R^{\frac{2}{3}} \times S_f^{\frac{1}{2}} \tag{7}$$

$$R = \frac{A}{P} \tag{8}$$

$$Q(x,t) = \frac{1}{\eta}\frac{A^{\frac{5}{3}} \times S_0^{\frac{1}{2}}}{P^{\frac{2}{3}}} \tag{9}$$

where, Q ($m^3/s$) is the discharge, A ($m^2$) is the cross-sectional area, R is the hydraulic radius, $S_f$ is the frictional slope equal to bed slope, P is the wetted perimeter, and $\eta$ is the Manning's roughness coefficient.

Even though Equation 4 carries a discharge (Q) term, the known parameter within the domain is the water level height, thus, Equation 4 is further simplified as follows:

$$\frac{\partial A(h)}{\partial t} + \frac{\partial Q(h)}{\partial x} = 0 \tag{10}$$

$$\frac{\partial A}{\partial h} \times \frac{\partial h}{\partial t} + \frac{\partial Q}{\partial h} \times \frac{\partial h}{\partial x} = 0 \tag{11}$$

where, $\frac{\partial A}{\partial h}$, $\frac{\partial h}{\partial t}$ and $\frac{\partial h}{\partial x}$ terms, which are the derivatives of area and water levels, can be derived based on the available data. Thus, $\frac{\partial Q}{\partial h}$ term should be substituted with the terms from available data as follows, using the first derivative of Manning's Equation.

$$\frac{dQ}{dh} = \frac{5}{3} \times \frac{1}{\eta} \times \frac{A^{\frac{2}{3}} \times {S_0}^{\frac{1}{2}}}{P^{\frac{2}{3}}} \times \frac{dA}{dh} - \frac{2}{3} \times \frac{1}{\eta} \times \frac{A^{\frac{5}{3}} \times {S_0}^{\frac{1}{2}}}{P^{\frac{5}{3}}} \times \frac{dP}{dh} \tag{12}$$

$$\frac{\partial A}{\partial h} \times \frac{\partial h}{\partial t} + \frac{{S_0}^{\frac{1}{2}}}{\eta} \left(\frac{5}{3} \times \frac{A^{\frac{2}{3}}}{P^{\frac{2}{3}}} \times \frac{dA}{dh} - \frac{2}{3} \times \frac{A^{\frac{5}{3}}}{P^{\frac{5}{3}}} \times \frac{dP}{dh}\right) \times \frac{\partial h}{\partial x} = 0 \tag{13}$$

Thus, as the final PDE that is used to train the PINN code, Equation 13 was utilized. And using that trained code, the water levels along the stream were simulated and tested.

To initiate the Physics-Informed Neural Network (PINN) framework for learning the unknown spatiotemporal dynamics of water level variation in the mentioned urban canal system, a fully connected deep neural network (DNN) was used to approximate the latent solution $h(x,t,r)$. Mathematically, the DNN-based approximation of the true water level function can be expressed as:

$$h(x,t,r) = \hat{h}\ (x,t,r;\theta) \tag{14}$$

where x denotes the spatial location along the channel, t denotes the time, and r denotes the corresponding rainfall intensity at the same spatial-temporal coordinate, $\hat{h}\ (x,t,r;\theta)$ is the surrogate function of the neural network, and $\theta$ denotes a set of trainable parameters, including the weights and the biases.

The architecture of the DNN is fully connected to a feed-forward network (FNN), where the first layer is the input layer, the last layer is the output layer, and the intermediate layers are the hidden layers. The input vector $z = [x, t, r]^T$ is passed through a sequence of hidden layers (4 or 5), each containing a prescribed number of neurons (256 or 530). All hidden layers employ an activation function from the following options: ReLU, tanh, sigmoid, swish, and GELU, based on their effectiveness in preserving nonlinearity while preventing vanishing gradients. The network architecture follows a shared-truck dual-head design, where the final layer gets branched into two distinct output heads that correspond to the two water level monitoring stations, Station 01 and Station 02, in the selected canal networks as mentioned in Section 3.1.1. These two stations correspond to the starting (x=0) and end locations of the canals. This dual-head structure enables the network to capture shared physical dynamics along the canal reach, while also learning station-specific hydrodynamic responses. Further, this allows simulating the water levels at intermediate points along the canal within the given time frame of input data. These intermediate points are called the collocation points, and these points allow the approach to compare the spatial variation of water levels along the canal.

The forward propagation of the DNN proceeds layer-wise as follows:

$$y^{(1)} = \sigma\left(W^{(1)}z + b^{(1)}\right) \tag{15}$$

$$y^{(i+1)} = \sigma\left(W^{(i)}y^{(i)} + b^{(i)}\right),\ i = 1,2,\ldots\ldots n_l\text{-}1 \tag{16}$$

where,

$z = [x, t, r]^T$ - the input vector consisting of spatial coordinate x, time t, and rainfall intensity r

$W^{(i)}$ - the weight matrix connecting the $i^{th}$ layer to the $(i+1)^{th}$ hidden layer (A matching matrix with the number of neurons in the $i+1$ layer)

$b^{(i)}$ - the bias vector of the hidden layer $(i+1)$

$\sigma$ - the selected activation function out of ReLU, tanh, sigmoid, swish, and GELU

$y^{(i)}$ - output of the $i^{th}$ hidden layer

The recursive propagation, in Equation 16, is carried through the network depth, learning the features of the input parameters, allowing the model to train. At the output layer, as in Equation 17, station-wise predictions are given for station 01 and station 02, through $\widehat{h}^{\,s}$, where s is either station 1 or 2.

$$\widehat{h}^{\,s}(x,t,r;\,\theta) = y^{(n_l+1)} = \left(W^{(n_l)}y^{(n_l)} + b^{(n_l)}\right), \qquad s \in \{1,2\} \tag{17}$$

The next step is model training, by adjusting the parameter, $\theta = \{W^{(i)}, b^{(i)}\}$. These parameters include all weight matrices and bias vectors associated with the hidden and output layers of the DNN. The goal of training is to adjust these parameters such that the predicted water levels $\widehat{h}^{\,s}(x,t,r;\,\theta)$, for each station s $\in$ {1,2}, match the observation data while simultaneously satisfying the governing PDE for the system. Similarly, as in neural networks, model training is performed by minimizing the loss function and optimizing the weights and biases through back-propagation. But, in the particular scenario, the issue is due to the availability of a limited number of data points to model the flood peaks and to execute 1D flood routing. As a solution to this issue, an additional loss function is created as the residual loss, which is generated through the PDE (Equation 20) used within the PINN code. Thus, within this PINN code, a composite loss function is utilized, integrating Mean Squared Errors (MSE) of data losses, initial condition losses, boundary condition losses, and a physics-informed loss function as Equation 18.

$$\mathcal{L}_{total} = \propto_1 \times MSE_d + \propto_2 \times MSE_r + \propto_3 \times MSE_0 + \propto_4 \times MSE_b \tag{18}$$

where,

$MSE_d$ - The data loss, computed as the mean squared error between predicted and observed water levels at the monitoring stations (Equation 19)

$MSE_r$ - The physics residual loss, quantifying the deviation of the governing PDE at collocation points (Equation 20)

$MSE_0$ - The initial condition loss, enforcing the agreement between the model-predicted and known water level distributions at x=0 and t=0 (Equation 21)

$MSE_b$ - The boundary condition loss, ensuring the agreement between model-predicted and known water level distributions at x=L and t=t (Equation 22)

$\propto_1, \propto_2, \propto_3, \propto_4$ - weight coefficients that control the relative importance of each loss term.

The equations for calculating each loss term are as follows:

$$MSE_d = \frac{1}{N_d}\sum[\widehat{h}^{\,s}(x_i, t_i, r_i;\ \theta) - h^{obs,s}(x_i, t_i, r_i;\ \theta)]^2 \tag{19}$$

$$MSE_r = \frac{1}{N_f}\sum[\frac{\partial A}{\partial t}\left(x_j, t_j, r_j\right) + \frac{\partial Q}{\partial x}\left(x_j, t_j, r_j\right)]^2 \tag{20}$$

$$MSE_0 = \frac{1}{N_0}\sum[\hat{h}\left(x_{0,}0\right) - h\left(x_{0,}0\right)]^2 \tag{21}$$

$$MSE_b = \frac{1}{N_b}\sum[\hat{h}\left(x_{L,}t\right) - h\left(x_{L,}t\right)]^2 \tag{22}$$

where, $N_d$ is the number of data points, $N_f$ is the number of collocation points to check residual loss, $N_0$ is the number of initial data points at t=0, and $N_b$ is the number of boundary data points at x=L and t=t. Once the total loss is computed, it is used to update the network parameters θ (weights and biases) through back-propagation using gradient-based optimization. The gradients of the loss with respect to each weight and bias are computed using automatic differentiation, considering the first derivative as the gradient. This process is integrated with the allocated learning rate and is repeated iteratively across the number of epochs using the Adaptive Moment Estimation (Adam) optimizer. For the canal systems, a suitable learning rate (0.00009) and epochs (1000 or 1200) were allocated based on hyperparameter tuning. By increasing the number of epochs, the accuracy of the predicted data can be further increased, but it reduces the model's generalizing ability; thus, the minimum number of adequate epochs was used in all three canal systems. Considering the optimizers, the main optimizers that are commonly used in PINN are Adam, Limited-memory Broyden-Fletcher-Goldfarb-Shanno (L-BFGS), or a hybrid version of Adam and L-BFGS (Niu et al., 2023). Even though L-BFGS has the ability for higher-precision tuning, the main constraints under usage of L-BFGS, including its complexity to implement in TensorFlow, slowness, and the need for higher memory intensity (Niu et al., 2023), lead to the selection of Adam as optimizer. Adam is a favorable optimizer for fast convergence in early epochs and to handle noisy data, but it also has a probability of getting deviated at local minima or flat data regions (Luo et al., 2024). The optimization is run until the loss function converges or the early stopping criteria are satisfied. During training, model checkpoints are used to save the best-performing weights based on the validation loss values. This training approach enables the PINN model to not only fit observed water level data but also to enforce physical consistency across space and time, yielding a robust and generalizable surrogate model of canal hydrodynamics.

Apart from the main flow under model training, hyperparameter tuning can be identified as a joint approach to optimize the learning performance and generalization capability of the PINN code. Hyperparameters are the parameters that are not learned from the data but rather have a critical role in influencing the convergence, accuracy, and stability of the model. In the present study, the key hyperparameters, including the learning rate ($\eta$), number of hidden layers, number of neurons per layer, activation function ($\sigma$), and loss component weights ($\alpha_1$, $\alpha_2$, $\alpha_3$, $\alpha_4$), were subjected to iterative tuning under distinct canal systems. This approach was conducted in a hybrid mode within the study using both manual and Bayesian Optimization approaches to identify the optimal set of hyperparameters that minimizes the total loss function. Unlike the manual method, which explores the search space blindly, Bayesian Optimization builds a probabilistic model of the objective function (NSE and RMSE) and selects hyperparameters based on a balanced strategy. The selection of hyperparameters for three canal networks is mentioned in Section 4.1 in more detail.

The trained PINN model was evaluated on its ability to predict water levels at the two monitoring stations (Station 01 and Station 02). The predicted water levels $\widehat{h}^{s}(x,t,r;\,\theta)$ were compared with observation data in the given time domain, and NSE and RMSE values were computed. The models were run several times till a higher agreement was reached on the calculated objective functions, confirming a favorable model training phase. Following the training phase, the trained PINN model was subjected to a structured validation process to assess its predictive accuracy, generalization capacity, and compliance with physical principles. The validation was conducted using both observed water level data and analytically derived residuals of the governing continuity equation. The developed PINN models were subjected to a comprehensive spatiotemporal validation using two complementary approaches. In the first approach, the models were evaluated based on their ability to simulate the highest flood peak within the observed time domain. The corresponding rainfall input and temporal range were externally provided, and the predicted water surface elevations were directly compared against field observations at the monitoring stations. In the second approach, the models were used to predict water levels at several intermediate spatial locations, designated as collocation points, along the canal reach. These predictions were evaluated against both observed water level measurements and outputs from the HEC-RAS model. The predictive accuracy at these points was quantified using standard performance metrics, NSE and RMSE. For both the training and validation phases, multiple forms of visualization were employed to support model interpretability. These included time series plots comparing observed and predicted water levels, residual plots illustrating the total loss function over epochs, and PDE residual plots showing the model's compliance with the underlying physical law as presented in Section 3.3.1. As the final output, these analyses provide a comprehensive evaluation of the model's capacity to generalize across space and time while respecting domain-specific physical constraints.

## 3.4 HEC-RAS Model Development

To complement the PINN approach and provide a physics-based benchmark for hydrodynamic behavior, a series of one-dimensional (1D) flood routing models was developed using the HEC-RAS software. These models were specifically tailored to simulate flood propagation through the canal networks located within the Colombo Metropolitan Area, Sri Lanka. A total of three separate HEC-RAS models were constructed, corresponding to three major canal systems in the study area. The primary objective was to simulate a known flood event and evaluate model performance against observed and PINN-predicted water levels.

Initially, the HEC-RAS approach starts with digitizing the canal; for that, the topographic data were used. For that, the Copernicus Global Land Service (2023) raster Digital Elevation Model (DEM) with a 30 m × 30 m spatial resolution was utilized in the study. The canal digitizing was performed manually with the use of global satellite images to sketch the actual canal path and to identify cross-section locations. Representing the actual canal path, the river center line, bank lines, flow paths, junctions, and cross-section locations are added. Along the canal, cross sections were updated and incorporated into the model domain for each canal, ensuring appropriate spatial resolution of the hydraulic profile. These cross sections included key locations such as water level monitoring locations, which served as a reference for mid-reach validation. These HEC-RAS models were constructed using the unsteady flow analysis module within the 1D simulation environment. The upstream boundary condition for each canal system was defined by a stage hydrograph at the corresponding headwater location, specifically derived from water level observations at designated monitoring stations. The downstream boundary condition was represented using a normal depth assumption (based on slope estimates derived from terrain analysis) or using stage hydrographs. The Manning's roughness coefficient was uniformly set at $n$=0.04 for all canal systems, selected based on visual inspection and reference to similar studies (Liu et al., 2019), reflecting moderate channel flow resistance due to vegetation along the canal banks.

The HEC-RAS models are calibrated based on water level data from an observed flood event, adjusting parameters such as Manning's roughness factor and the normal depth value at the instances where it is applicable. The models run at a 5-minute computation interval, allowing a warmup period of 10,000 initial steps. The model validation is conducted by comparing predicted water levels with observed water levels along the canal and calculating NSE and RMSE values. These HEC-RAS outputs were also compared with PINN model outputs at the same spatiotemporal points, facilitating a triangulated validation of the event, enhancing confidence in both the PINN and HEC-RAS simulations.

## 3.5 Data Collection

The data required for both the PINN and HEC-RAS modeling frameworks were obtained through the Urban Water Management Center of the Sri Lanka Land Development Corporation (SLLDC). The datasets included:

i). Rainfall records from multiple rain gauge stations distributed across the Colombo Metropolitan Region

ii). Water level time series at critical monitoring points along the canal networks

iii). Cross-sectional profiles of the urban canals, including geospatial coordinates and elevation details necessary for hydraulic modeling

The rainfall data and water level data were available at 5-minute time steps. These datasets formed the foundational input for model calibration, training, and validation, and were cross-verified against some historical rainfall records from the Department of Meteorology, Sri Lanka. Tables 2, 3, and Figure 6 show a summary of the data points under water level monitoring stations and rainfall gauges.

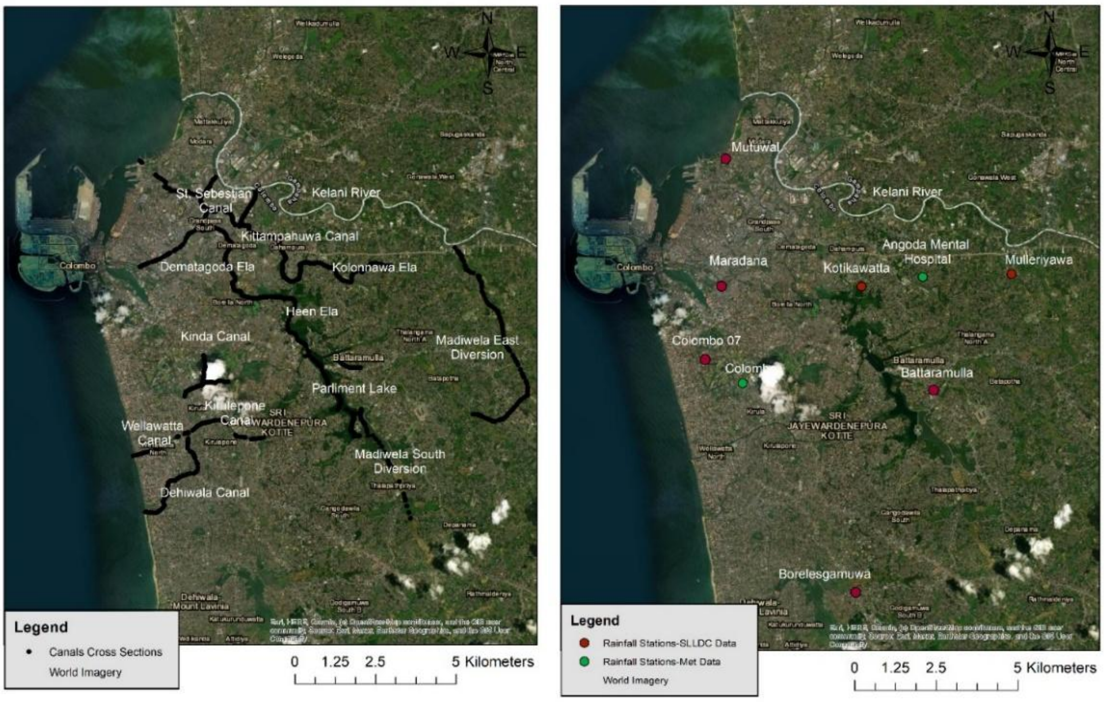


*Figure 6: Canal cross-section points along the canals and data available from rainfall stations*

*Table 2: Number of canal cross sections and water level monitoring points along the canals*

| Canal Name | Number of Cross-Section Points | Water Level Monitoring Locations along the Canal (From 2022 to 2025) |
|---|---|---|
| Dehiwala Canal | 70 Points | Dehiwala Canal Outfall |
| Kirillapone Canal | 46 Points | Near Lanka Hospital<br>Nawala Road Bridge |
| Wellawatta Canal | 32 Points | Wellawatta Canal Outfall |
| Madiwela East Diversion | 118 Points | Rajasinghe MW Bridge<br>Chandrika MW Bridge<br>Ambathale Downstream |
| Dematagoda Canal | 77 Points | Yakbedda Bridge |

| Canal Name | Number of Cross-Section Points | Water Level Monitoring Locations along the Canal (From 2022 to 2025) |
|---|---|---|
| Kollonnawa Canal | 81 Points | SLLDC Bridge<br>Wallampitiya Bridge |
| Main Drain | 49 Points | Ingurukade Junction |
| Mutuwal Tunnel | 5 Points | New Mutual Tunnel Outlet |
| Parliament Bridge | 6 Points | Parliament Bridge |
| Parliament lake | 73 Points | Diyasuru Uyana Gate |
| St Sebastian East | 68 Points | Orugodawatta |
| St Sebastian North | 39 Points | Nagalagama Street |
| Torrington Canal | 38 Points | Torington Canal<br>Kirimandala Mw Bridge |

*Table 3: Rainfall stations where data was collected by the Urban Water Management Center, SLLDC, and data available time domains*

| Rainfall Station | Duration of Data Availability (5-min Incremental Data Range) |
|---|---|
| Mutwal | 2020 - 2025 |
| Battaramulla | 2019 - 2025 |
| Kotikawaththa | 2019 - 2020 |
| Mulleriyawa | 2020 - 2025 (Missing Data -2022) |
| Borelesgamuwa | 2019 - 2025 |
| Maradana | 2021 - 2025 |
| Colombo 07 | 2019 - 2025 |

Based on these data for canal cross-sections, water level monitoring stations, and canal interconnectivity, three (3) canal systems were selected for modelling as:

i). Madiwela East Diversion

ii). Dehiwala-Wellawatta-Kirillapone Canal System

iii). Parliament Lake - Kiththampahuwa - Kinda - Dematagoda Canal System

The three canal systems are shown in Figure 7, and they were modelled in PINN and HEC-RAS, generating six (6) models.

Several factors should be satisfied with the available data to select a canal system that can be used for modelling. The availability of at least three water level monitoring stations along the canal, the availability of a satisfactory amount of canal cross-section data, and having stage hydrographs in the prescribed time domain are the criteria.

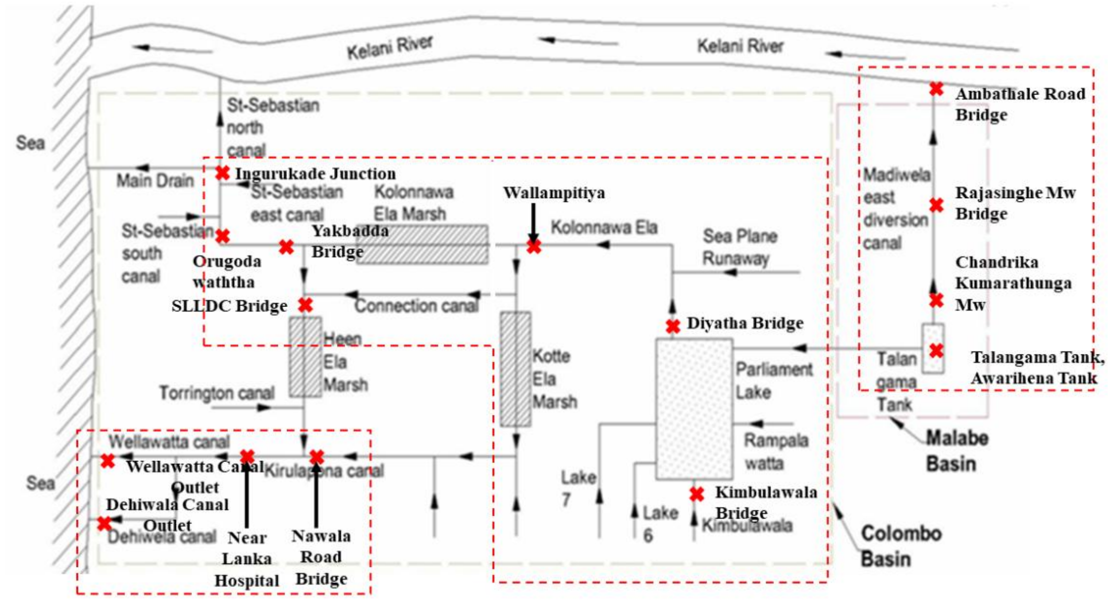


*Figure 7: A schematic diagram showing the selected canal systems covering the total canal network in the Colombo Metropolitan Area*

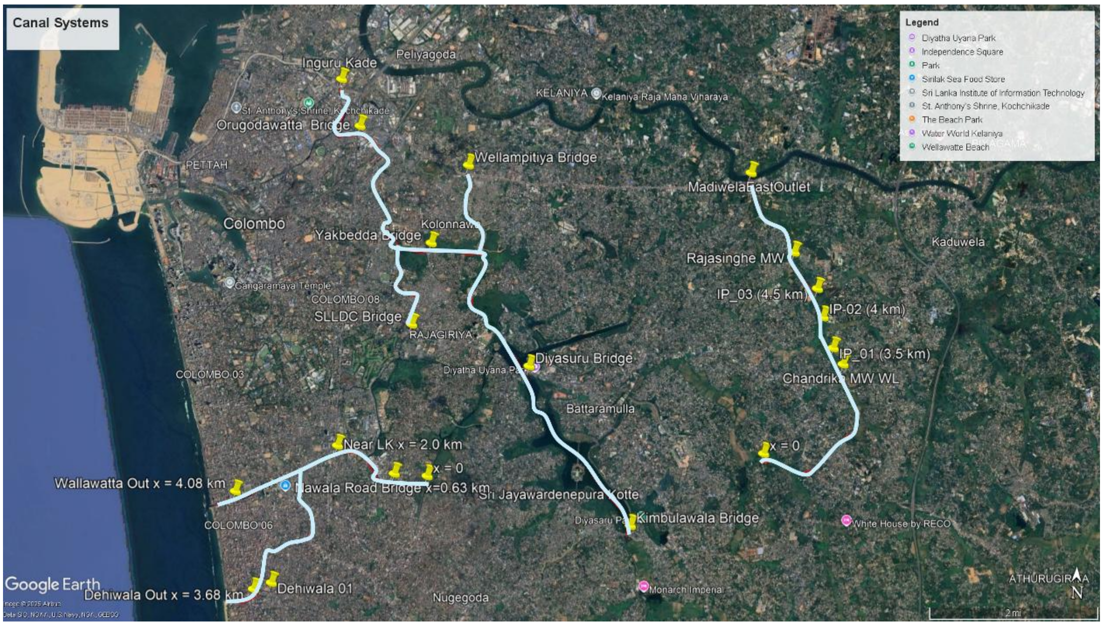


*Figure 8: A Google satellite image with marked canal paths in red used as three distinct canal systems*

## 3.5 Data Processing

This section outlines the procedures followed to preprocess the raw hydrometeorological data into meaningful inputs suitable for model development. The initial step involved identifying a representative flood event that occurred within the available observational data period. To facilitate this selection, time series plots of canal water levels were generated and visually analyzed to detect instances of elevated water stages as an indicator of flood conditions. Several high-water-level events were shortlisted based on their magnitude and temporal distribution across the monitoring stations. From these, a single flood event that was common to all three canal systems was selected to serve as the reference event for both PINN and HEC-RAS modelling. This approach ensured consistency across model domains and enabled a unified evaluation of flood dynamics within the study area.

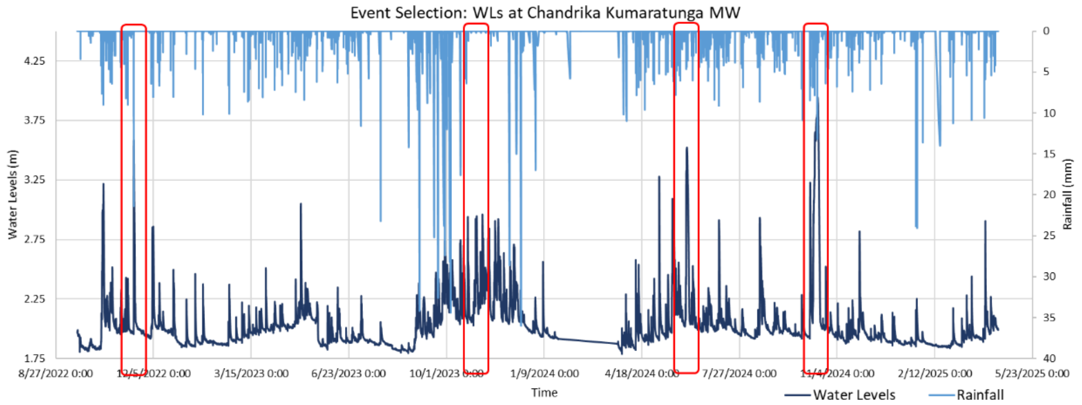


*Figure 9: Time series plot of water levels vs time and rainfall vs time at the Chandrika Kumarathunga MW water level monitoring location representing the Madiwela East Diversion (Canal System 01)*

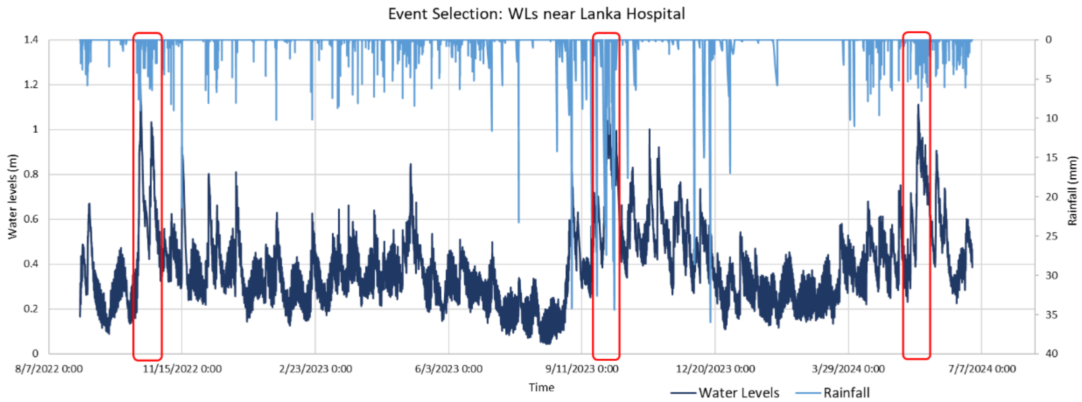


*Figure 10: Time series plot of water levels vs time and rainfall vs time near Lanka Hospital water level monitoring location representing the Dehiwala-Wellawatta-Kirillapone Canal System (Canal System 02)*

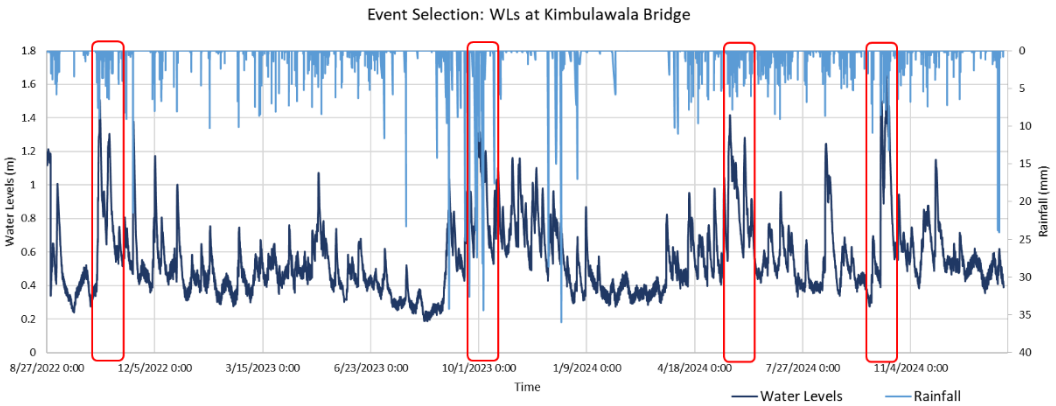


*Figure 11: Time series plot of water levels vs time and rainfall vs time at Kimbulawala Bridge monitoring location representing the Parliament Lake-Dematagoda canal system (Canal System 03)*

As in Figures 9, 10, and 11, the distinct water level peaks coincide with the intense rainfall events, supporting the identification of potential flood occurrences. The identified flood events are highlighted using red boxes for further evaluation. These selected events from observations were cross-verified against official flood occurrence reports and warning notifications issued by the Department of Meteorology, Sri Lanka, and the Disaster Management Centre (DMC). Based on this corroboration, the following dates were confirmed as actual flood events impacting the selected canal system.

i). 13th to 17th November 2022

ii). 5th to 9th November 2023

iii). Mid May to 5th June 2024

iv). 12th to 16th Octomber 2024

Among these, the flood event of 13th to 17th November 2022 was selected as the representative flood scenario for model calibration and validation, as it was evident across all three systems and occurred within a period of consistent monitoring data. Even though the November 2023 flood event and the June 2024 flood event were also prominent in the graphs for selected water level monitoring stations, the November 2022 flood event showed higher flood peaks, thus, the particular event was selected. The extreme weather reports mention that this particular rainfall event caused huge damage not only in Colombo, but also in districts like Kandy, Nuwara-Eliya, Rathnapura, and Gampaha (United Nations Office for the Coordination of Humanitarian Affairs (OCHA), 2023).

Following the identification of a representative flood event, the next step is to check about missing data percentages across the selected monitoring stations. Specifically, the time series datasets of water levels at various locations were examined to identify missing data segments and quantify the percentage of data gaps. These missing data statistics are summarized in Table 4. A preliminary screening revealed that most data gaps were short, randomly distributed, and limited to a small number of missing points. In many cases, the total number of missing observations originated from several short-duration interruptions, rather than systematic data losses for a long period of time. Such characteristics suggested that the missing sequences were manageable under an interpolation-based missing data patching method. Accordingly, a linear interpolation technique was adopted for gap filling. This method estimates the missing values by drawing a straight line between the last available observation before the gap and the first valid observation after the gap, thereby ensuring a smooth and physically reasonable transition (Bikše et al., 2023; Niedzielski & Halicki, 2023). This data patching procedure ensured the continuity of time series inputs, which is crucial for the accurate training and validation of the PINN and HEC-RAS models.

*Table 4: Missing data percentages for water levels on important locations along the canals*

| Canal Name | Canal System | Time Duration | Missing Data Percentage |
|---|---|---|---|
| Chandrika Kumaratunga MW | Canal System 01 | 2022/10/11 to 2022/10/15 | 14/1440 = 0.97% |
| Rajasinghe MW | | | 21/1440 = 1.45% |
| Ambathale Downstream | | | 10/1440 = 0.69% |
| Dehiwala Outlet | Canal System 02 | 2022/10/11 to 2022/10/17 | 14/1729 = 0.89% |
| Wallewatta Oulet | | | 20/1729 = 1.15% |
| Near Road Bridge (Kirullepone Canal) | | | 20/1729 = 1.15% |
| Lanka Hospital (Kirullepone Canal) | | | 21/1729 = 1.21 |
| Kimbulawala Bridge | Canal System 03 | 2022/10/11 to 2022/10/20 | 10/2592 = 0.39% |
| Diyatha Bridge | | | 34/2592 = 1.31% |
| Ingurukade Junction | | | 36/2592 = 1.31% |
| Orugodawatta Bridge | | | 26/2596 = 1.00% |
| Yakbedda | | | 30/2592 = 1.16% |

From Table 4, it is evident that the total missing data percentages were less than 1.5%, which can be applied with linear interpolation theories, due to their short random behavior. Forcing on rainfall data, there were zero (0) missing stations within the prescribed time duration, and to represent each canal system, a closer rainfall gauging station was used as in Table 5, based on a Theisen polygon approach as in Figure 12.

*Table 5: Used rainfall gauging station for each canal system*

| Canal System | RF station |
|---|---|
| Madiwela East Diversion | Battaramulla |
| Dehiwala-Wellawatta-Kirillapone Canal System | Colombo 07 |
| Parliament Lake - Kiththampahuwa - Kinda - Dematagoda Canal System | Battaramulla |

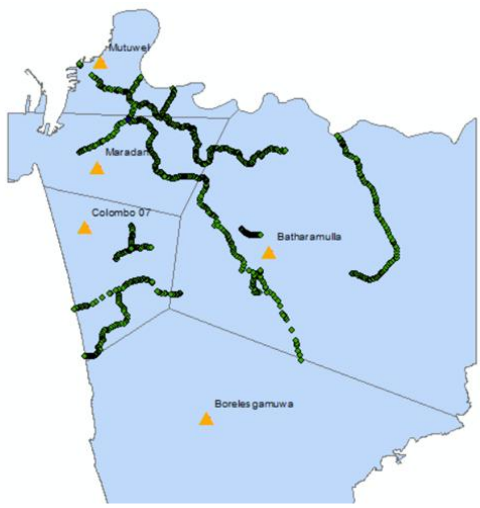


*Figure 12: Thiessen polygons for rainfall stations*

From the gap-filled data, the flood event was identified at several water level monitoring locations along the canal systems as follows in Figures 13, 14, and 15.

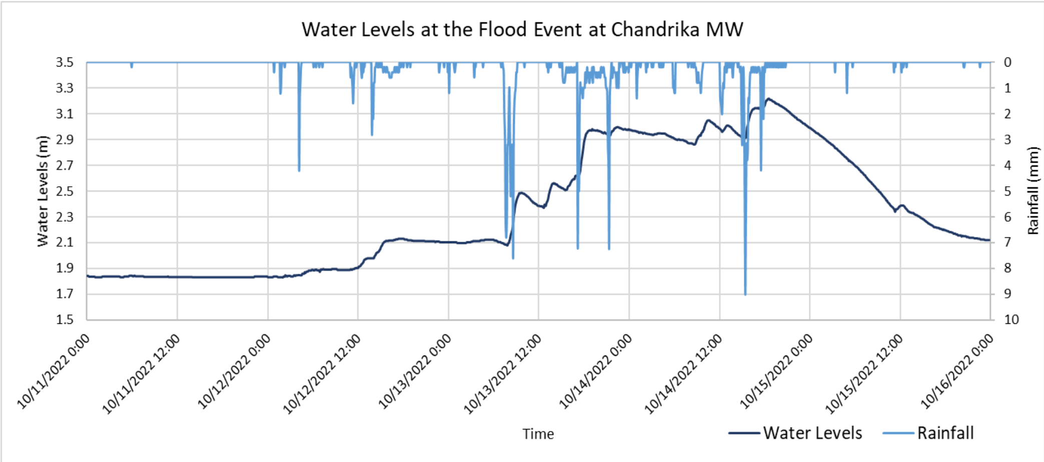


*Figure 13: Selected flood event with elevated water levels at Chandrika Kumarathunga MW, representing Madiwela East Diversion (Canal System 01)*

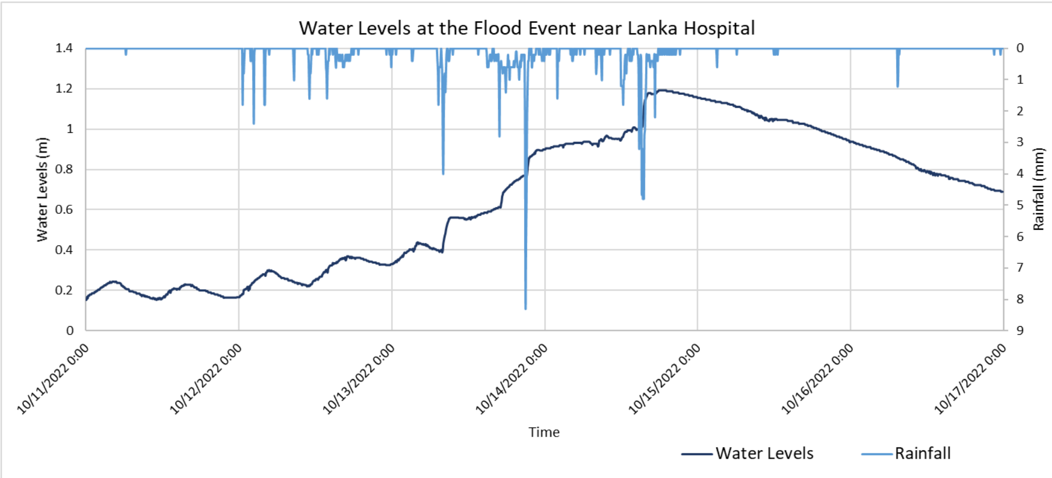


*Figure 14: Selected flood event with elevated water levels near Lanka Hospital, representing Dehiwala-Wellawatta-Kirillapone Canal System (Canal System 02)*

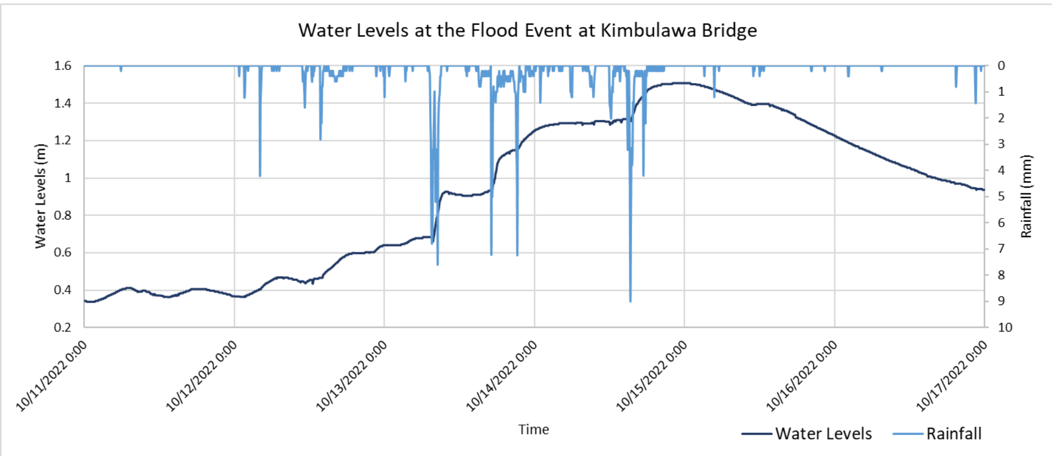


*Figure 15: Selected flood event with elevated water levels at Kimbulawa Bridge, representing Parliament Lake - Kiththampahuwa - Kinda - Dematagoda Canal System (Canal System 03)*

The time series plots illustrating the relationship between rainfall intensity and canal water levels clearly indicate that the flood peak is occurring on 15th November 2022. Accordingly, the rise in water levels associated with this peak will be reproduced by both modeling approaches, the PINN and HEC-RAS model, to evaluate their respective performances. The simulated outputs will subsequently be compared against the gap-filled observed water level records, as described in Section 3.3, to assess the accuracy and reliability of the predictions. A detailed interpretation and comparative analysis of the modeled results will be presented in the following Results and Discussion chapter.

## 3.6 Summary

This chapter outlines the comprehensive methodology adopted to simulate and compare flood propagation in selected canal systems of the Colombo Metropolitan Area using two distinct modeling approaches: the traditional 1D hydrodynamic model HEC-RAS and the data-efficient deep learning model PINN. The methodology involves selecting representative canal systems, collecting and preprocessing hydrometeorological data, and developing both PINN and HEC-RAS models to evaluate their performance in predicting spatiotemporal flood behavior during an observed flood event.

In the study, three canal systems were selected based on the availability of water level monitoring stations, cross-sectional canal data, and proximity to reliable rainfall gauge stations. The datasets included water level time series, 5-minute rainfall records, and canal geometry, which were preprocessed to patch missing values through linear interpolation. A representative flood event occurring between 13th and 17th November 2022 was selected for calibration due to its intensity and consistent data availability across the selected canal systems.

The PINN model was developed using the kinematic wave formulation, derived from the simplified Saint-Venant equations, and incorporated as a residual loss function within the neural network's training process. A dual-head PINN architecture was employed to simultaneously predict water levels at two monitoring stations while enforcing physical laws across space and time through collocation points. Model training was carried out using the Adam optimizer, with composite loss terms representing data loss, initial and boundary conditions, and physics residuals. Hyperparameter tuning was performed using both manual and Bayesian optimization methods to ensure convergence and generalization. Additionally, HEC-RAS 1D models were developed for each canal system using cross-section data and stage hydrographs. Boundary conditions were defined using stage hydrographs. The models were calibrated and validated using the same flood event, with roughness coefficients and boundary conditions fine-tuned to match observed water levels.

Both models, PINN and HEC-RAS, were evaluated based on their ability to simulate peak flood levels and spatial water surface variation along canal reaches. Their outputs were compared using NSE and RMSE, along with visual comparisons including time series and spatial plots.

# CHAPTER 4

# RESULTS AND DISCUSSION

## 4.1 Chapter Introduction

This section presents the outcomes of the developed PINN and HEC-RAS models. The results of hyperparameter tuning conducted to finalize the PINN architecture, validation and comparison between PINN-predicted water levels and observations, validation of HEC-RAS simulated outputs against observed water levels, and direct comparison between the water levels generated by the PINN and HEC-RAS models are presented. These comparative analyses aim to evaluate the ability of the PINN approach in modeling flood peaks and performing 1D flood routing, thereby assessing its suitability as an alternative approach to conventional hydrodynamic modeling tools.

## 4.3 Hyperparameter Optimization

In this section, the selection of suitable values for different hyperparameters, including the number of layers, the number of neurons, the learning rate, the activation function, and loss weights, as mentioned under Section 3.1.2. are presented. The NSE and RMSE value variations are considered as the selection criterion for deciding parameter values giving optimum results in the PINN model. This task was conducted for all three canal systems that were selected for the analysis.

Within the task, the number of hidden layers was varied between 2 and 6, while the number of neurons per layer was tested across 64, 128, 256, and 512 units to assess the impact of network depth and capacity. In terms of activation functions, five commonly used types, ReLU, tanh, sigmoid, Swish, and GELU(Szandała, 2021), were evaluated. Among these, Swish consistently yielded superior performance in capturing nonlinear hydrodynamic behavior and was therefore selected as the preferred activation function. The learning rate was selected based on values commonly adopted in recent neural network literature. Accordingly, values were tested in the vicinity of 0.0001 to ensure clear and stable convergence (Jepkoech et al., 2021; Zhang et al., 2023), and 0.00085 was selected as the learning rate, with a higher NSE value and a lower RMSE value. Although the model did not explicitly use learning rate decay or adaptive learning rate schedulers, the convergence was further guided by an early stopping mechanism with a patience value of 600 epochs and a minimum delta threshold of 0.00001. This ensures that, during training, the total loss must decrease by at least 0.00001 compared to the best recorded loss to be considered a meaningful improvement, otherwise, such minor changes are treated as insignificant, leading to early stopping triggering. Additionally, the loss weighting coefficients (e.g., for data loss, physics loss, initial and boundary conditions) were varied around a baseline of 0.5, with adjustments made in ±0.025 increments on either side to balance the contribution of each loss component during training. And 0.45 was selected as the best weight for loss weights.

### 4.3.1 Hyperparameter Tuning for Madiwela East Diversion (Canal System 01)

The following graphs, in Figures 16, 17, 18, 19, 20, and 21, show a visual representation of NSE and RMSE variation with the varying parameter inputs.

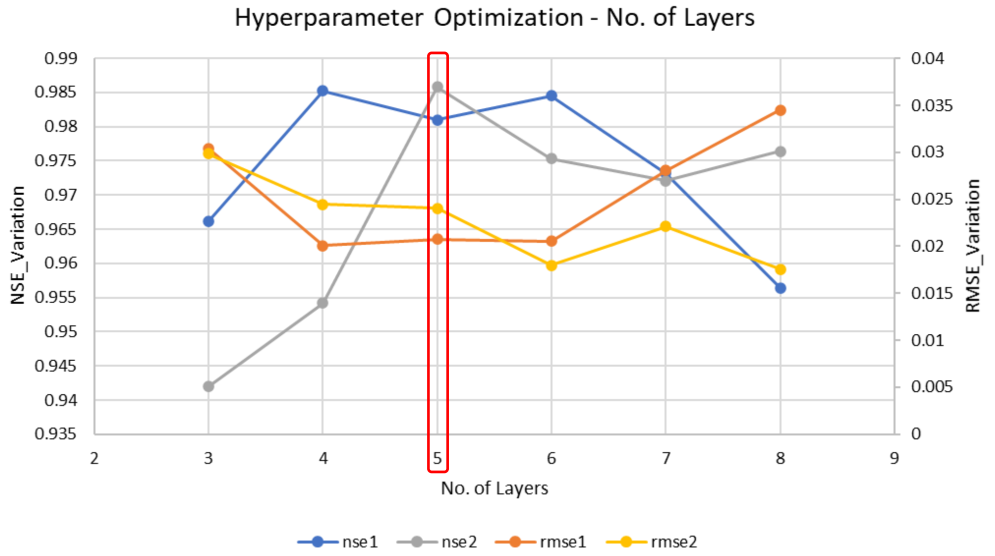


*Figure 16: Tests conducted to identify the most preferable layer count in the PINN code*

*(nse1- variation of NSE value for station 01, nse2- variation of NSE value for station 02, rmse1- variation of RMSE value for station 01, rmse2- variation of RMSE value for station 02)*

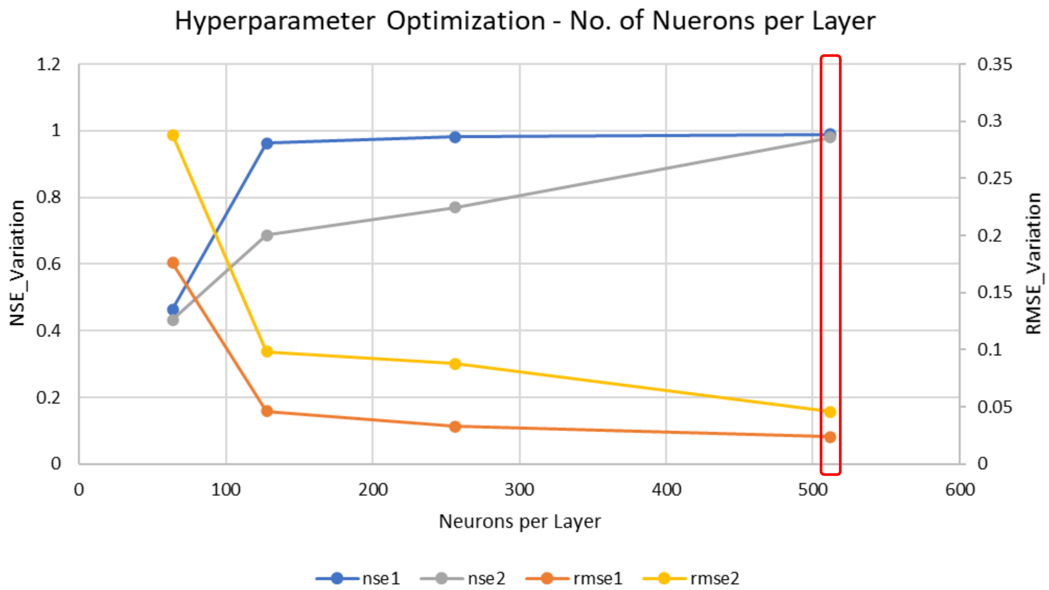


*Figure 17: Tests conducted to identify the most preferable neurons per layer PINN code*

*(nse1- variation of NSE value for station 01, nse2- variation of NSE value for station 02, rmse1- variation of RMSE value for station 01, rmse2- variation of RMSE value for station 02)*

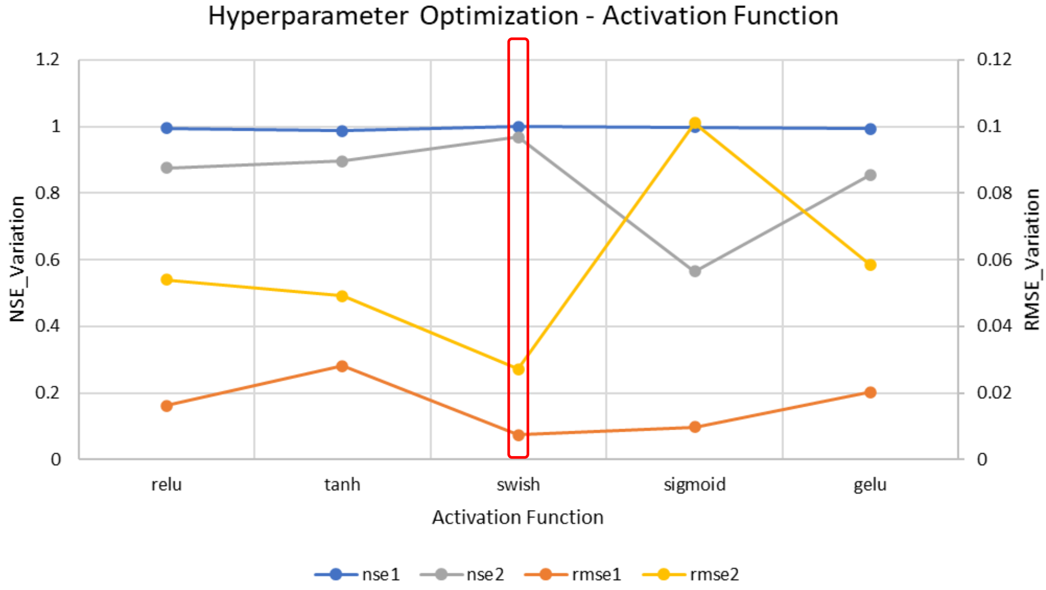


*Figure 18: Tests conducted to identify the most preferable activation function for the PINN code*

*(nse1- variation of NSE value for station 01, nse2- variation of NSE value for station 02, rmse1- variation of RMSE value for station 01, rmse2- variation of RMSE value for station 02)*

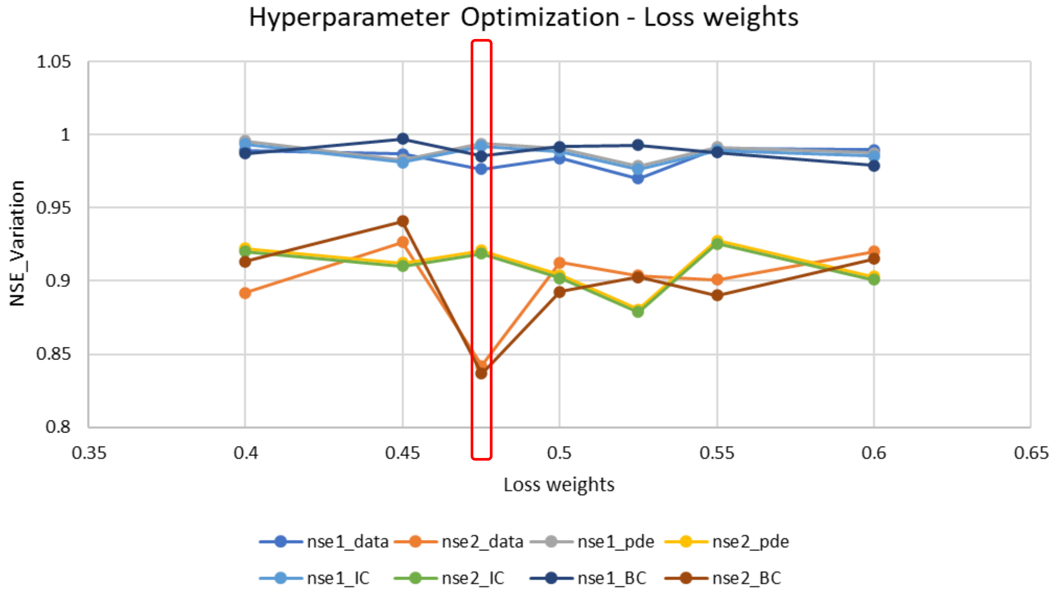


*Figure 19: Tests conducted to identify the most preferable loss weights for the PINN code*

*(nse[i]_data- variation of NSE value for station [i] with variation of data loss weight, nse[i]_pde- variation of NSE value for station [i] with variation of PDE loss weight, nse[i]_IC- variation of NSE value for station [i] with variation of initial condition loss weight, nse[i]_BC-variation of NSE value for station [i] with variation of boundary condition loss weight, [i]={1,2})*

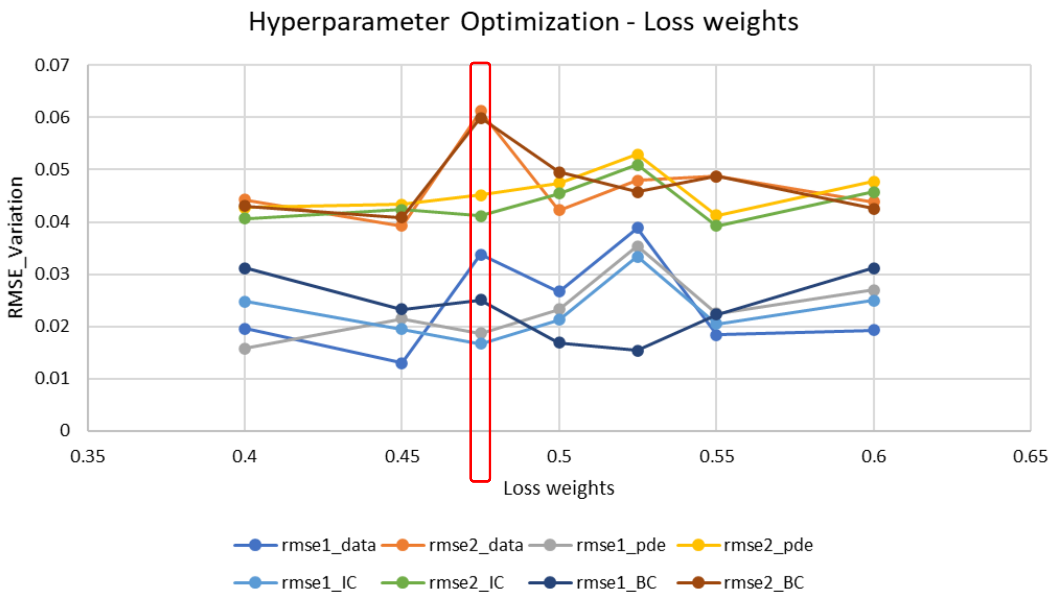


*Figure 20: Tests conducted to identify the most preferable loss weights for the PINN code*

*(rmse[i]_data- variation of RMSE value for station [i] with variation of data loss weight, rmse[i]_pde- variation of RMSE value for station [i] with variation of PDE loss weight, rmse[i]_IC- variation of RMSE value for station [i] with variation of initial condition loss weight, rmse[i]_BC- variation of RMSE value for station [i] with variation of boundary condition loss weight, [i]={1,2})*

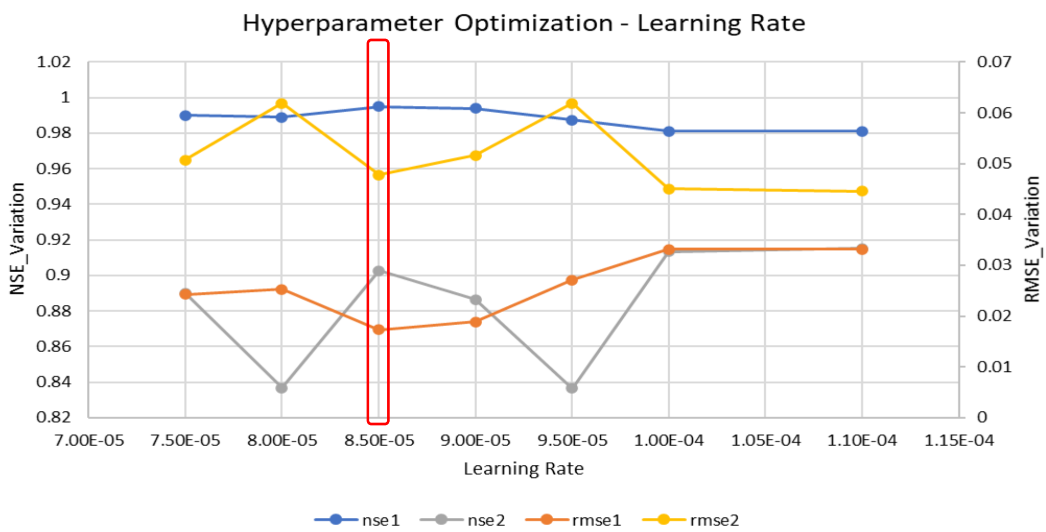


*Figure 21: Tests conducted to identify the most preferable activation function for the PINN code*

*(nse1- variation of NSE value for station 01, nse2- variation of NSE value for station 02, rmse1- variation of RMSE value for station 01, rmse2- variation of RMSE value for station 02)*

The parameters giving a higher NSE value and a lower RMSE value are selected as the optimum parameters. A summary of selected parameters for the PINN model developed for Madiwela East Diversion is as follows:

i). Number of layers = 5 layers

ii). Number of Neurons per layer = 512 neurons

iii). Activation function = Swish

iv). Learning rate = 0.00085

v). Loss weights

   a. Data loss = 0.45

   b. PDE loss = 0.45

   c. Initial condition loss = 0.45

   d. Boundary condition loss = 0.45

### 4.3.2 Hyperparameter Tuning for Dehiwala-Wellawatta-Kirillapone Canal System (Canal System 02)

The following graphs, in Figures 22, 23, 24, 25, 26, and 27, show a visual representation of NSE and RMSE variation with the varying parameter inputs.

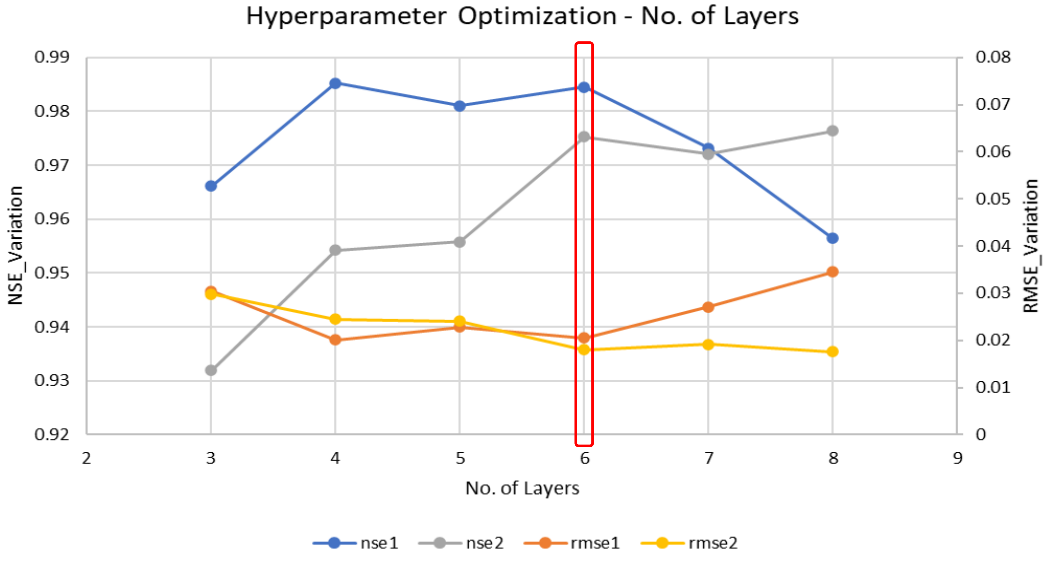


*Figure 22: Tests conducted to identify the most preferable layer count in the PINN code*

*(nse1- variation of NSE value for station 01, nse2- variation of NSE value for station 02, rmse1- variation of RMSE value for station 01, rmse2- variation of RMSE value for station 02)*

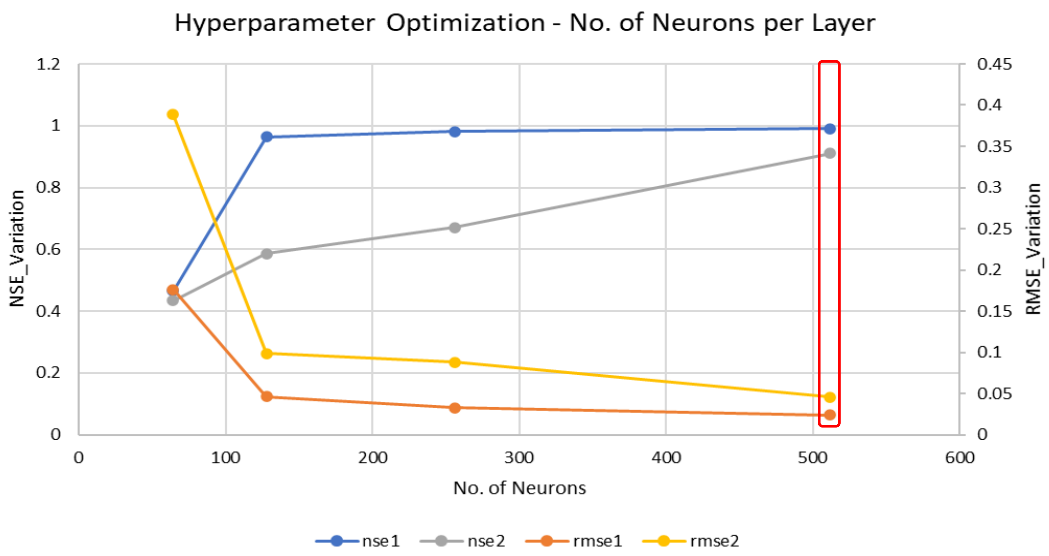


*Figure 23:Tests conducted to identify the most preferable neurons per layer PINN code*

*(nse1- variation of NSE value for station 01, nse2- variation of NSE value for station 02, rmse1- variation of RMSE value for station 01, rmse2- variation of RMSE value for station 02)*

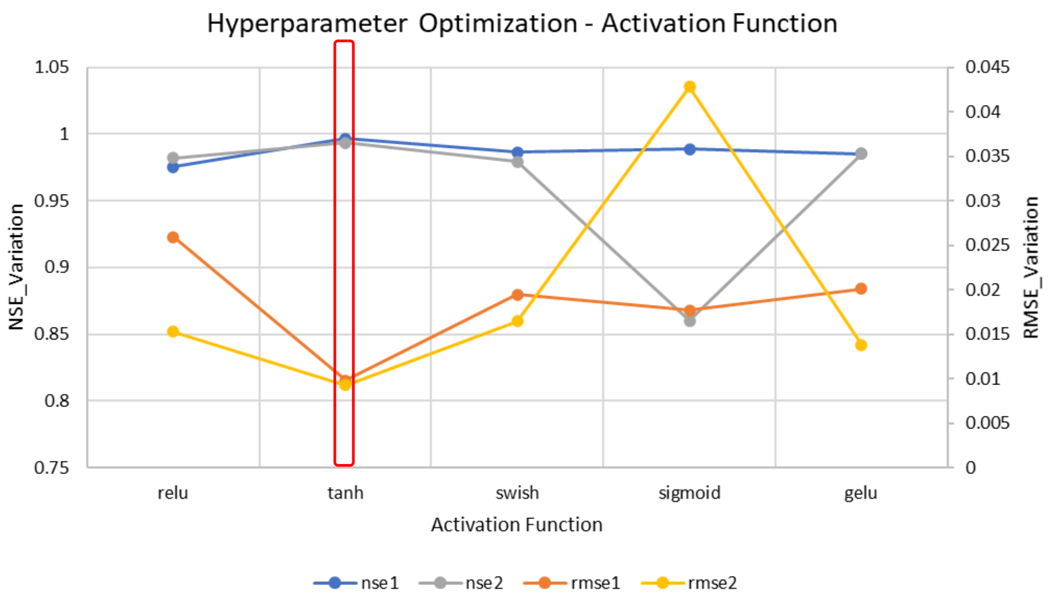


*Figure 24: Tests conducted to identify the most preferable activation function for the PINN code*

*(nse1- variation of NSE value for station 01, nse2- variation of NSE value for station 02, rmse1- variation of RMSE value for station 01, rmse2- variation of RMSE value for station 02)*

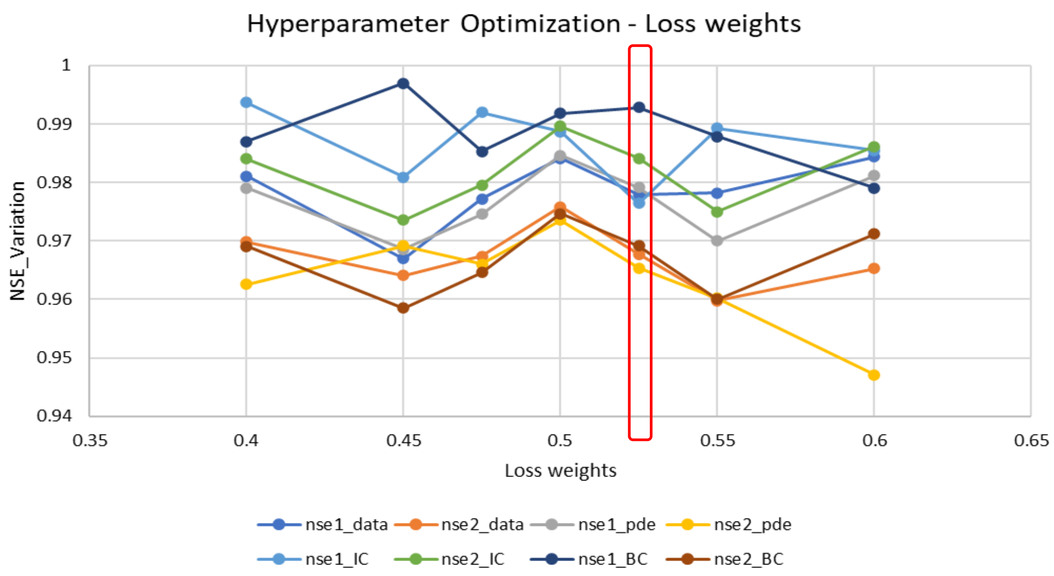


*Figure 25: Tests conducted to identify the most preferable loss weights for the PINN code*

*(nse[i]_data- variation of NSE value for station [i] with variation of data loss weight, nse[i]_pde- variation of NSE value for station [i] with variation of PDE loss weight, nse[i]_IC- variation of NSE value for station [i] with variation of initial condition loss weight, nse[i]_BC-variation of NSE value for station [i] with variation of boundary condition loss weight, [i]={1,2})*

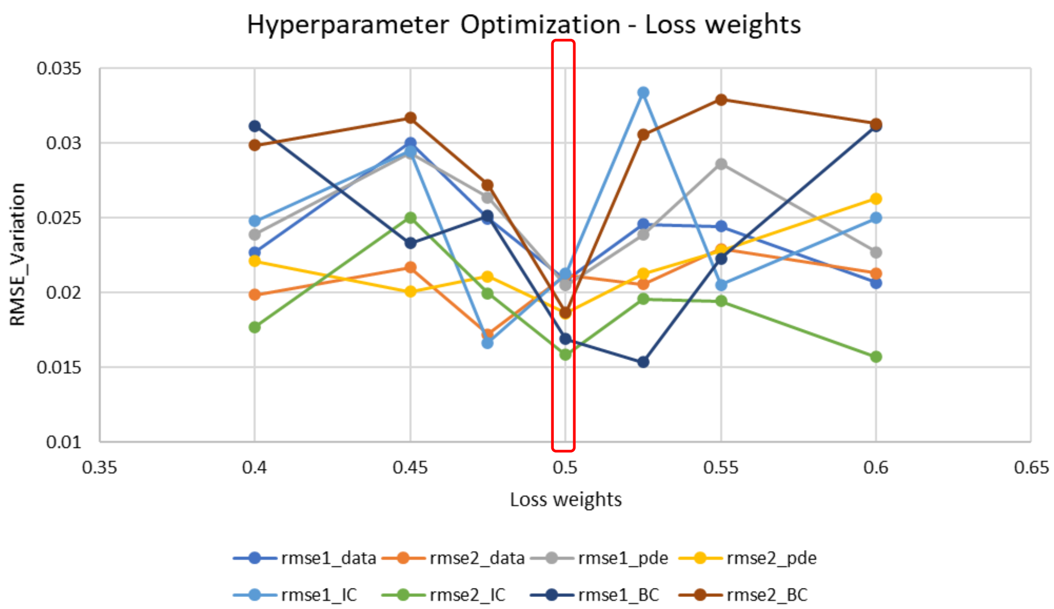


*Figure 26: Tests conducted to identify the most preferable loss weights for the PINN code*

*(rmse[i]_data- variation of RMSE value for station [i] with variation of data loss weight, rmse[i]_pde- variation of RMSE value for station [i] with variation of PDE loss weight, rmse[i]_IC- variation of RMSE value for station [i] with variation of initial condition loss weight, rmse[i]_BC- variation of RMSE value for station [i] with variation of boundary condition loss weight, [i]={1,2})*

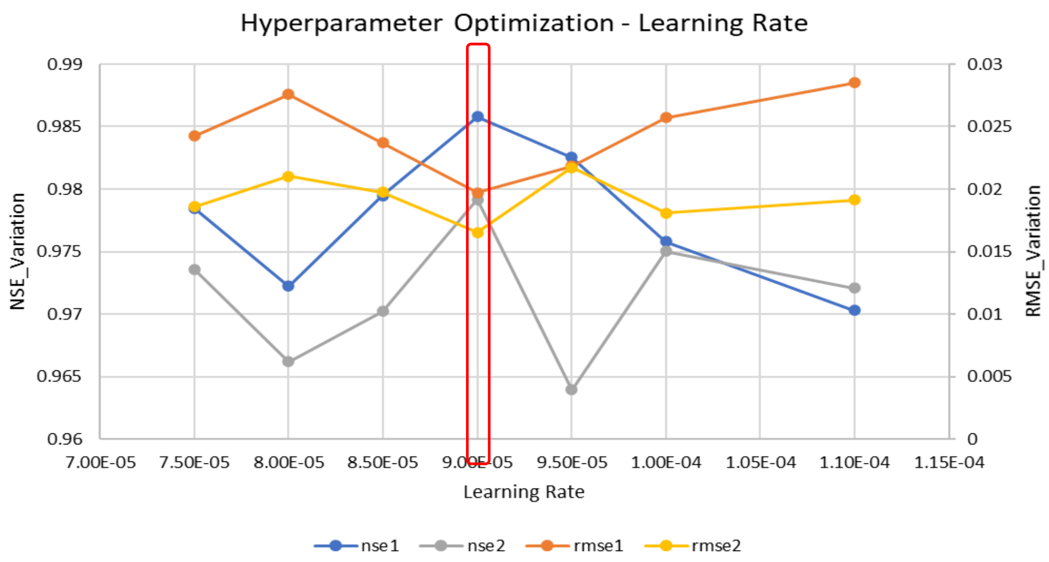


*Figure 27:Tests conducted to identify the most preferable activation function for the PINN code*

*(nse1- variation of NSE value for station 01, nse2- variation of NSE value for station 02, rmse1- variation of RMSE value for station 01, rmse2- variation of RMSE value for station 02)*

The parameters giving a higher NSE value and a lower RMSE value are selected as the optimum parameters. A summary of selected parameters for the PINN model developed for Madiwela East Diversion is as follows:

i). Number of layers = 6 layers

ii). Number of Neurons per layer = 512 neurons

iii). Activation function = Tanh

iv). Learning rate = 0.00009

v). Loss weights

a. Data loss = 0.5

b. PDE loss = 0.5

c. Initial condition loss = 0.5

d. Boundary condition loss = 0.5

### 4.3.2 Hyperparameter Tuning for Parliament Lake-Kiththampahuwa-Kinda-Dematagoda Canal System (Canal System 03)

The following graphs, in Figures 28, 29, 30, 31, 32, and 33, show a visual representation of NSE and RMSE variation with the varying parameter inputs.

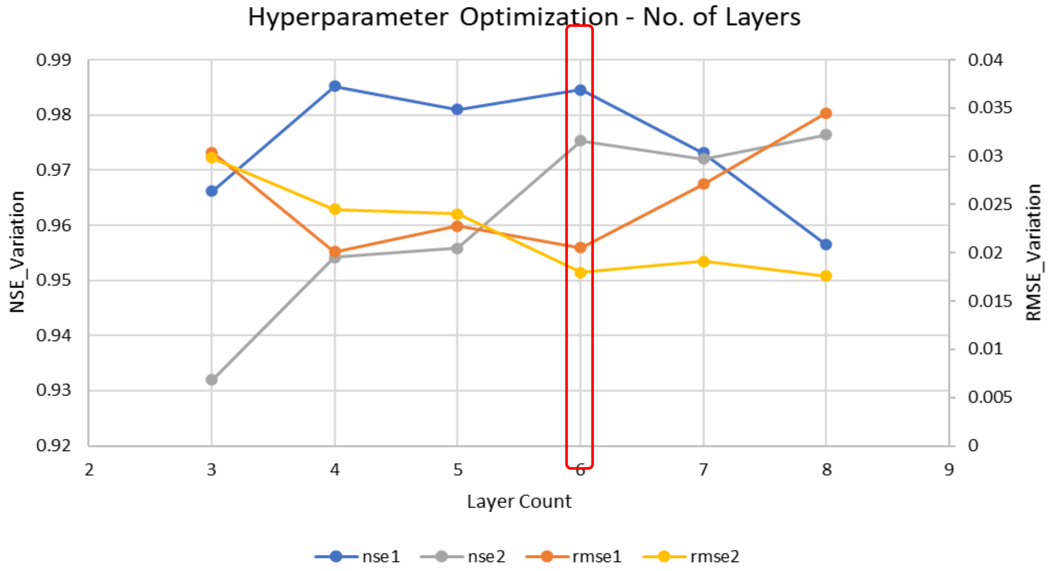


*Figure 28: Tests conducted to identify the most preferable layer count in the PINN code*

*(nse1- variation of NSE value for station 01, nse2- variation of NSE value for station 02, rmse1- variation of RMSE value for station 01, rmse2- variation of RMSE value for station 02)*

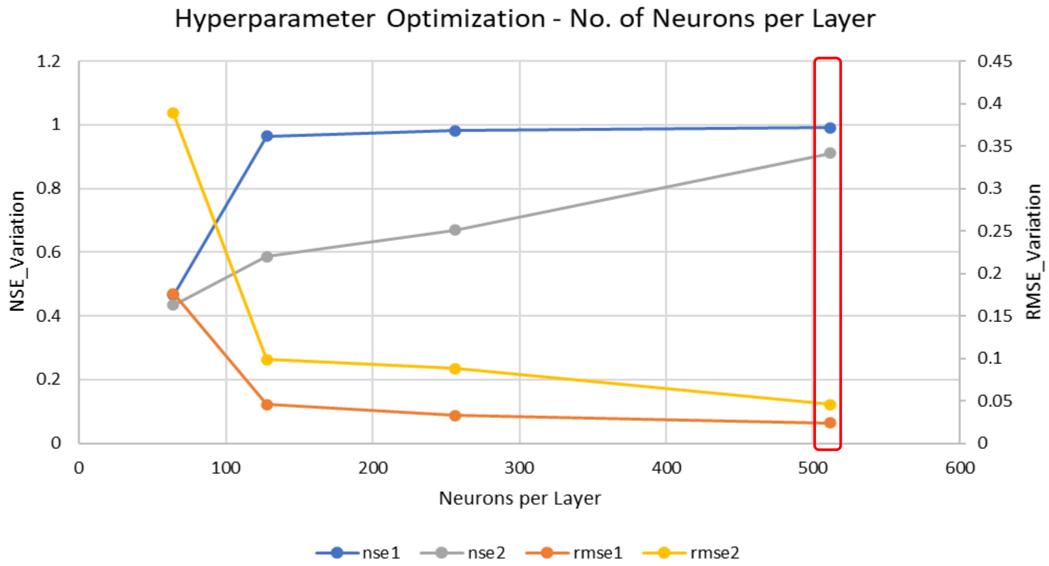


*Figure 29: Tests conducted to identify the most preferable neurons per layer PINN code*

*(nse1- variation of NSE value for station 01, nse2- variation of NSE value for station 02, rmse1- variation of RMSE value for station 01, rmse2- variation of RMSE value for station 02)*

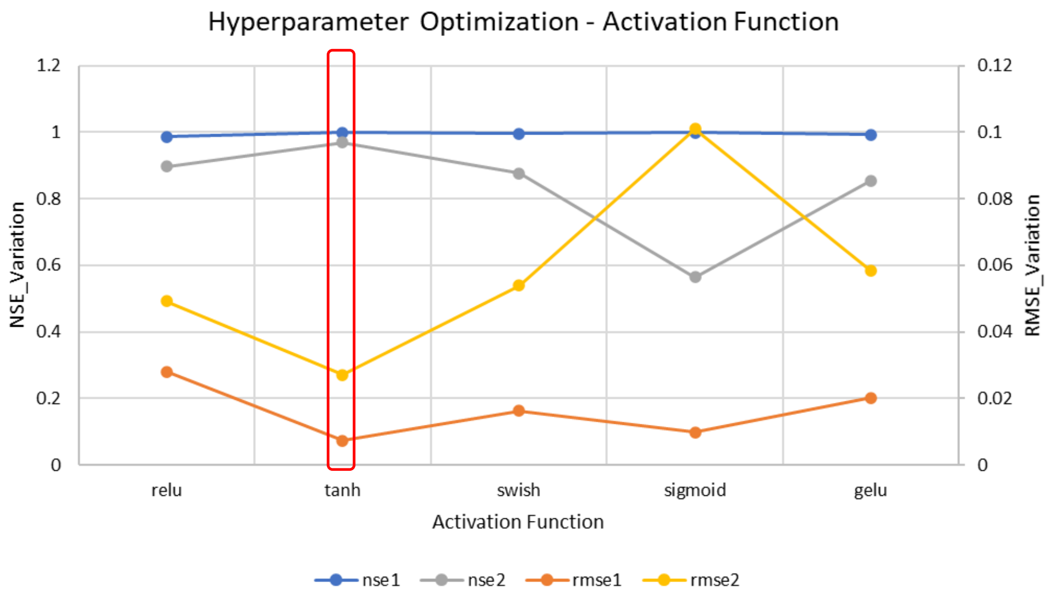


*Figure 30:Tests conducted to identify the most preferable activation function for the PINN code*

*(nse1- variation of NSE value for station 01, nse2- variation of NSE value for station 02, rmse1- variation of RMSE value for station 01, rmse2- variation of RMSE value for station 02)*

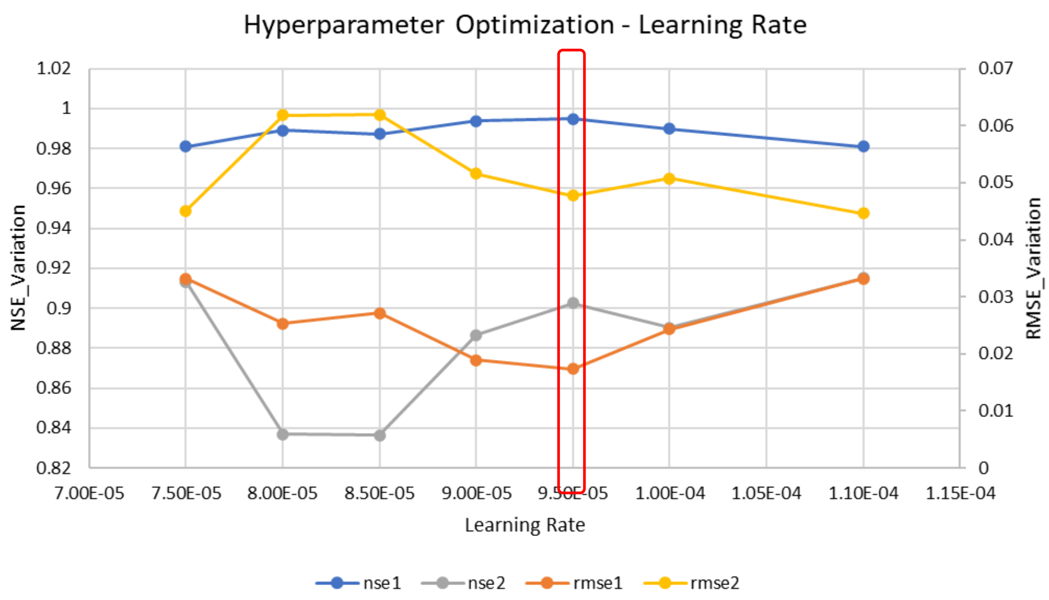


*Figure 31:Tests conducted to identify the most preferable activation function for the PINN code*

*(nse1- variation of NSE value for station 01, nse2- variation of NSE value for station 02, rmse1- variation of RMSE value for station 01, rmse2- variation of RMSE value for station 02)*

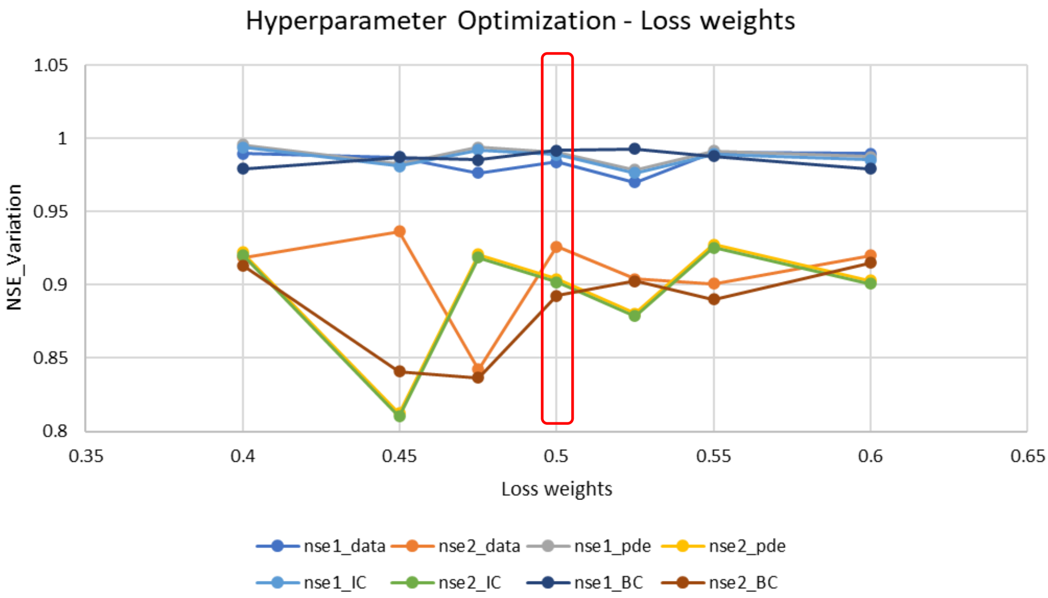


*Figure 32:Tests conducted to identify the most preferable loss weights for the PINN code*

*(nse[i]_data- variation of NSE value for station [i] with variation of data loss weight, nse[i]_pde- variation of NSE value for station [i] with variation of PDE loss weight, nse[i]_IC- variation of NSE value for station [i] with variation of initial condition loss weight, nse[i]_BC-variation of NSE value for station [i] with variation of boundary condition loss weight, [i]={1,2})*

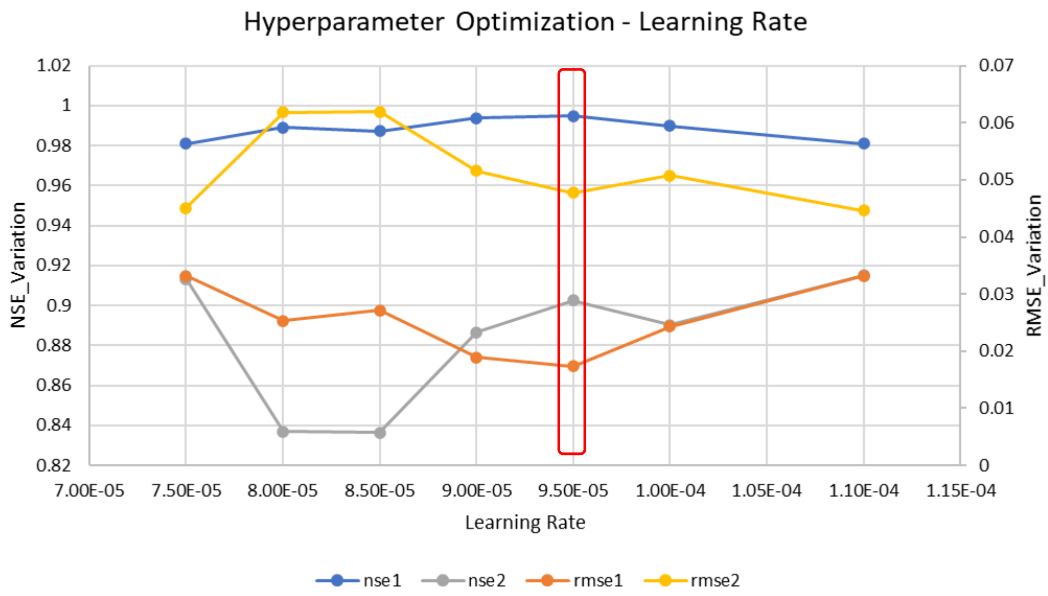


*Figure 33:Tests conducted to identify the most preferable loss weights for the PINN code*

*(rmse[i]_data- variation of RMSE value for station [i] with variation of data loss weight, rmse[i]_pde- variation of RMSE value for station [i] with variation of PDE loss weight, rmse[i]_IC- variation of RMSE value for station [i] with variation of initial condition loss weight, rmse[i]_BC- variation of RMSE value for station [i] with variation of boundary condition loss weight, [i]={1,2})*

The parameters giving a higher NSE value and a lower RMSE value are selected as the optimum parameters. A summary of selected parameters for the PINN model developed for the Madiwela East Diversion is as follows:

i). Number of layers = 6 layers

ii). Number of Neurons per layer = 512 neurons

iii). Activation function = Tanh

iv). Learning rate = 0.000095

v). Loss weights

   a. Data loss = 0.5

   b. PDE loss = 0.5

   c. Initial condition loss = 0.5

   d. Boundary condition loss = 0.5

Based on the tuned hyperparameters, the PINN codes for three canal systems were developed. The next section explains the results obtained by the PINN codes and the HEC-RAS models.

## 4.4 Model Outputs

The water level stations were categorized under input data and validation points for PINN and HEC-RAS models, as in Figure 34.

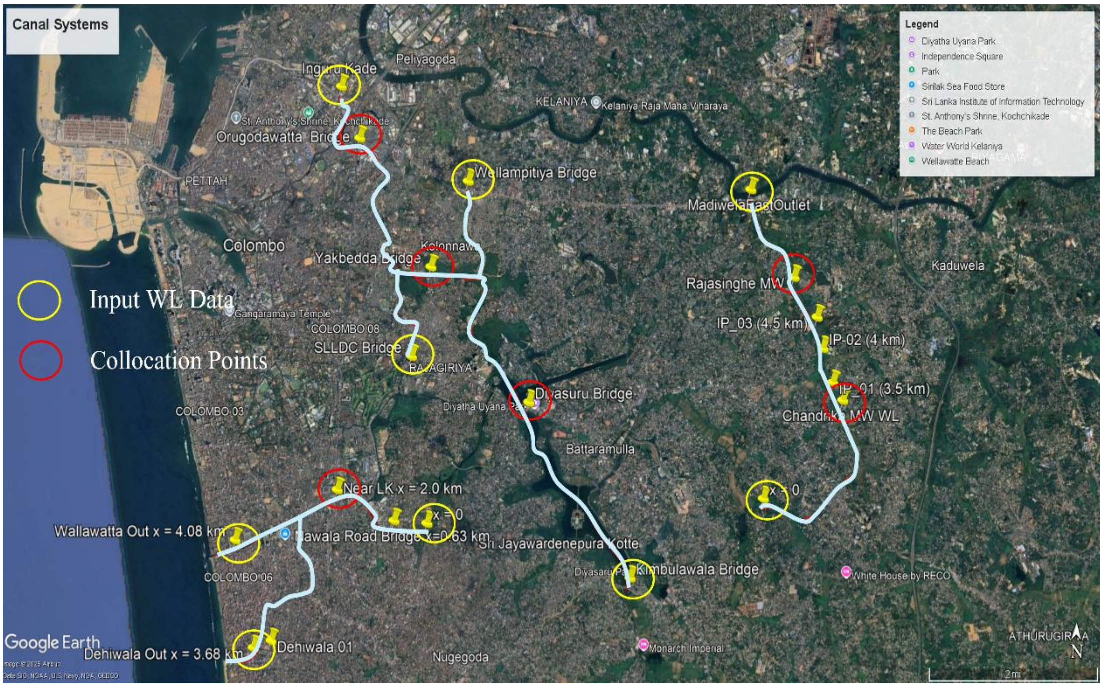


*Figure 34: Input water level station and collocation points used in spatial validation and intermediate points in canal networks*

### 4.4.1 Madiwela East Diversion

The Madiwela East Diversion (Canal System 01) is a critical drainage canal located within the Colombo Metropolitan Area, Sri Lanka, with a total length of approximately 7.50 km (Figure 35). For the analysis and model validation, two water level (WL) monitoring stations were considered along this canal reach, namely the Chandrika Kumarathunga Mw Station, Rajasinghe MW, and Ambathale Downstream Station, located at 3.32 km, at 5.60 km, and at 7.50 km respectively, from the canal origin (x = 0 m). The Baththaramulla rainfall station was selected as the representative precipitation input source for this canal system (Table 5). The modelled flood event corresponds to the period between October 11$^{th}$ and 16$^{th}$, 2022, which captured a significant rainfall-induced water level rise across the canal. In addition to the two gauge locations, several interpolated water level prediction points were also analyzed along the canal at x = 3,500 m, 4,000 m, and 4,500 m, enabling detailed spatiotemporal evaluation of the simulated hydrodynamics within the PINN and HEC-RAS models.

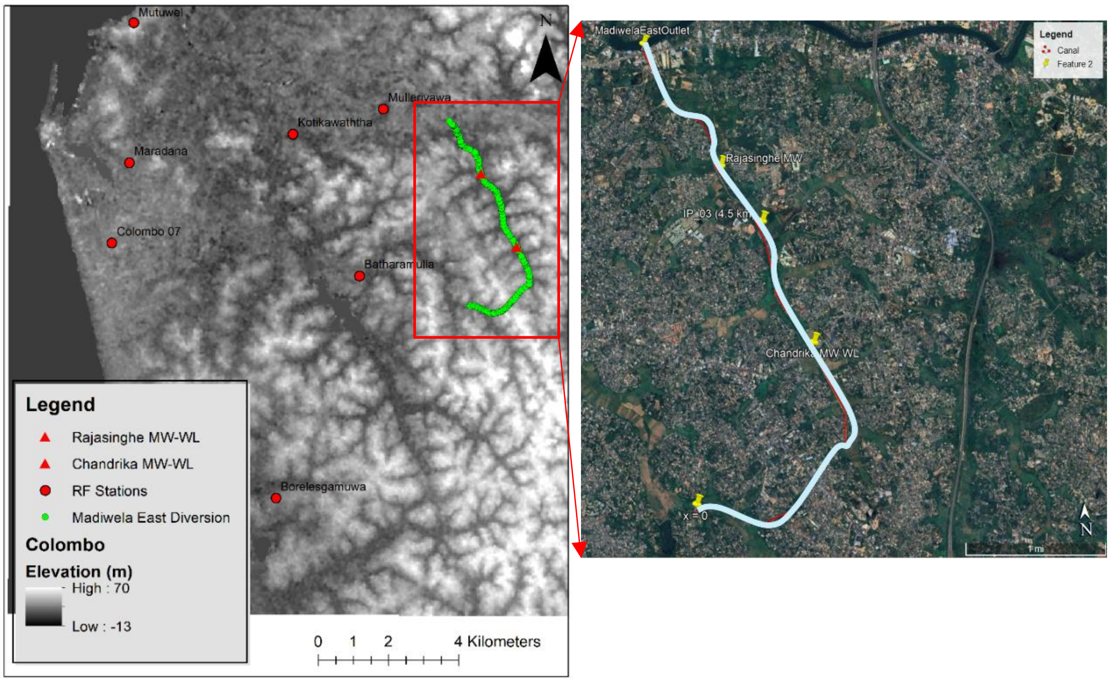


*Figure 35: Madiwela East Diversion and x=0, x=L, and collocation points including three water level monitoring locations, Chandrika Kumarathunga MW, Rajasinghe MW, and Ambathale Downstream*

#### 4.4.1.1 PINN Approach

Within this section, the results from running the PINN code, developed as in Section 3.3. with optimized hyperparameters (Section 4.3.1.) are presented. As the input data, rainfall, canal cross sections, distance to cross sections along the canal (x), stage hydrographs, and time step were sent to the code. The model was trained for stage hydrographs at Chandrika MW and Ambathale Downstream, considering them as Station 01 and Station 02, as in Figure 36. And based on their agreement rates with inputted observation data, the NSE and RMSE values were calculated (Table 6).

Further, to avoid over-fitting, the reduction of the PDE loss function and the total loss function was also checked, as in Figure 37.

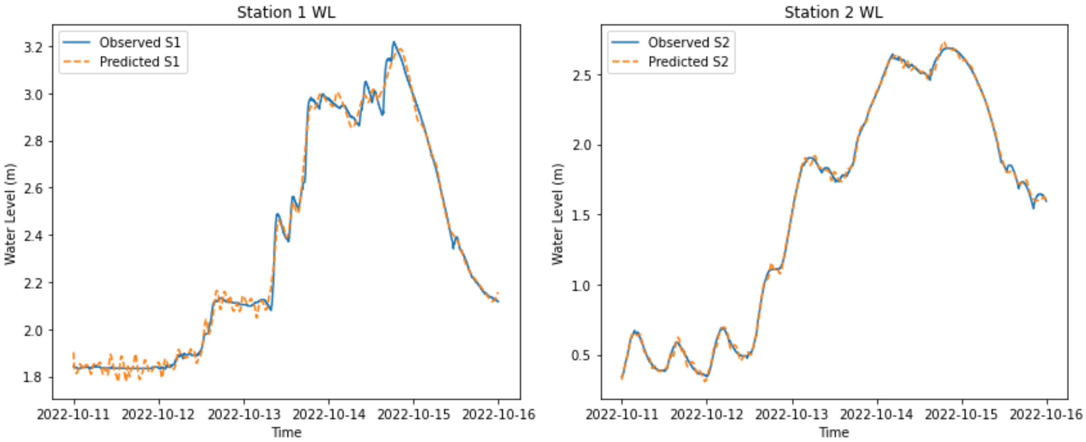


*Figure 36: Training for Chandrika Kumarathunga MW (Station 01) and Ambathale Downstream (Station 02) along the Madiwela East Diversion*

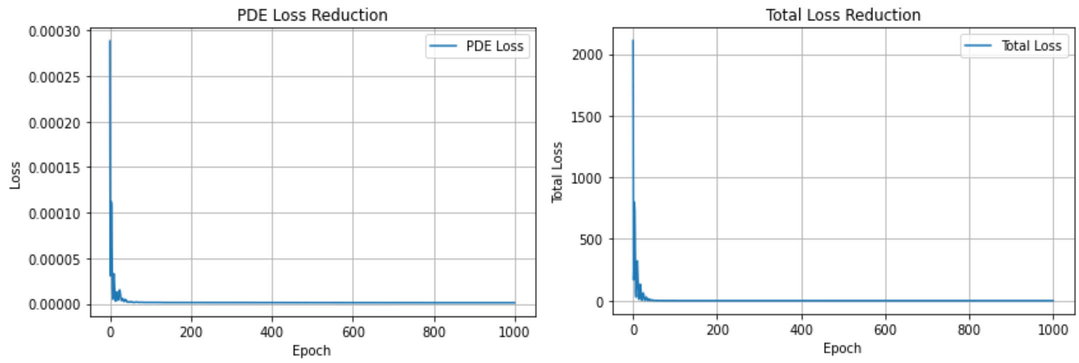


*Figure 37: PDE loss reduction and total loss reduction along with 1000 epochs in the PINN code*

*Table 6: The training NSE and RMSE values for accuracy*

| **Station Name** | **Training NSE** | **Training RMSE (in m)** |
|---|---|---|
| Chandrika MW (Station 01) | 0.9932 | 0.0301 |
| Ambathale Downstream (Station 02) | 0.9984 | 0.0227 |

The model demonstrated excellent predictive accuracy during the training phase at both monitoring stations. For Chandrika MW (Station 01), a high NSE of 0.9932 and a low RMSE of 0.0301 m indicate a near-perfect fit between predicted and observed water levels. Similarly, Ambathale Downstream (Station 02) achieved an even higher NSE of 0.9984 with a RMSE of only 0.0227 m, confirming the model's strong ability to capture the underlying hydrodynamics at both locations. The subsequent step involves validating the trained model through a multi-faceted approach. Three validation strategies were employed. First, the predicted flood peaks at the two water level monitoring stations were visually and quantitatively compared against observed flood peaks to assess the model’s temporal accuracy. Second, water level predictions at intermediate locations along the canal were compared with observed values to evaluate spatial consistency. Third, water levels at selected intermediate collocation points were compared with simulated outputs from the HEC-RAS 1D hydraulic model. Thus, for the Madiwela East Diversion, model validation was primarily based on these methods, (i) the alignment of flood peaks at observed stations under externally provided rainfall input (Figure 38), (ii) the agreement of model predictions with water levels at Rajasinghe MW observation point and (iii) a spatial comparison with HEC-RAS model predictions at key locations along the canal at x = 3,500 m, 4,000 m, and 4,500 m (Figures 42,43, and 44). The detailed comparison between PINN-predicted and HEC-RAS-simulated water levels is presented later in the section under PINN–HEC-RAS Comparison.

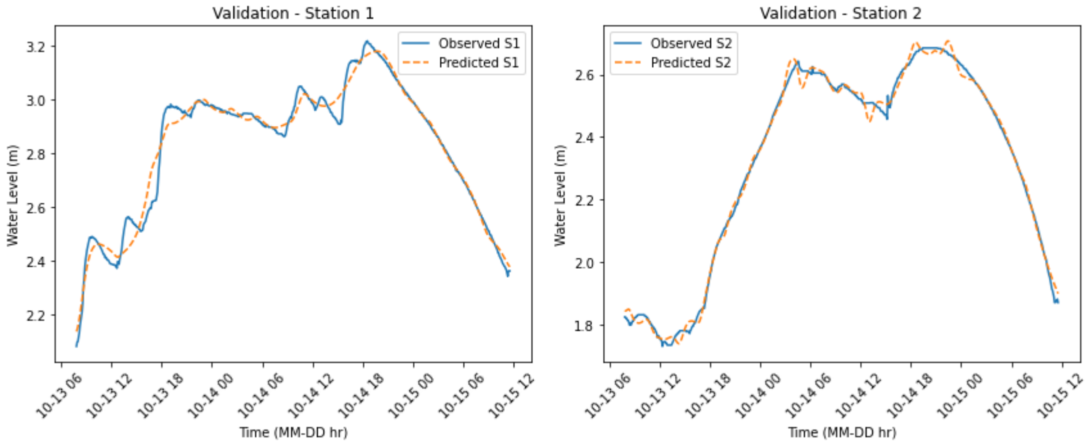


*Figure 38: Validation for flood peaks to check the ability of modelling flood peaks (for Stations 01 and 02)*

*Table 7: The testing NSE and RMSE values for accuracy*

| Station Name | Testing NSE | Testing RMSE (in m) |
|---|---|---|
| Chandrika MW (Station 01) | 0.9740 | 0.0345 |
| Ambathale Downstream (Station 02) | 0.9951 | 0.0254 |

As in Table 7, the model shows a good performance during the validation phase, with NSE values of 0.9740 and 0.9951 for Chandrika MW (Station 01) and Ambathale Downstream (Station 02), respectively. The corresponding RMSE values of 0.0345 m (3.45 cm) and 0.0254 m (2.54 cm) further indicate high accuracy and minimal deviation between the predicted and observed water levels. As the secondary step for validation, the PINN model predicted water levels for the Rajasinghe MW were compared with the observed data for the period, allowing a spatiotemporal validation for the model, as in Figure 39. The high NSE values of 0.9929 and low RMSE values of 0.0690 m (7 cm), show a higher agreement between the observed and predicted values, justifying the accuracy of the PINN model.

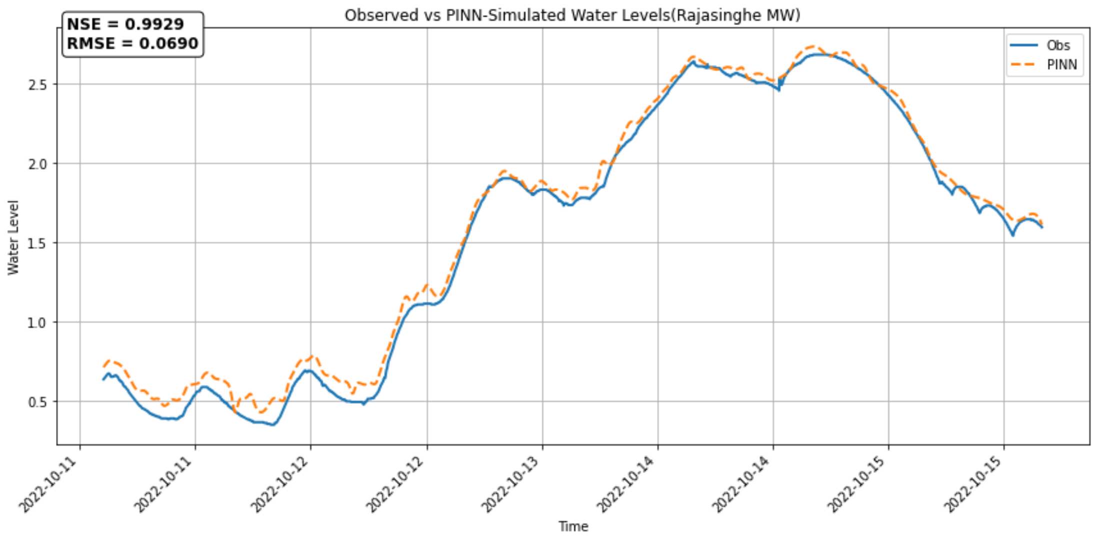


*Figure 39: Spatiotemporal validation for water levels in the given time domain in the flood period at the Rajasinghe water level monitoring location (x = 5.60 km)*

Furthermore, the PINN model-predicted water levels at the intermediate collocation points located at x = 3,500 m, 4,000 m, and 4,500 m are illustrated in Figure 40. These predictions were specifically extracted for comparison with the corresponding HEC-RAS simulation results. This intermediate-point validation approach, alongside the earlier discussed validation technique, was employed to assess the reliability of the PINN model in estimating water levels at locations where direct monitoring data is unavailable. The results demonstrate that water levels at any given point along the canal, measured from x = 0, can be effectively estimated using the PINN model. This capability highlights the potential of the PINN framework for real-time flood forecasting and early warning systems, offering a more computationally efficient and responsive alternative to traditional hydrodynamic models such as HEC-RAS, which are often time-intensive.

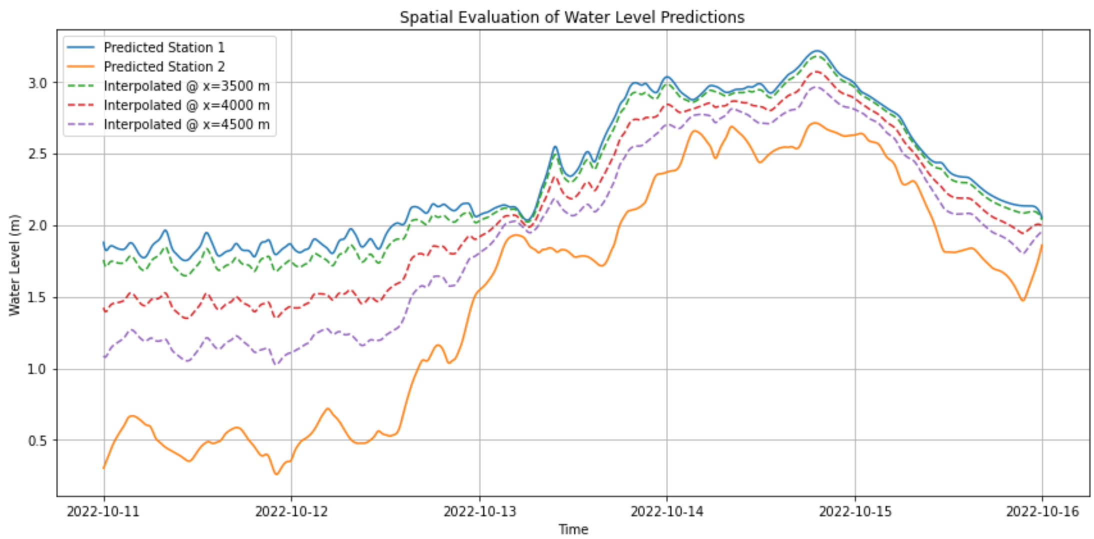


*Figure 40: Predicted water levels at intermediate locations, x=3,500 m; 4,000 m; and 4,500 m*

### 4.4.1.2 HEC-RAS Approach

The 1D hydraulic model of the Madiwela East Diversion canal was constructed in HEC-RAS to simulate the selected flood event and to provide a comparative benchmark against the PINN-predicted and observed water levels.

In the model, the terrain data used to define the canal geometry was obtained from the Copernicus Open Access Hub, with a 30 m × 30 m spatial resolution. The DEM and Google satellite imagery were used to manually delineate the canal alignment, ensuring consistency with ground-based references, as in Figure 41. A total of 17 cross-sections were provided and input data into the model, covering the entire canal reach from its origin to the downstream boundary. Among these, key monitoring locations such as the Rajasinghe MW station were included to facilitate validation. A Manning’s n value of 0.04 was provided for roughness throughout the reach. It was selected based on the prevailing channel conditions mixed with vegetation, which was observed along the bank (Raczyński & Dyer, 2022). The upstream boundary condition was defined using a stage hydrograph derived from observed water level data at the Chandrika Kumarathunga MW station, as in Figure 42. For the downstream boundary, the stage hydrograph for the Ambathale Downstream water level monitoring location was used.

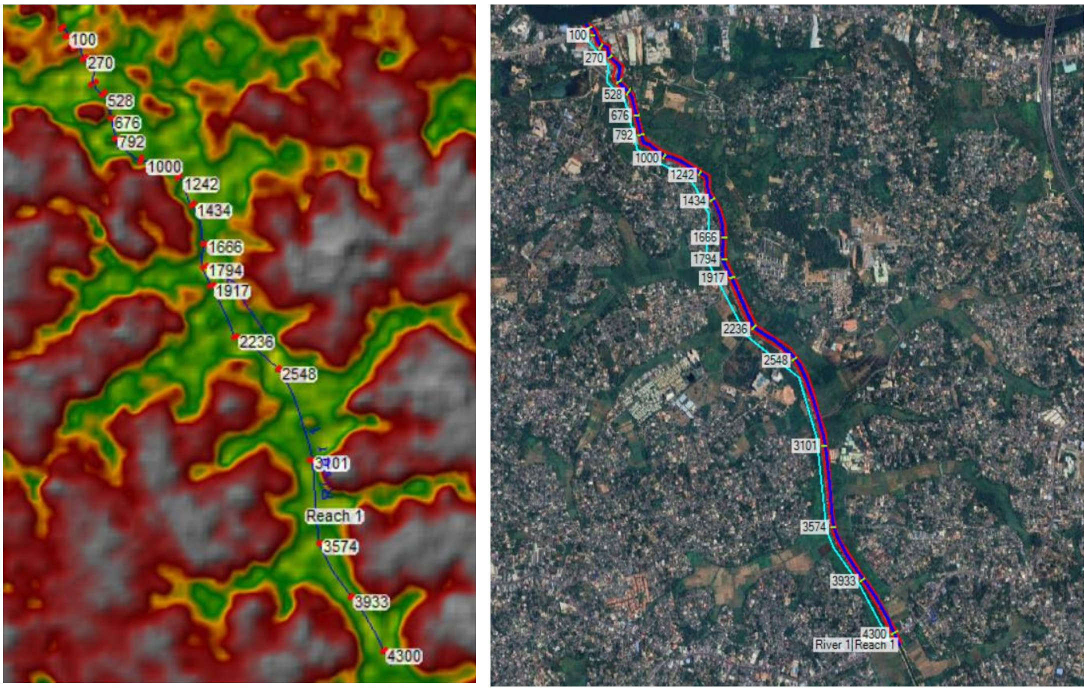


*Figure 41: Channel geometry, including the canal center line, bank lines, flow lines, and cross sections, which was drawn manually with the support of Google satellite imagery*

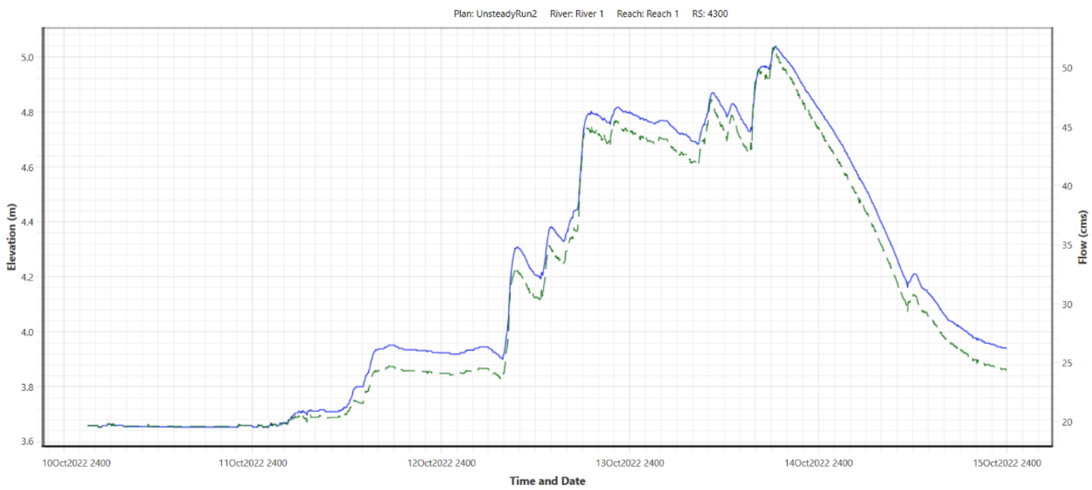


*Figure 42: Stage hydrograph at Chandrika Kumarathunga MW water level station used as the upstream boundary condition for Madiwela East Diversion*

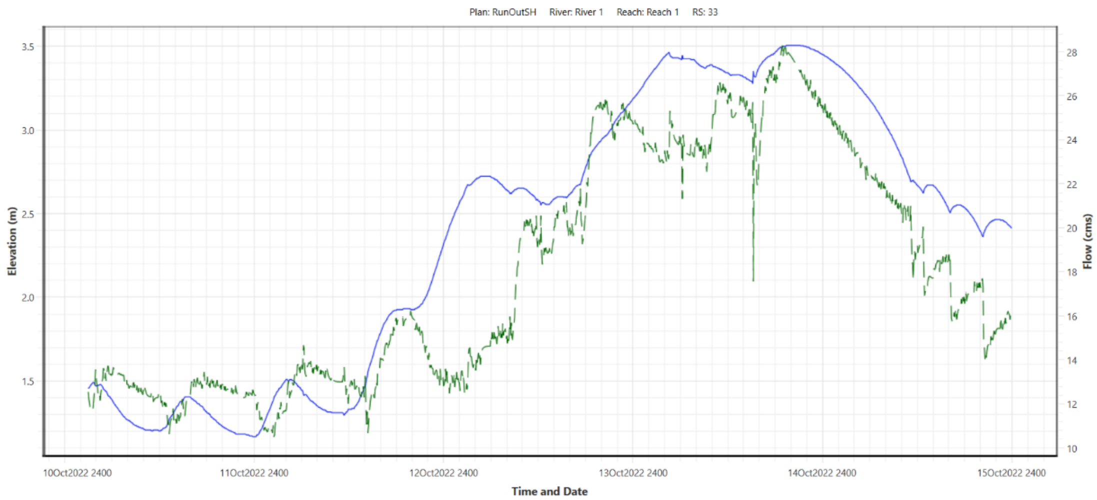


*Figure 43: Stage hydrograph at Ambathale Downstream water level station used as the downstream boundary condition for Madiwela East Diversion*

Based on the defined input data and boundary conditions, the HEC-RAS model for the Madiwela East Diversion was executed with a computational time interval of 1 minute and a warm-up period of 1,000 time steps to ensure numerical stability and convergence. Key spatial reference points within the model domain were associated with specific cross-section numbers. The Rajasinghe MW water level monitoring station was assigned to cross-section number 1,917, enabling the extraction of predicted water levels at the cross-section for validation. Additionally, stage hydrographs from three locations at distances of 3,500 m, 4,000 m, and 4,500 m from the canal origin were extracted. Those locations were given references intentionally, to match with cross-section numbers 3,933 m, 3,101 m, and 2,548 m, respectively. These locations were selected to match the PINN model's collocation points to facilitate spatial validation of water level predictions across both modeling approaches.

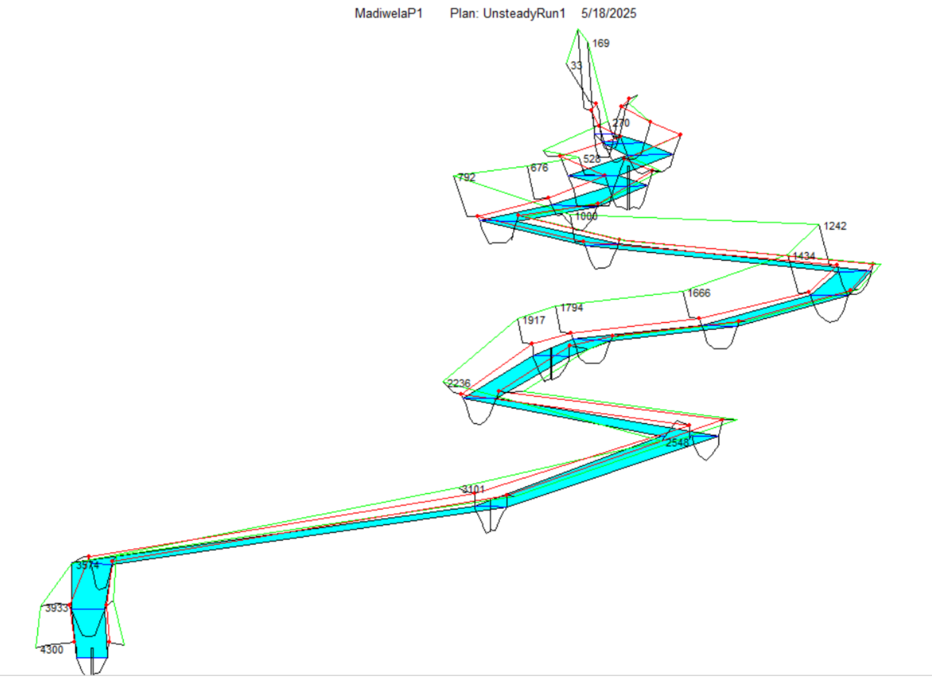


*Figure 44: Maximum flood condition along the Madiwela East Diversion on 10/14/2025*

The downstream end of the Madiwela East Diversion directly connects to the Kelani River. Thus, due to the proximity of the Rajasinghe MW water level monitoring station to this connecting point, water levels at this location are significantly influenced by backwater effects and fluctuations in the Kelani River. Figure 45 shows the comparison of water levels predicted by the HEC-RAS model and the observed water levels in the time domain. The higher NSE value of 0.9851 and lower RMSE value of 0.10 (10 cm) show a high agreement of model predictions and observed data, justifying the model accuracy.

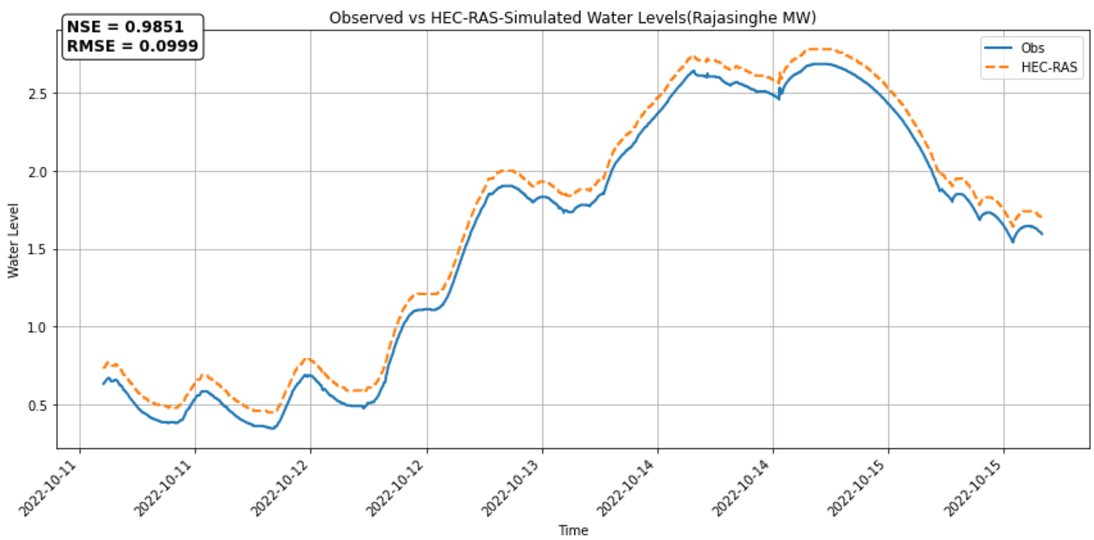


*Figure 45: HEC-RAS predicted water level and observational data for the Rajasinghe MW water level monitoring location*

#### 4.4.1.2 Comparison of PINN and HEC-RAS Results

As the second approach of validation, the PINN results and HEC-RAS results were compared, for x=3,500 m, 4,000 m, and 4,500 m as in Figures 46, 47, and 48. For quantifying the variations, the NSE and RMSE are calculated.

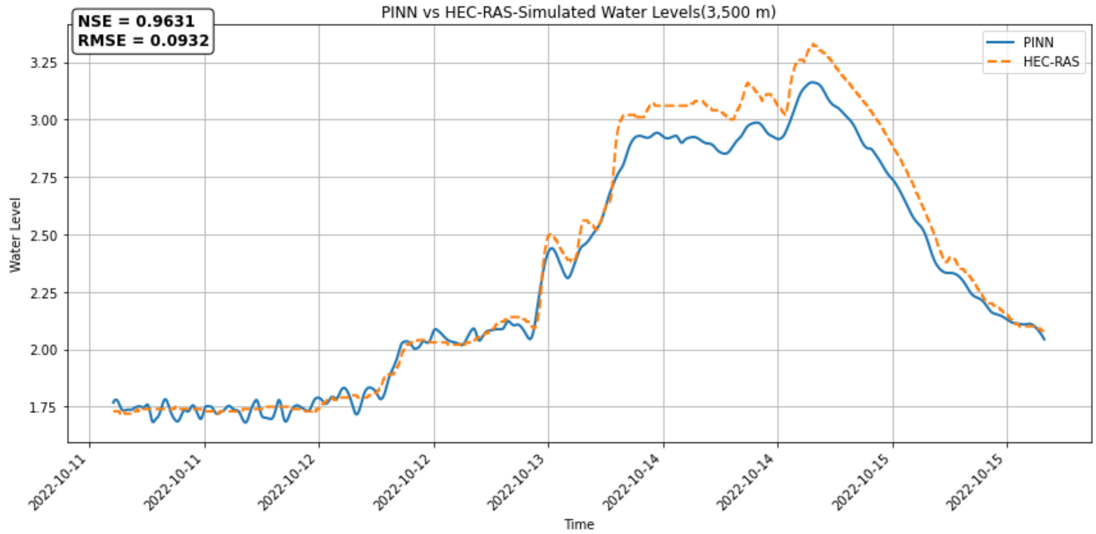


*Figure 46: Comparison of predicted water levels from PINN and HEC-RAS at x = 3,500 m from the origin (x = 0)*

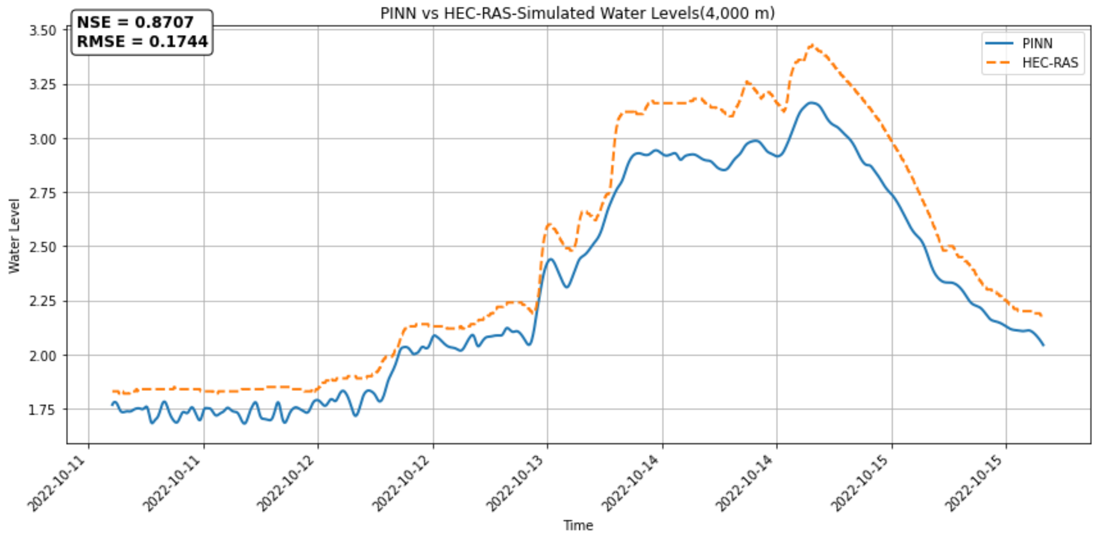


*Figure 47: Comparison of predicted water levels from PINN and HEC-RAS at x = 4,000 m from origin (x = 0)*

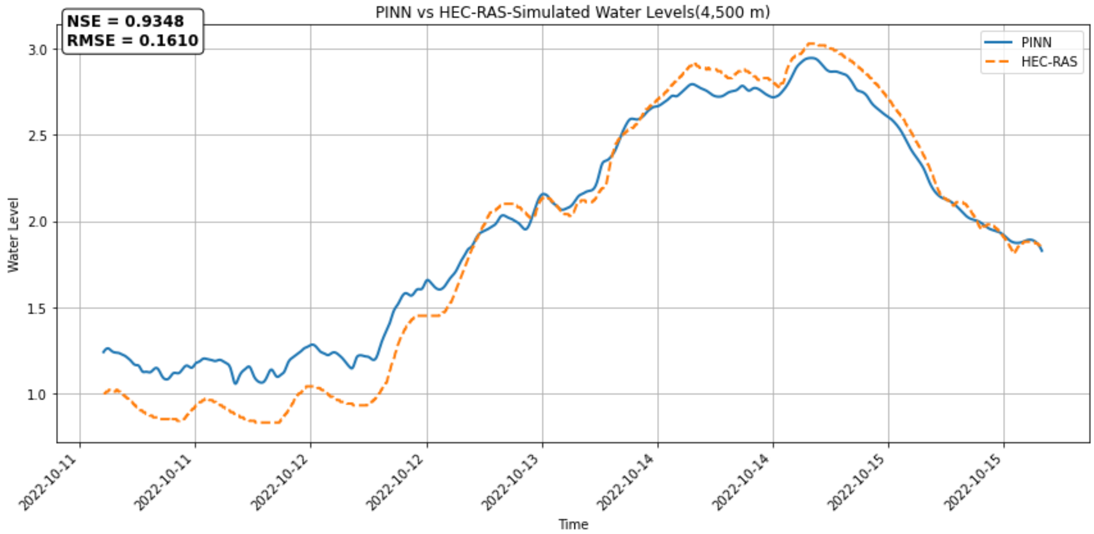


*Figure 48: Comparison of predicted water levels from PINN and HEC-RAS at x = 4,500 m from origin (x = 0)*

Before the direct comparison of intermediate predictions between the two models, the spatial validation was carried out using observed data from the Rajasinghe MW station, as summarized in Table 8. While both the PINN and HEC-RAS models exhibit high NSE values, indicating strong agreement with observed data, RMSE provides a more precise perspective on predictive accuracy by quantifying the average deviation between predicted and observed water levels. For the Rajasinghe MW station, the PINN model achieved an RMSE of 0.07 m (7 cm), in contrast to 0.10 m (10 cm) for the HEC-RAS model. In the context of flood modelling, a 10 cm discrepancy during a peak flow event can be significant in terms of warning, showing the higher reliability of the PINN model in this case.

*Table 8: Comparison of agreements of predicted water levels with observation data at the Rajasinghe MW*

| Intermediate Location | PINN Model | | HEC-RAS Model | |
|---|---|---|---|---|
| | NSE Value | RMSE Value | NSE Value | RMSE Value |
| Rajasinghe MW | 0.9987 | 0.0700 | 0.9851 | 0.1000 |

Moreover, a similar trend is observed in Figures 46, 47, and 48, where HEC-RAS predictions consistently overestimate water levels relative to the PINN model, as for the observed data. Despite all three model comparisons at 3,500 m, 4,000 m, and 4,500 m maintaining high NSE values (generally above 0.87), the RMSE values fluctuate between 9 cm to 17 cm across the intermediate locations. This common overestimation highlights a systematic bias in the HEC-RAS model under the given boundary conditions and supports the utility of PINN for more accurate predictions.

### 4.4.2 Dehiwala-Wellawatta-Kirillapone Canal System

The Wellawatta, Dehiwala, and Kirullapone Canal System (Canal System 02) forms an integral component of the urban stormwater drainage infrastructure within the Colombo Metropolitan Area. This canal network comprises two primary reaches, as the combination of Wellawatta and Kirullapone Canal, spanning approximately 4.460 km, and the Dehiwala Canal, extending 4.040 km. For hydrodynamic modelling and validation, four (4) key water level monitoring stations were considered along the system as, Nawala Road Bridge (0.63 km), Near Lanka Hospital (2.00 km), Wellawatta Canal Outlet (4.08 km) from the canal origin (x = 0 m) at the Kirullapone Canal, and Dehiwala Canal Outlet (3.68 km) from the connection junction of Dehiwala Canal and Wellawatta Canal. In the PINN model, only the reach connecting Wellawatta and Kirullapone Canal was considered, but in the HEC-RAS model, the total canal system was used. The Colombo 07 rainfall station was selected as the representative precipitation input source (Table 5) for the simulation. The selected flood event for this canal system occurred between October 13$^{th}$ and 17$^{th}$, 2022, which was characterized by intense rainfall and rapid water level response. Model validation was focused on the Lanka Hospital WL monitoring location. For further spatial validation of simulated water levels, multiple points at x = 1,000 m, 3,000 m, and 4,000 m were used to assess the performance of the PINN and HEC-RAS models under urban flood conditions.


*Figure 49:Dehiwala-Wellawatta-Kirillapone Canal System, showing four water level monitoring stations, Nawala Road Bridge (0.63 km), near Lanka Hospital (2.00 km), Wellawatta Canal Outlet (4.08 km) from the canal origin (x = 0 m) in the Kirullapone Canal, and Dehiwala Canal Outlet (3.68 km) from the connection junction*

#### 4.4.2.1 PINN Approach

Within this section, the results from running the PINN code, developed as in Section 3.1. with optimized hyperparameters (Section 4.1.1.) will be presented. As the input data, rainfall, canal cross sections, distance to cross sections along the canal (x), stage hydrographs, and time step were input to the code. The model was trained for stage hydrographs at Nawala Road Bridge and Wellawatta Canal Outlet, considering them as Station 01 and Station 02, as in Figure 50.

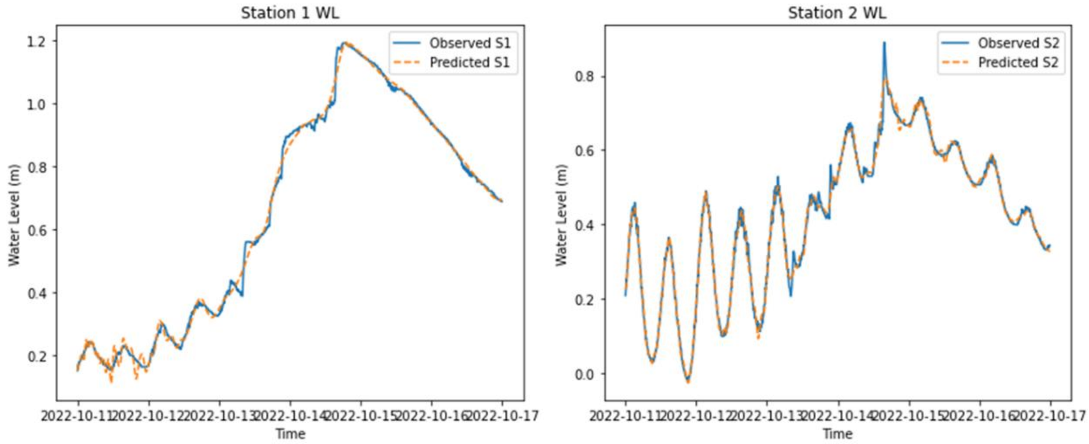


*Figure 50: Training for Nawala Road Bridge (Station 01) and Wellawatta Canal Outlet (Station 02) along the Canal System 02*

And based on their agreement rates with inputted observation data, the NSE and RMSE values were calculated (Table 9). Further, to avoid over-fitting, the reduction of the PDE loss function and the total loss function were also checked, as in Figure 51.

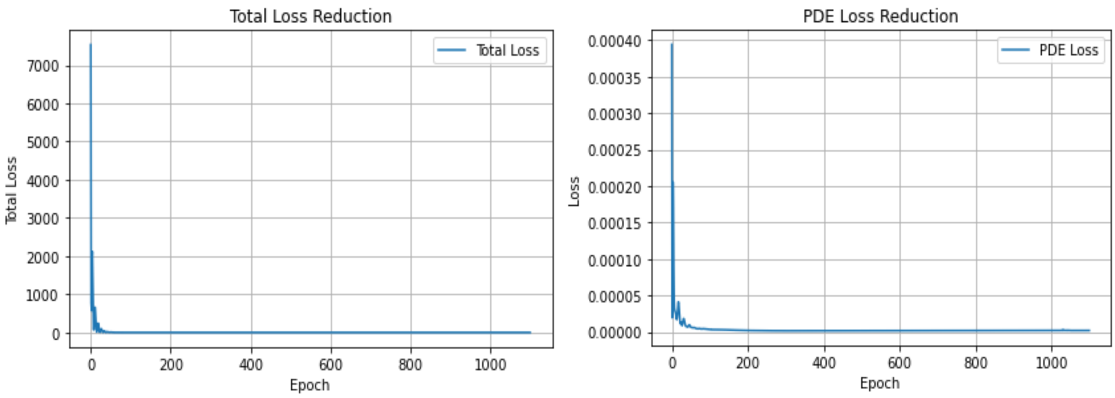


*Figure 51: PDE loss reduction and total loss reduction along with 1,200 epochs in the PINN code*

*Table 9: The training NSE and RMSE values for accuracy*

| Station Name | Training NSE | Training RMSE (in m) |
|---|---|---|
| Nawala Road Bridge (Station 01) | 0.9980 | 0.0190 |
| Wellawatta Outlet (Station 02) | 0.9964 | 0.0151 |

The model demonstrated excellent predictive accuracy during the training phase at both monitoring stations. For Nawala Road Bridge (Station 01), a high NSE of 0.9980 and a low RMSE of 0.0190 m (2 cm) indicate a near-perfect fit between predicted and observed water levels. Similarly, Wellawatta outlet (Station 02) achieved an even higher NSE of 0.9964 with a RMSE of only 0.0151 m (1.5 cm), confirming the model's strong ability to capture the underlying hydrodynamics at both locations. The subsequent step involves validating the trained model through a multi-faceted approach. The three validation strategies mentioned in Section 4.2.1 were employed. Thus, for the Dehiwala-Wellawatta-Kirillapone Canal System, model validation was primarily based on, (i) the alignment of flood peaks at observed stations under externally provided rainfall input (Figure 52), (ii) the agreement of model predictions with water levels near Lanka Hospital observation point and (iii) a spatial comparison with HEC-RAS model predictions at key locations along the canal at x = 1,000 m, 3,000 m, and 4,000 m (Figures 53,54, and 55).

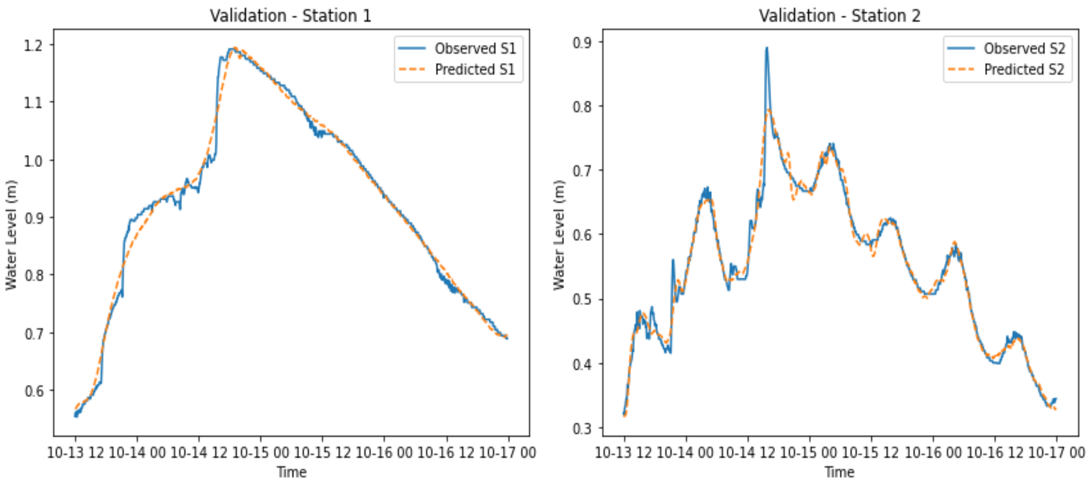


*Figure 52:Validation for flood peaks to check the ability of modelling flood peaks (for Stations 01 and 02)*

*Table 10: The testing NSE and RMSE values for accuracy*

| Station Name | Testing NSE | Testing RMSE (in m) |
|---|---|---|
| Nawala Road Bridge (Station 01) | 0.9840 | 0.0216 |
| Wellawatta Outlet (Station 02) | 0.9776 | 0.0176 |

As shown in Table 10, the model demonstrates strong predictive performance during the testing phase, achieving NSE values of 0.9840 and 0.9776 for the Nawala Road Bridge (Station 01) and Wellawatta Outlet (Station 02), respectively. The corresponding RMSE values of 0.0216 m (2.16 cm) and 0.0176 m (1.76 cm) further confirm the model’s high accuracy and minimal deviation between the predicted and observed water levels at both locations. As the secondary step for validation, the PINN model predicted water levels for the station near Lanka Hospital were compared with the observed data for the period, allowing a spatiotemporal validation for the model, as in Figure 53. The high NSE value of 0.9825 and low RMSE value of 0.0179 m (2 cm) show a higher agreement between the observed and predicted values, justifying the accuracy of the PINN model. Although the model predictions exhibit strong overall agreement with the observed data, a key limitation is the inability to capture the flood peak with complete accuracy, showing a deviation of approximately 10 cm at the crest. This discrepancy could potentially be mitigated by increasing the number of training epochs, which would enable the network to more closely fit the peak values. However, extending the training beyond the current epoch count would likely compromise the generalization ability of the model when applied to other canal systems, increasing the risk of overfitting. Given the already high level of agreement achieved under the current configuration, the same epoch count was retained for subsequent spatiotemporal validations at additional locations along the canal (x = 1,000 m, 3,000 m, and 4,000 m).

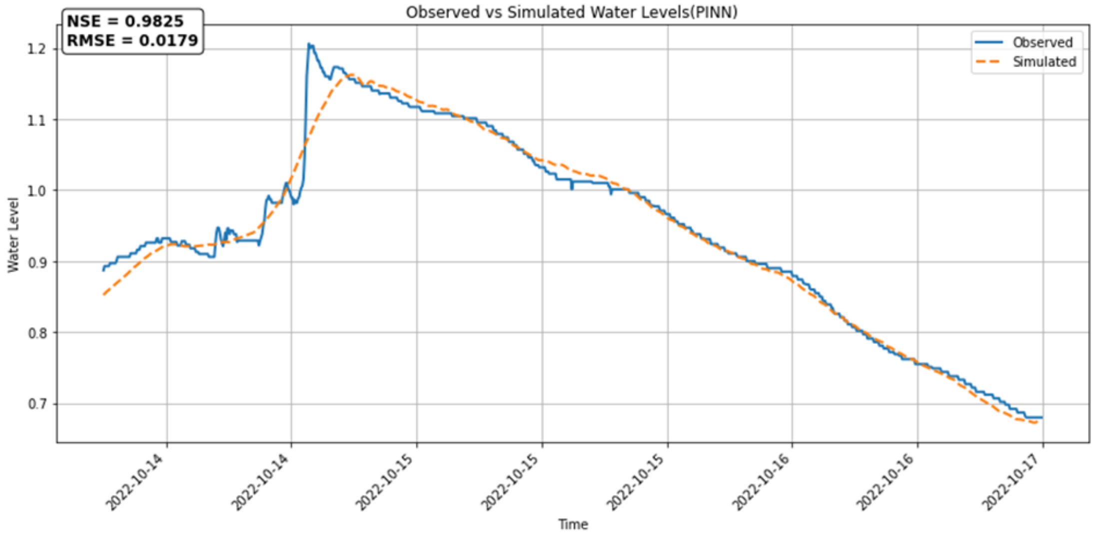


*Figure 53: Spatiotemporal validation for water levels in the given time domain in the flood period near Lanka Hospital water level monitoring location (x = 2 km)*

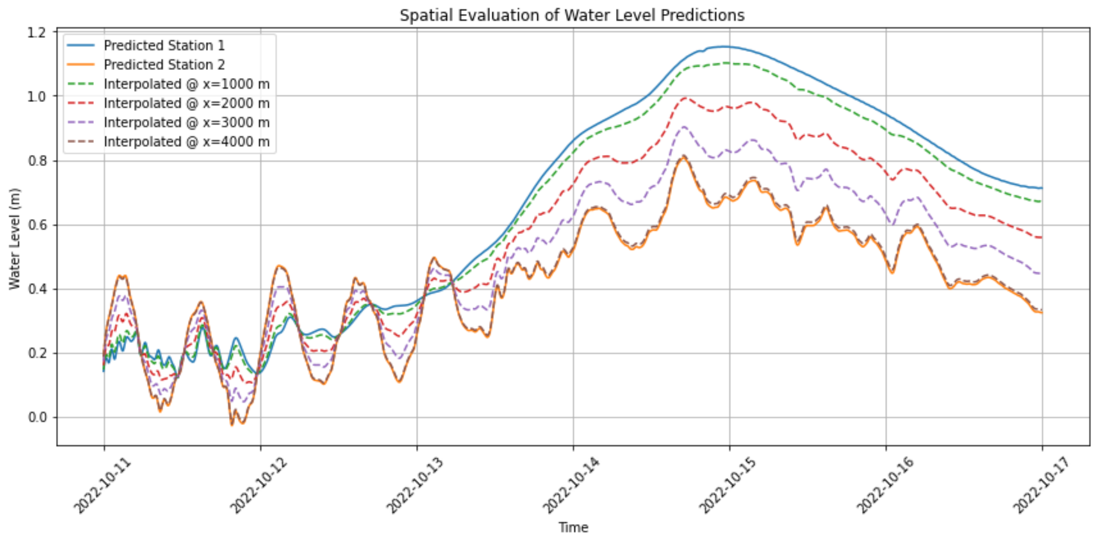


*Figure 54:Predicted water levels at intermediate locations, x=1,000 m; 3,000 m; and 4,000 m*

These PINN-predicted water levels were extracted to compare with HEC-RAS simulations and to validate model performance at ungauged locations. The results confirm that PINN can reliably estimate water levels at any point along the canal, making it well-suited for real-time flood forecasting and early warning, offering a faster, more efficient alternative to time-consuming models like HEC-RAS.

#### 4.4.2.2 HEC-RAS Approach

The 1D hydraulic model of the Dehiwala-Wellawatta-Kirillapone Canal System was constructed in HEC-RAS to simulate the selected flood event and to provide a comparative benchmark against the PINN-predicted and observed water levels. In the model, the terrain data used to define the canal geometry was obtained from the Copernicus Open Access Hub, with a 30 m × 30 m spatial resolution. The DEM and Google satellite imagery were used to manually delineate the canal alignment, ensuring consistency with ground-based references, as in Figure 55. A total of 56 cross-sections were provided and input data into the model, covering the entire canal reach from its origin to the downstream boundary. Among these, key monitoring locations such as the station near the Lanka Hospital were included to facilitate validation. A Manning’s *n* value of 0.04 was provided for roughness throughout the reach. It was selected based on the prevailing channel conditions mixed with vegetation, which was observed along the bank (Raczyński & Dyer, 2022). The upstream boundary condition was defined using a stage hydrograph derived from observed water level data at the Nawala Road Bridge, as in Figure 56. For the downstream boundary, the stage hydrographs at Dehiwala Canal Output (Figure 57) and Wellawatta Canal Output (Figure 58) water level monitoring locations were used.

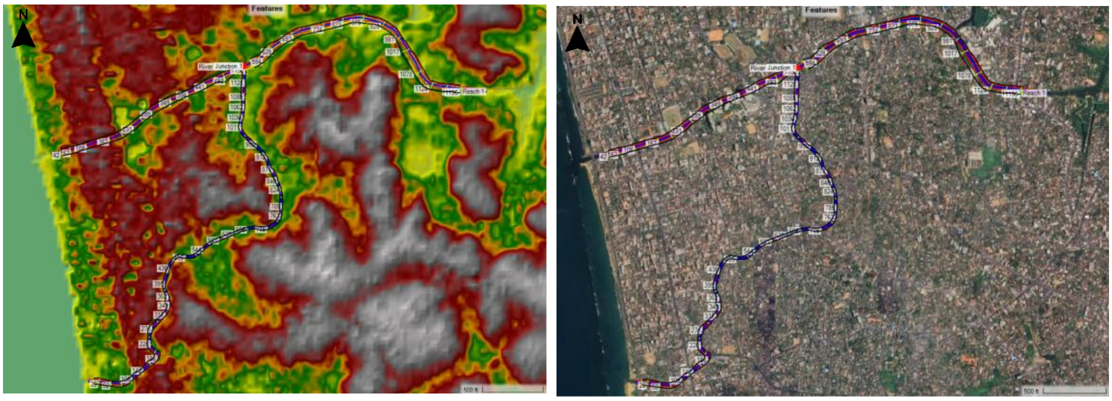

*Figure 55: Channel geometry, including the canal center line, bank lines, flow lines, and cross sections, which was drawn manually with the support of Google satellite imagery*

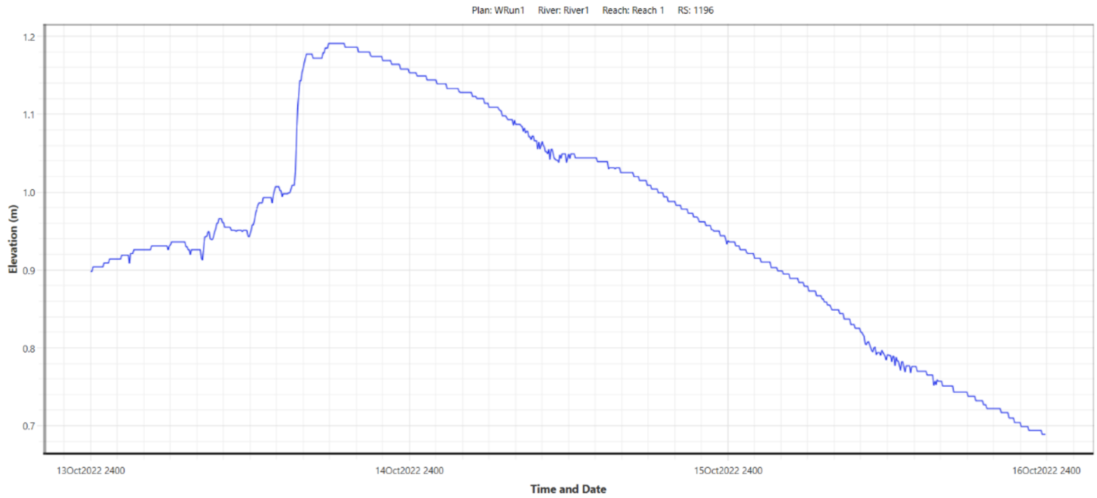


*Figure 56: Stage hydrograph at Nawala Road Bridge water level station used as the upstream boundary condition for Canal System 02*

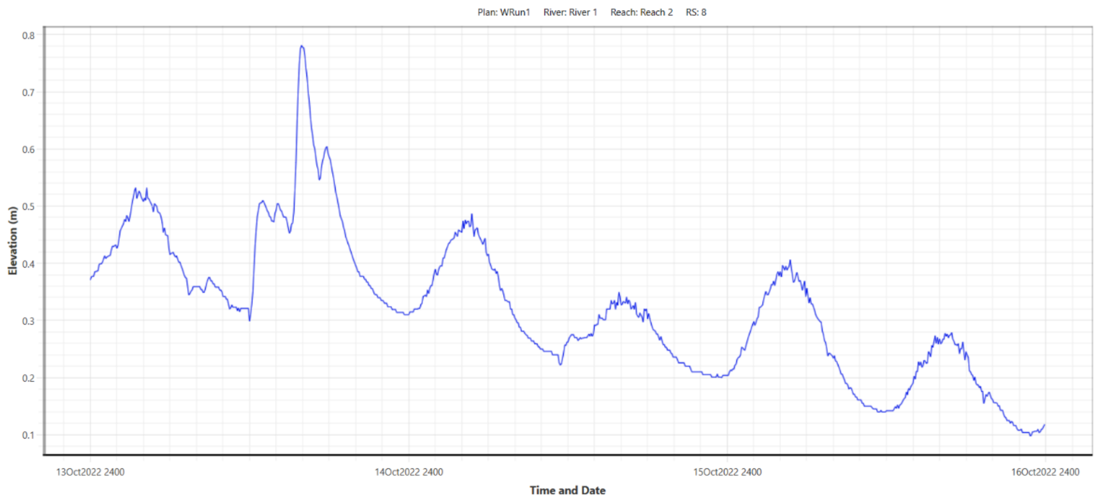


*Figure 57: Stage hydrograph at Dehiwala Canal Outlet water level station used as the downstream boundary condition for Canal System 02*

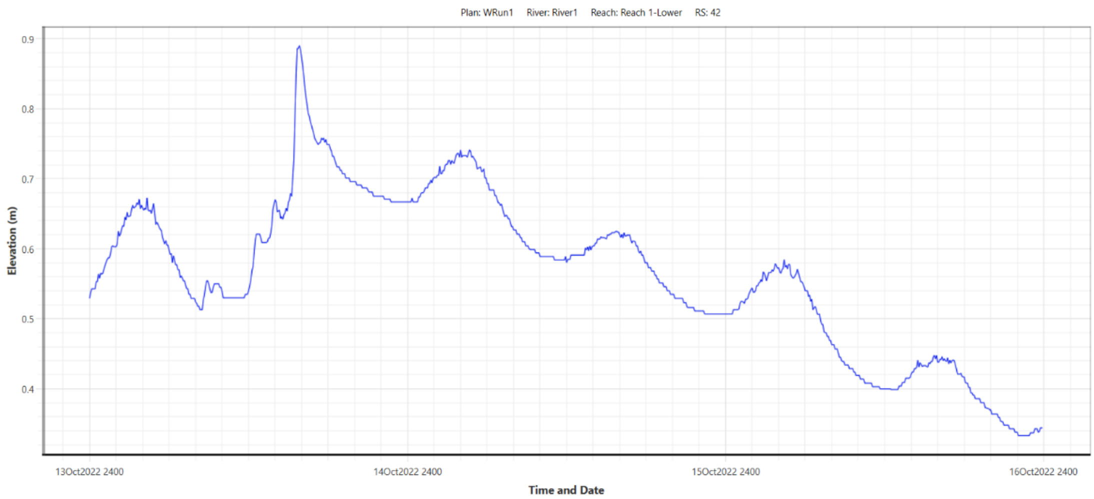


*Figure 58: Stage hydrograph at Wellawatta Canal Outlet water level station used as the downstream boundary condition for Canal System 02*

Based on the defined input data and boundary conditions, the HEC-RAS model for the Dehiwala-Wellawatta-Kirulapone canal systems was executed with a computational time interval of 1 minute and a warm-up period of 1,000 time steps to ensure numerical stability and convergence. Key spatial reference points within the model domain were associated with specific cross-section numbers.

The water level monitoring station near Lanka hospital was assigned to cross-section number 774, enabling the extraction of predicted water levels at the cross-section for validation. Additionally, stage hydrographs from three locations at distances of 1,000 m, 3,000 m, and 4,000 m from the canal origin were extracted. Those locations were given references intentionally, to match the cross-section numbers 1,078, 519, and 200, respectively. These locations were selected to match the PINN model's collocation points, facilitating spatial validation of water level predictions across both modeling approaches.


*Figure 59: Maximum flood condition along the Dehiwala-Wellawatta-Kirulapone canal system on 10/14/2025*

For the validation process, the stage hydrograph at the water level monitoring station near Lanka hospital (Figure 60) was used. The predicted water levels were compared with observation data at the location, as in Figure 61.

The higher NSE value of 0.9487 and lower RMSE value of 0.030 m (3 cm) show a high agreement of model predictions and observed data, justifying the model accuracy. From the results, it is evident that both models demonstrated strong performance, but the PINN model outperformed the HEC-RAS model, achieving a higher NSE value of 0.9825 and a lower RMSE of 0.0179 m (2 cm) compared to the HEC-RAS NSE and RMSE values. Indicating a higher performance level.

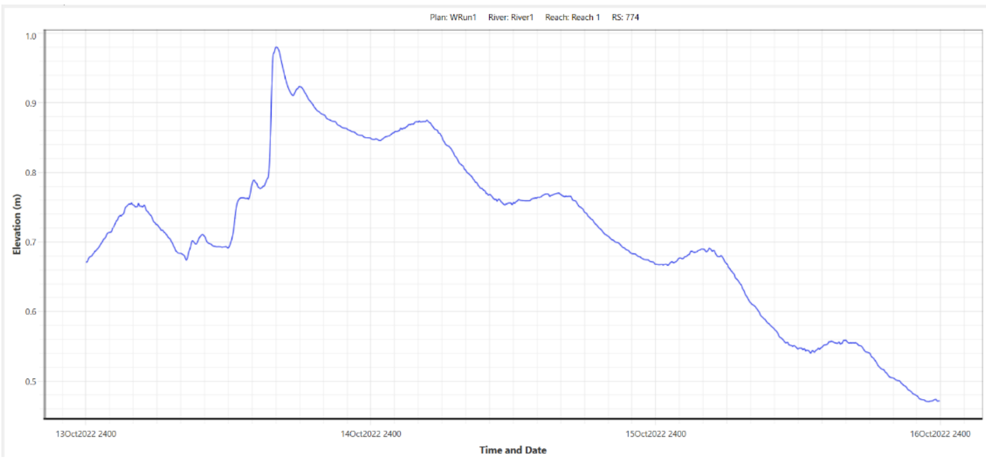


*Figure 60: Stage hydrograph at the water level monitoring station near Lanka hospital for the considered time domain*

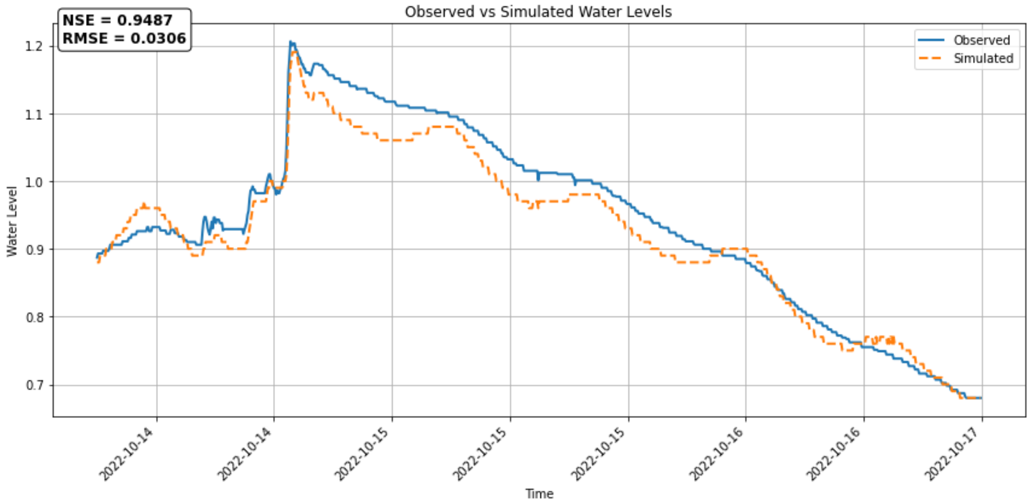


*Figure 61:Spatiotemporal validation for water levels in the given time domain in the flood period near Lanka Hospital water level monitoring location (x = 2 km)*

#### *4.4.2.3 Comparison of PINN and HEC-RAS results*

As the third approach of validation, the PINN results and HEC-RAS results were compared, for x=1,000 m, 3,000 m, and 4,000 m as in Figures 62, 63, and 64.

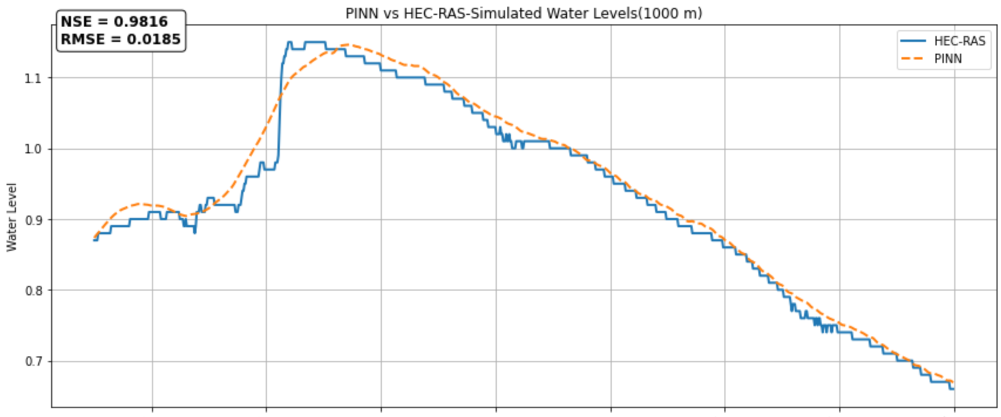


*Figure 62: Comparison of predicted water levels from PINN and HEC-RAS at x = 1,000 m from the origin (x = 0)*

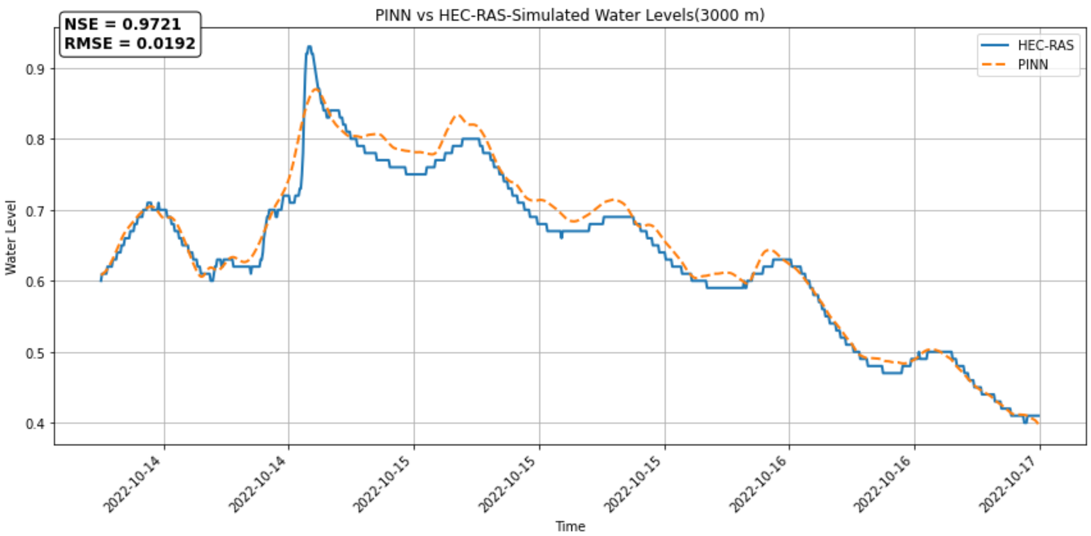


*Figure 63: Comparison of predicted water levels from PINN and HEC-RAS at x = 3,000 m from the origin (x =0)*

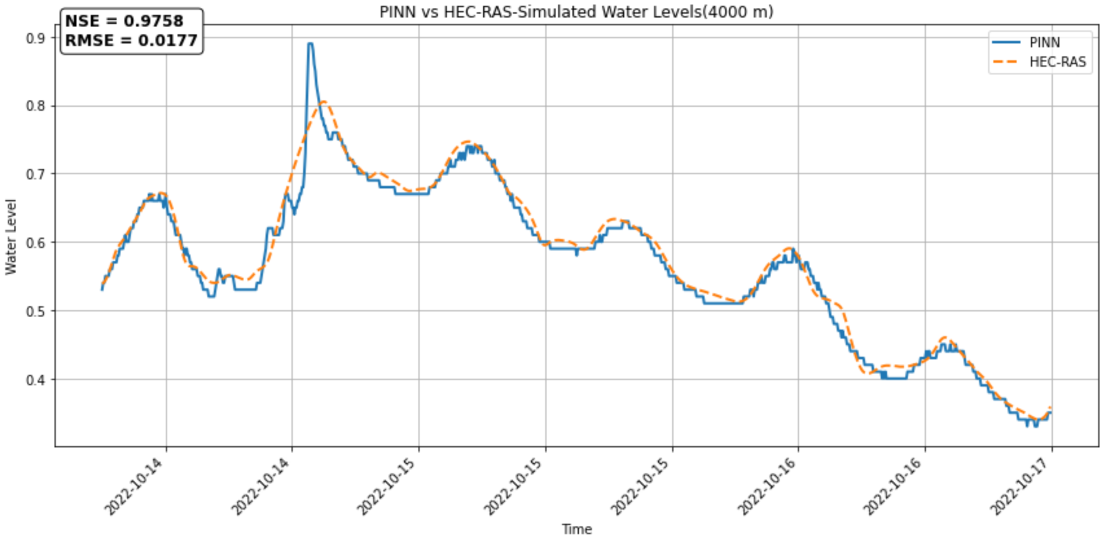


*Figure 64:Comparison of predicted water levels from PINN and HEC-RAS at x = 4,000 m from the origin (x = 0)*

Figures 62, 63, and 64 demonstrate a strong agreement between the water levels predicted by the PINN and HEC-RAS models. This consistency is expected, as both models independently showed high agreement with observed data, with the PINN model outperforming HEC-RAS (Table 11). However, in Figures 62 and 63, the PINN-predicted peaks appear slightly reduced, by approximately 5 to 10 cm. This reduction likely results from the PDE training strategy, which blends the influence of both boundary stations. While increasing the number of training epochs could improve peak accuracy, the current epoch count was selected to preserve the model's generalization capability across different canal systems.

*Table 11: Comparison of agreements of predicted water levels with observation data near Lanka hospital*

| Intermediate Location | PINN Model | | HEC-RAS Model | |
|---|---|---|---|---|
| | **NSE Value** | **RMSE Value** | **NSE Value** | **RMSE Value** |
| Lanka Hospital Station | 0.9825 | 0.0179 | 0.9487 | 0.0306 |

### 4.4.3 Parliament Lake - Kiththampahuwa - Kinda - Dematagoda Canal System

The Parliament Lake-Kiththampahuwa-Kinda-Dematagoda Canal System (Canal System 03) constitutes a vital drainage corridor within the Colombo Metropolitan Area, contributing significantly to flood management and urban water regulation. This interconnected canal network is composed of three main reaches as: the Parliament Lake to Dematagoda Canal stretch, spanning approximately 12.10 km, the Kinda Canal extending 2.00 km, and the Kiththampahuwa Canal with a length of 1.82 km. For the purpose of hydrodynamic simulation and model validation, five (5) water level monitoring stations were identified along the primary canal reach as, Kimbulawala Bridge at the canal origin (x = 0 m), Diyatha Bridge (3.780 km), Yakbedda Bridge (7.530 km), Orugodawatta (10.900 km), and Ingurukade Junction (12.100 km). In the PINN framework, the Parliament Lake and Dematagoda reach was primarily used for modeling, while the full extent of the system was incorporated into the HEC-RAS 1D hydraulic simulation for a more comprehensive comparison (Figure 65). The Battaramulla rainfall station was selected as the representative precipitation input (Table 5), corresponding to the spatial coverage and proximity to the canal system. The selected flood event, which occurred between October $11^{th}$ and $19^{th}$, 2022, was marked by significant rainfall-induced surges in canal water levels and provided an ideal test case for model validation. The primary validation locations for both PINN and HEC-RAS models included the Diyatha Bridge, Yakbedda Bridge, and Orugodawatta monitoring stations.


*Figure 65: Parliament Lake-Kiththampahuwa-Kinda-Dematagoda Canal System, showing four water level monitoring stations, Kimbulawala Bridge at the canal origin (x = 0 m), Diyatha Bridge (3.780 km), Yakbedda Bridge (7.530 km), Orugodawatta (10.900 km), and Ingurukade Junction (12.100 km)*

#### 4.4.3.1 PINN Approach

Within this section, the results from running the PINN code, developed as in Section 3.1. with optimized hyperparameters (Section 4.1.1.) will be presented. As the input data, rainfall, canal cross sections, distance to cross sections along the canal (x), stage hydrographs, and time step were input to the code. The model was trained for stage hydrographs at Kimbulawala Bridge and Ingurukade Junction, considering them as Station 01 and Station 02, as in Figure 66.

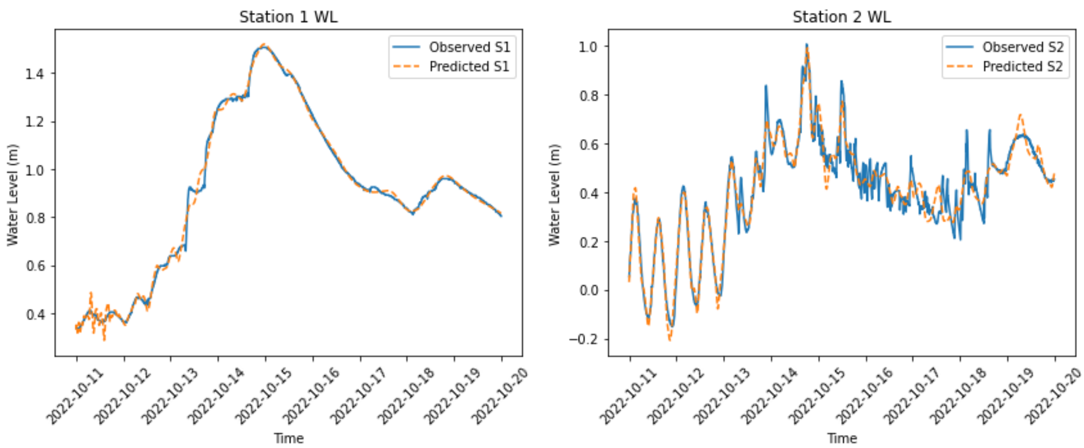


*Figure 66: Training for Kimbulawala Bridge (Station 01) and Ingurukade Junction (Station 02) along the Parliament Lake-Kiththampahuwa-Kinda-Dematagoda Canal System*

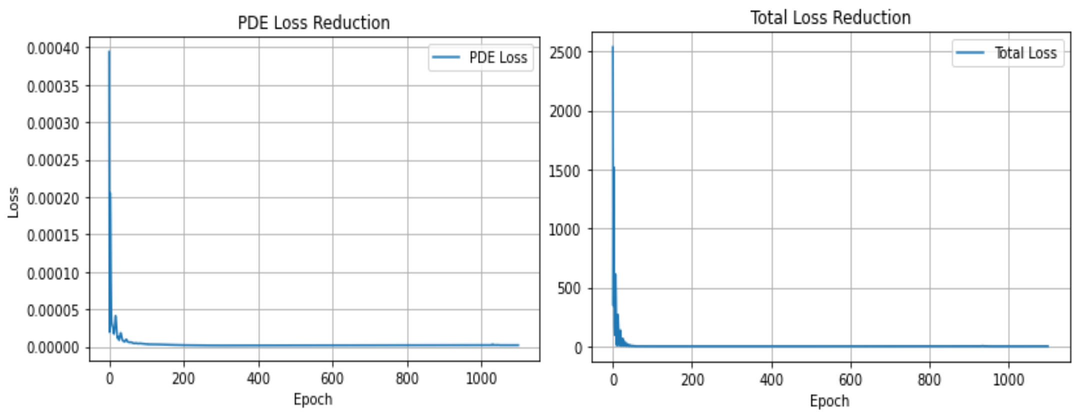


*Figure 67: PDE loss reduction and total loss reduction along with 1,200 epochs in the PINN code*

*Table 12: The training NSE and RMSE values for accuracy*

| Station Name | Training NSE | Training RMSE (in m) |
|---|---|---|
| Kimbulawala Bridge (Station 01) | 0.9923 | 0.0211 |
| Ingurukade Junction (Station 02) | 0.9338 | 0.0394 |

The model demonstrated excellent predictive accuracy during the training phase at both monitoring stations. For Kimbulawala Bridge (Station 01), a high NSE of 0.9923 and a low RMSE of 0.0211 m (2 cm) indicate a near-perfect fit between predicted and observed water levels. The relatively lower NSE value of 0.9338 and higher RMSE of 0.0394 m (4 cm) observed at Ingurukade Junction (Station 2), in contrast to other validation locations. This is due to the mismatch between model-predicted water levels and short-term, high-frequency fluctuations in observed water levels between October 15th and 17th.

As shown in Figure 66, these sharp oscillations may be caused by downstream influences such as backwater effects, tidal variations, due to the proximity to the sea, or urban flow dynamics. This mismatch led to localized residuals, affecting the NSE value of the PINN model, despite the modelling of the overall flood trend accurately. To improve the model's ability to reproduce such localized and rapid changes, the number of training epochs could be increased. A longer training duration may allow the network to better minimize small-scale errors and capture abrupt peaks more precisely. However, increasing epochs must be balanced carefully, as overfitting to one canal system can reduce the model's generalizability across different catchments. The subsequent step involves validating the trained model through a multi-faceted approach. Two validation strategies out of the three validation strategies mentioned in Section 4.2.1 were employed. Thus, for the Parliament Lake-Kiththampahuwa-Kinda-Dematagoda Canal System, model validation was primarily based on, (i) the alignment of flood peaks at observed stations under externally provided rainfall input (Figure 68), and (ii) the agreement of model predictions with water levels at Diyatha Bridge (3.780 km), Yakbedda Bridge (7.530 km), and Orugodawatta (10.900 km). The third validation approach, which involves direct comparison, was not applied in this case, as multiple water level monitoring stations with actual observed data were available along the canal system.

*Figure 68: Validation for flood peaks to check the ability of modelling flood peaks (for Stations 01 and 02)*

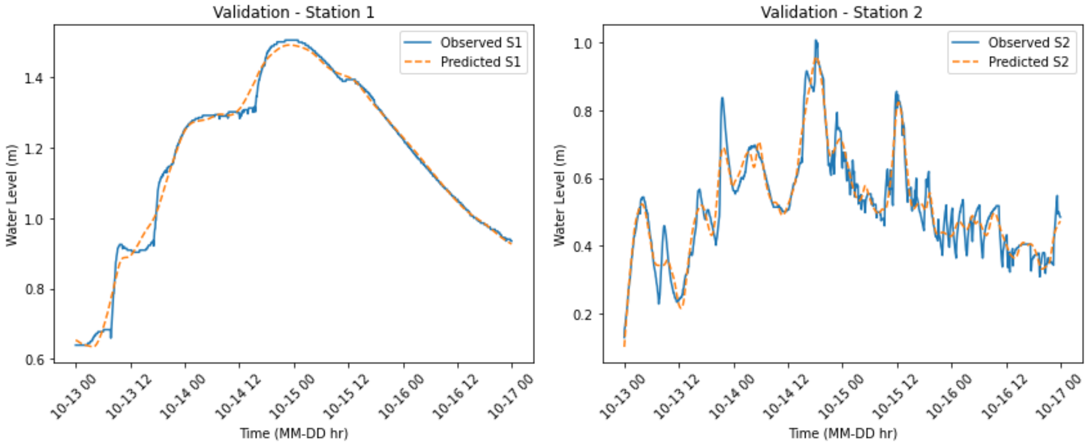


*Table 13: The testing NSE and RMSE values for accuracy*

| Station Name | Testing NSE | Testing RMSE (in m) |
|---|---|---|
| Kimbulawala Bridge (Station 01) | 0.9941 | 0.0271 |
| Ingurukade Junction (Station 02) | 0.9755 | 0.0335 |

As shown in Table 12, the model demonstrates strong predictive performance during the testing phase, achieving NSE values of 0.9941 and 0.9755 for the Kimbulawala Bridge (Station 01) and Ingurukade Junction (Station 02), respectively. The corresponding RMSE values of 0.0271 m (3 cm) and 0.0335 m (3 cm) further confirm the model's high accuracy and minimal deviation between the predicted and observed water levels at both locations. As the secondary step for validation, the PINN model predicted water levels for the station near Diyatha Bridge, Yakbedda Bridge, and Orugodawatta (Figure 69) were compared with the observed data for the period, allowing a spatiotemporal validation for the model.

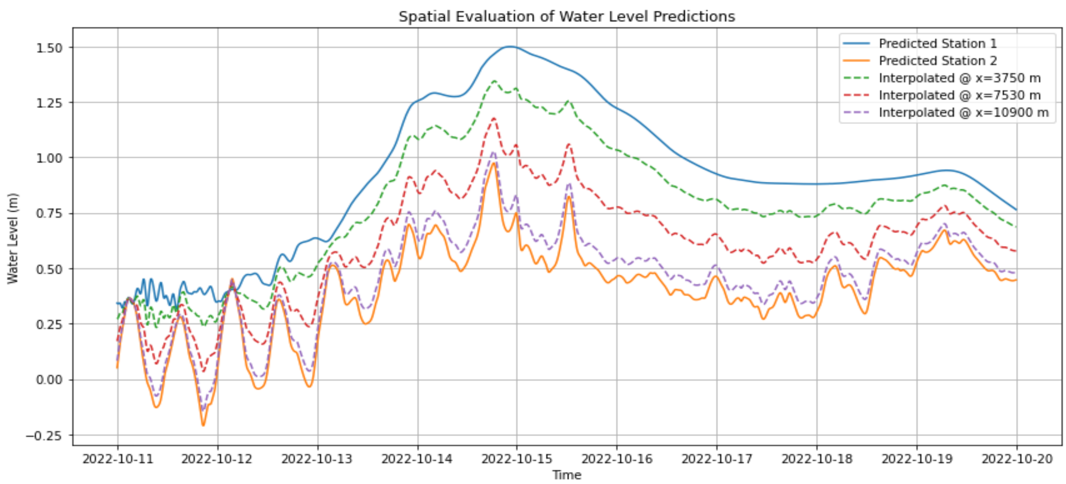


*Figure 69: Predicted water levels at Intermediate locations, at Diyatha Bridge (3.780 km), Yakbedda Bridge (7.530 km), Orugodawatta (10.900 km)*

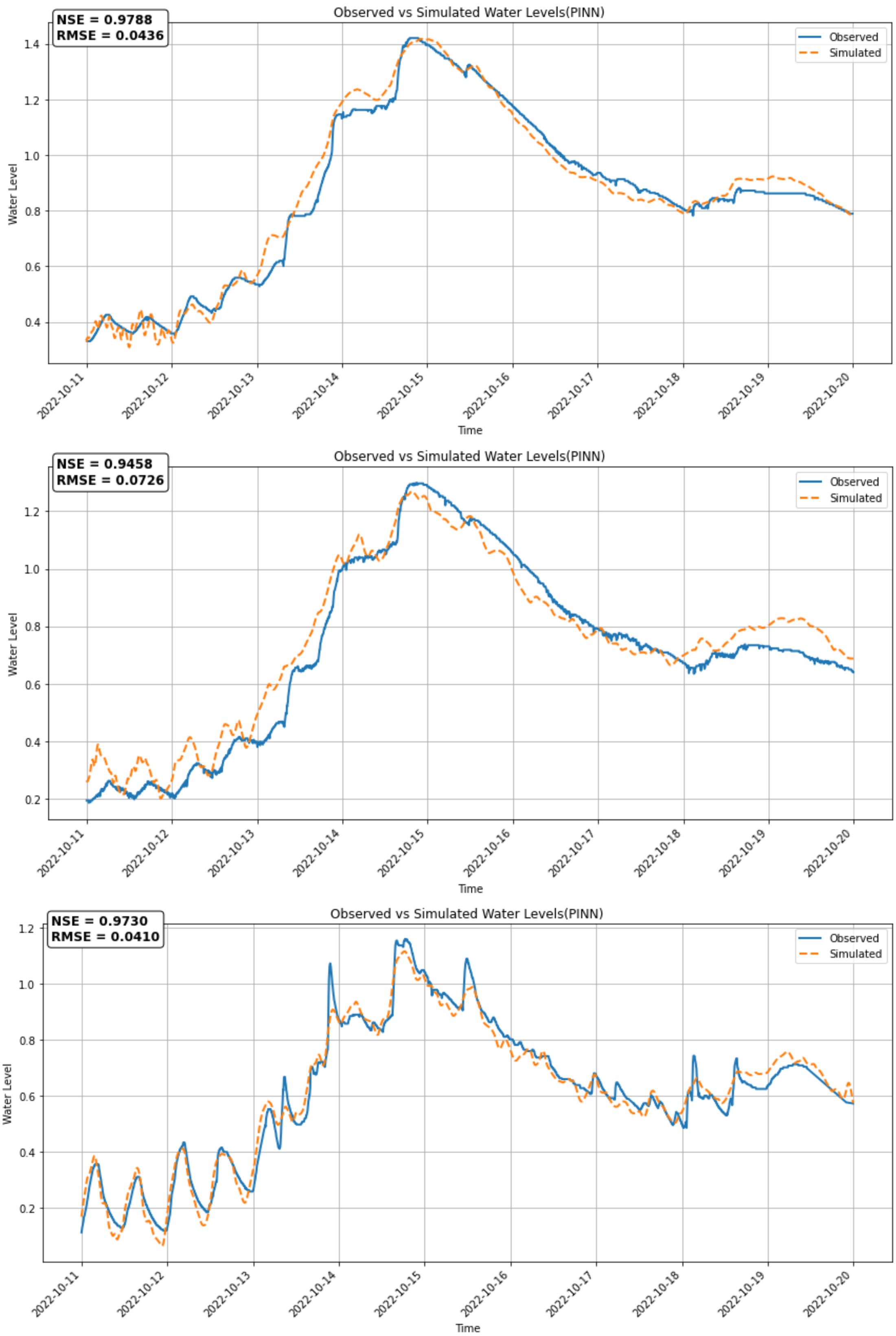


*Figure 70: Spatiotemporal validation using Intermediate stations for Diyatha Bridge (3.780 km), Yakbedda Bridge (7.530 km), Orugodawatta (10.900 km) along the Canal System 3*

The predicted water levels in Figure 69 were plotted with the observation hydrographs, as in Figure 70, and compared to check the accuracy. The NSE and RMSE values for the three monitoring stations are shown in Table 14.

*Table 14: NSE and RMSE values for the intermediate stations along the canal for the PINN model*

| Water Level Monitoring Station | NSE Value | RMSE Value |
|---|---|---|
| Diyatha Bridge | 0.9788 | 0.0436 |
| Yakbedda Bridge | 0.9458 | 0.0726 |
| Orugodawatta Bridge | 0.9730 | 0.0410 |

During the validation phase, the model demonstrated strong predictive performance across the selected water level monitoring stations. At Diyatha Bridge, an NSE value of 0.9788 and an RMSE of 0.0436 m were achieved, indicating excellent agreement with observed data. Similarly, Orugodawatta Bridge recorded an NSE of 0.9730 and an RMSE of 0.0410 m, reflecting high model accuracy. Although the performance at Yakbedda Bridge was slightly lower, with an NSE of 0.9458 and an RMSE of 0.0726 m, the results still demonstrate a robust level of agreement between predicted and observed water levels. The observed reduction in NSE and corresponding increase in RMSE values may be attributed to the proximity of the monitoring location to the junction where the Dematagoda Canal merges with the Kinda Canal, introducing additional flow complexities and variability into the observations.

#### 4.4.3.2 HEC-RAS Approach

The 1D hydraulic model of the Parliament Lake-Kiththampahuwa-Kinda-Dematagoda Canal System (Canal System 03) was developed using HEC-RAS to simulate the selected flood event and to serve as a comparative benchmark against both the observed and PINN model-predicted water levels. The terrain data required for defining the canal geometry was obtained from the Copernicus Open Access Hub, with a spatial resolution of 30 m × 30 m, which is particularly appropriate for modeling flood behavior across the flat, highly urbanized terrain typical of Sri Lanka's Wet Zone. To ensure spatial accuracy and consistency with existing infrastructure, Google satellite imagery was used in conjunction with the DEM to manually digitize the canal alignment, ensuring an accurate representation of all branches and joining points as junctions within the system. A total of 156 cross-sections were incorporated into the model, covering the full extent of the canal network from upstream sources to downstream outfalls (Figure 71). These cross-sections included critical locations such as Diyatha Bridge, Yakbedda Bridge, and Orugodawatta Bridge, which also served as key monitoring stations for model validation. A uniform Manning's roughness coefficient ($n$) of 0.04 was adopted throughout the canal reach. This value was selected based on prior studies (Liu et al., 2019) and field conditions, considering the moderate vegetation and channel irregularities observed along the canal banks. The upstream boundary conditions were defined using stage hydrographs derived from observed water level data at Kimbulawala Bridge and Wellampitiya Bridge. These hydrographs were reconstructed to reflect the timing and magnitude of upstream inflows during the selected flood event. Similarly, the downstream boundary conditions were input using stage hydrographs observed at SLLDC Bridge and Orugodawatta Bridge, representing the backwater effects from downstream hydraulic controls and system outlets.

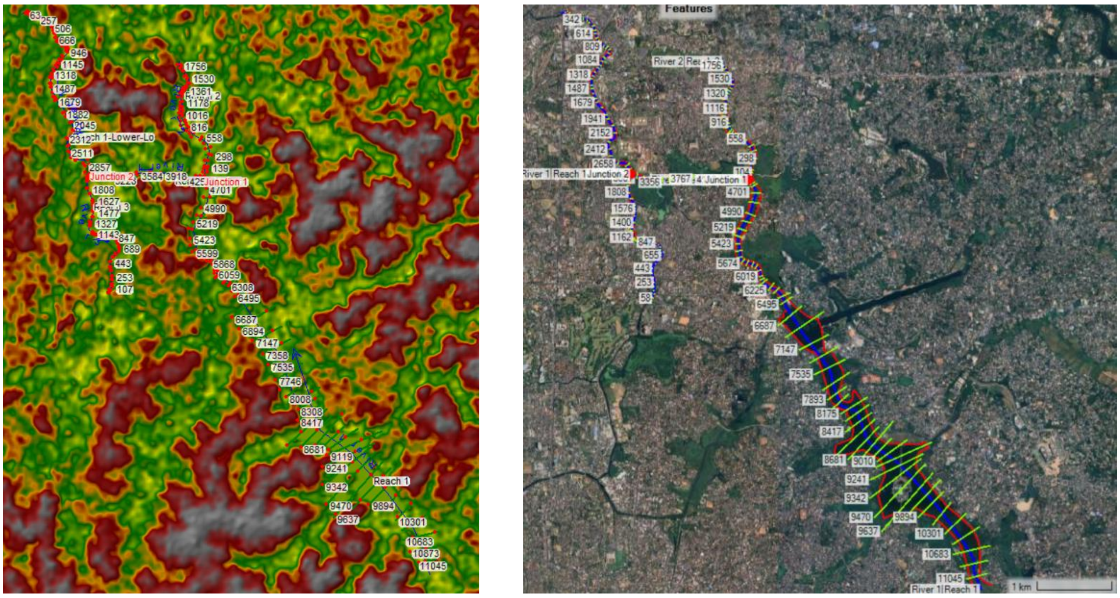

*Figure 71: Channel geometry, including the canal center line, bank lines, flow lines, and cross sections, which was drawn manually with the support of Google satellite imagery*


*Figure 72: Stage hydrograph at Kimbulawala Bridge water level station used as the upstream boundary condition for Canal System 3*

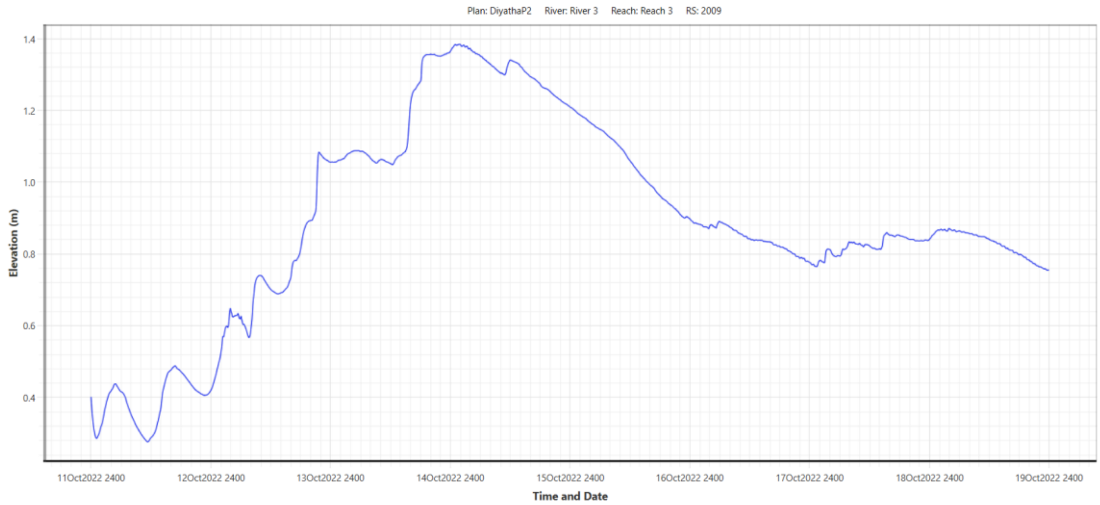


*Figure 73: Stage hydrograph at Wellampitiya Bridge water level station used as the upstream boundary condition for Canal System 3*

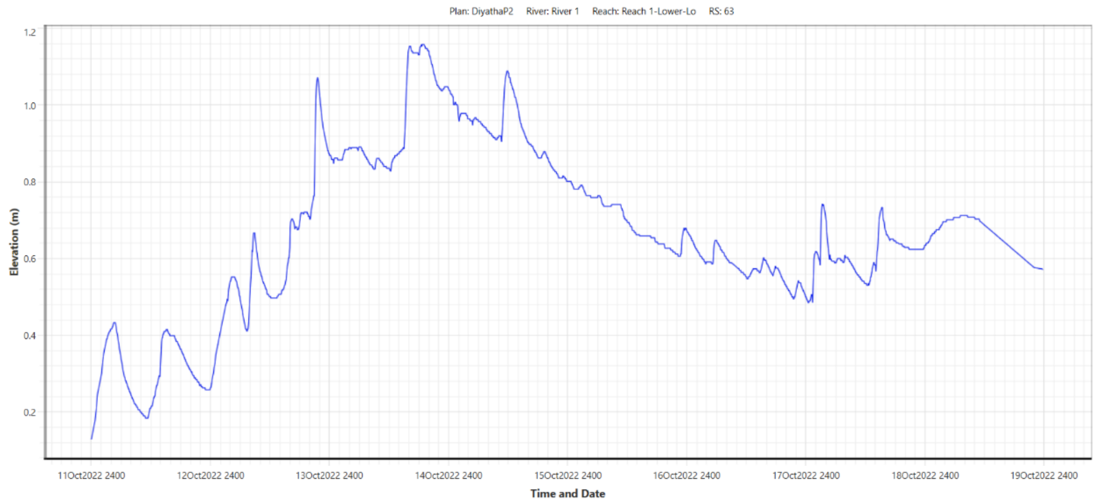


*Figure 74: Stage hydrograph at Orugodawatta Bridge used as the downstream boundary condition for Canal System 3*

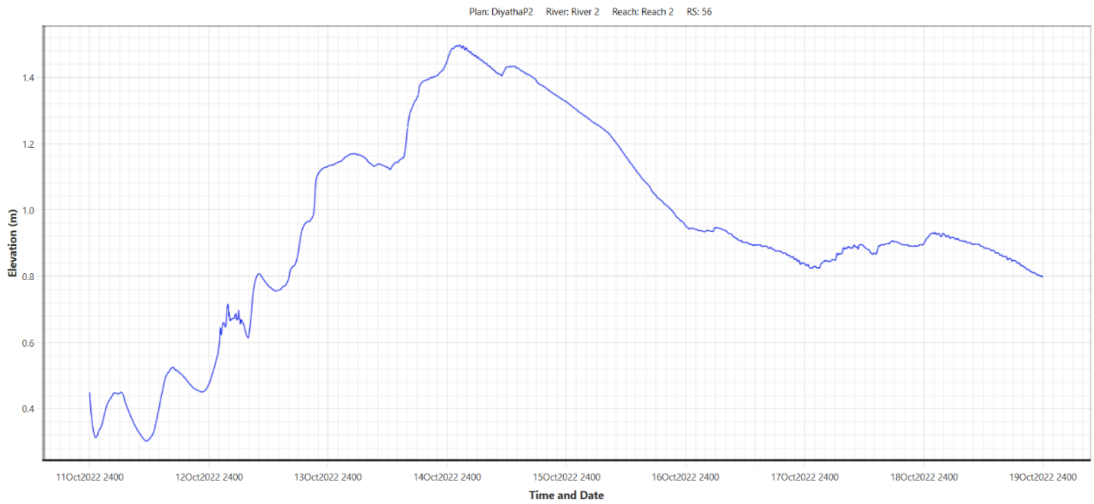


*Figure 75: Stage hydrograph at SLLDC Bridge used as the downstream boundary condition for Canal System 3*

Based on the defined input parameters and boundary conditions, the HEC-RAS model for the Parliament Lake-Kiththampahuwa-Kinda-Dematagoda Canal System was executed using a computational time interval of 1 minute and a warm-up period of 1,000 time steps, which helped ensure numerical stability and convergence of the unsteady flow computations.

Within the hydraulic model domain, key water level monitoring stations were mapped to specific cross-section numbers to enable direct comparison between observed and simulated results. In particular, the Diyatha Bridge station was associated with cross-section number 7358 (Reach 1), while the Yakbedda Bridge station was linked to cross-section number 3476 (Reach 1 – Lower). These two locations served as the primary validation points for the model, as both had reliable observed water level data available during the selected flood event. At each station, the simulated stage hydrographs were extracted and compared against the corresponding observed records, NSE and RMSE were calculated to assess the model's predictive accuracy. Unlike in previous canal systems, no additional intermediate validation locations were used in this case, due to the adequate availability of water level monitoring stations across the system. These comparisons form the basis for evaluating the HEC-RAS model's reliability in simulating spatiotemporal flood dynamics and for benchmarking its performance against the PINN model developed for the same system.

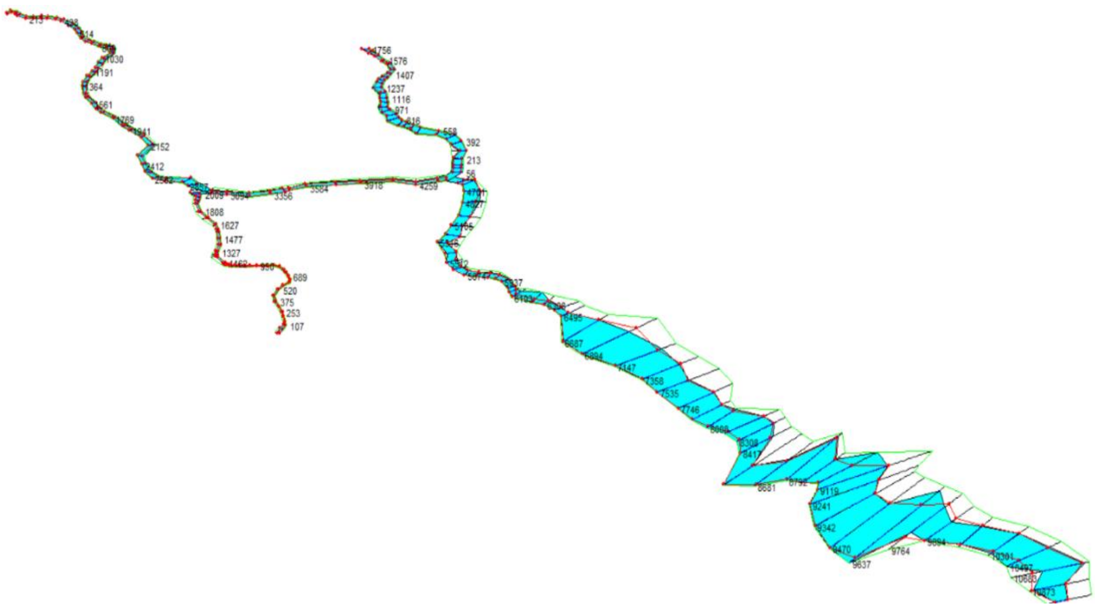

*Figure 76: Maximum flood condition along the Parliament Lake-Kiththampahuwa-Kinda-Dematagoda canal system on 10/14/2025*

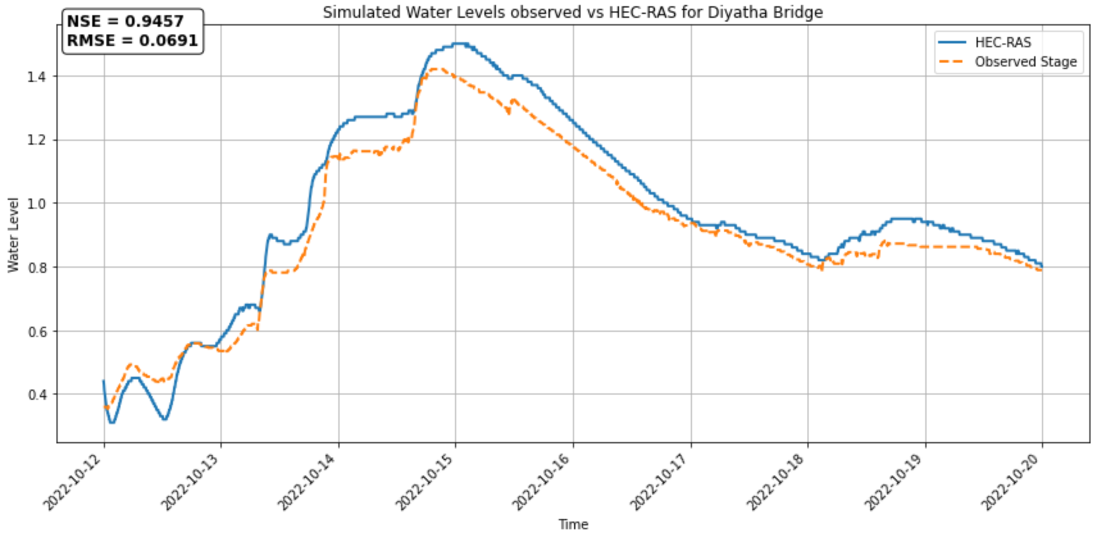


*Figure 77: Spatiotemporal validation using Intermediate stations at Diyatha Bridge along the Canal System 3*

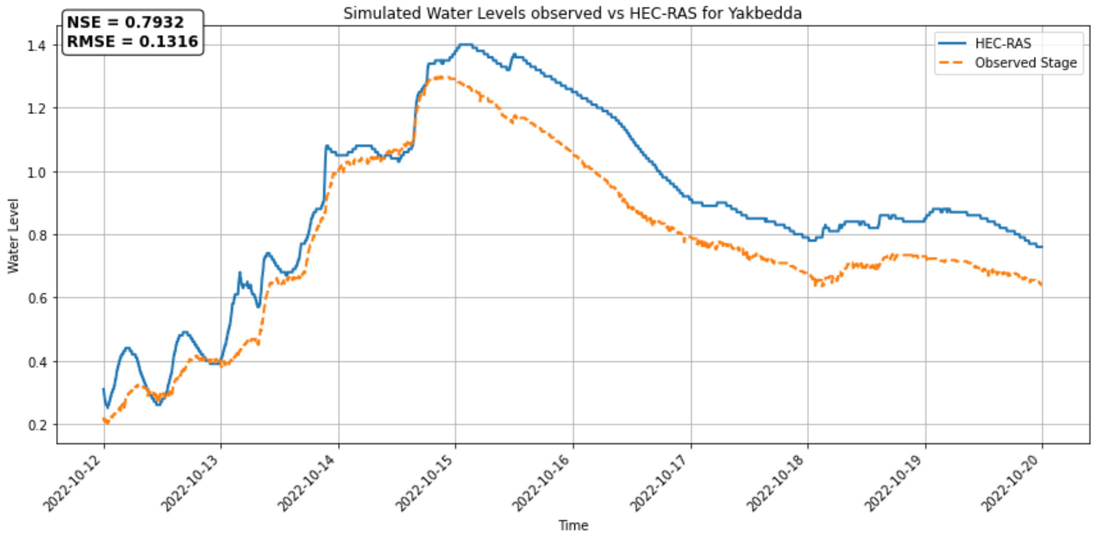


*Figure 78: Spatiotemporal validation using Intermediate stations at Yakkbedda Bridge along the Canal System 3*

*Table 15: NSE and RMSE values for the intermediate stations along the canal for the HEC-RAS model*

| Water Level Monitoring Station | NSE Value | RMSE Value |
|---|---|---|
| Diyatha Bridge | 0.9457 | 0.0691 |
| Yakbedda Bridge | 0.7932 | 0.1316 |

At Diyatha Bridge, both models exhibited strong performance, with the PINN model achieving a higher NSE of 0.9788 and a lower RMSE of 0.0436 m, compared to the HEC-RAS model's NSE of 0.9457 and RMSE of 0.0691 m. Figure 70 shows that the PINN model predicted water levels closely match the observed hydrograph, particularly during the rising limb and flood peak, with minimal overprediction or lag. However, as shown in the Figure 77, HEC-RAS model illustrated it showed a slight overestimation during the recession phase, which accounts for the higher RMSE. At the water level monitoring station at Yakbedda Bridge, the differences between the models became more significant. The PINN model maintained strong predictive performance with an NSE of 0.9458 and RMSE of 0.0726 m, while the HEC-RAS model showed a significant drop in performance, recording an NSE of 0.7932 and RMSE of 0.1316 m. As seen in Figure 78, the HEC-RAS model consistently overpredicted water levels throughout the event, especially during peak and post-peak phases. This deviation could be due to boundary condition effects that were not fully captured by the HEC-RAS model. In this section of the canal, there are several junctions incorporated in the model with different canal divisions, and there are several wetlands connected to the canal, which were not included due to data unavailability. Even, these conditions were not considered in the PINN model, the PINN model had higher predictive performance, highlighting the advantages of using PINN models in 1D flood routing.

## 4.5 Sensitivity Analysis-PINN code

A comprehensive sensitivity analysis was conducted to evaluate the impact of key hyperparameters on the performance of the PINN models developed for the three canal systems. The analysis focused on changes in two performance metrics, NSE and RMSE, as a function of variations in each hyperparameter (Equation 23). The rate of change was calculated using a normalized difference formula, which captures the maximum deviation relative to the highest observed performance.

$$\text{Representative parameter} = \frac{\max(y)-\min(y)}{\max(y)} \tag{23}$$

As in Table 16, Canal System 01, the analysis revealed that the number of neurons was the most influential parameter, with a sensitivity rate of 0.53 for NSE and a significantly higher 0.88 for RMSE. The number of layers (0.32 NSE, 0.36 RMSE) and activation function (0.21 NSE, 0.69 RMSE) also had notable effects. In contrast, learning rate and loss component weights (PDE, IC, BC, and data loss weights) demonstrated only a moderate influence. This indicates that model architecture plays a dominant role in controlling both the accuracy and stability of predictions in this system. For the Canal System 02, the number of neurons again showed the highest sensitivity of 0.67 for NSE and 0.92 for RMSE, confirming its strong effect on performance. The number of layers also had a moderate influence on NSE (0.32), but all other parameters, including activation function, learning rate, and loss weights, exhibited very low sensitivity for NSE ($\leq 0.02$), suggesting a relatively stable response in terms of accuracy. However, RMSE values were more sensitive to changes in activation function (0.69) and loss weights (0.21-0.28), indicating that these parameters affect error magnitudes even if overall efficiency metrics remain high (Table 16). In the canal System 03, as in Table 16, the sensitivity pattern was more varied. The number of neurons (0.54 NSE, 0.77 RMSE) and activation function (0.21 NSE, 0.62 RMSE) again emerged as influential parameters. However, unlike the previous systems, the RMSE values in Canal 03 showed greater sensitivity to physics-related loss weights, such as PDE (0.32), IC (0.26), and BC (0.29). This highlights that in more complex canal configurations with multiple boundary interactions, tuning the physics-informed components of the loss function becomes more critical to achieving lower prediction error. In all three canal systems, the number of neurons consistently demonstrated the highest sensitivity in both NSE and RMSE, underscoring its central role in defining the model's learning capacity. The activation function and number of layers also contributed significantly to model performance, particularly in reducing error. On the other hand, parameters such as learning rate and data loss weight had minimal influence on NSE, though they still affected RMSE to a lesser extent. Notably, the physics-based loss weights (PDE, IC, BC) showed increasing importance in more hydrologically complex settings like Canal System 03.

*Table 16: Sensitivity analysis for Canal Systems 01,02, and 03 for No. of layers, neurons per layer, and the activation function were found to be the most sensitive parameters*

| **Canal System 01** | | | | | | | | |
|---|---|---|---|---|---|---|---|---|
| **Parameter** | **No. of layers** | **Neurons** | **Activation function** | **Learning rate** | **PDE weight** | **Data weight** | **IC weight** | **BC weight** |
| **Rate of Change of NSE** | 0.32 | 0.53 | 0.21 | 0.04 | 0.06 | 0.03 | 0.06 | 0.04 |
| **Rate of Change of RMSE** | 0.36 | 0.88 | 0.69 | 0.27 | 0.21 | 0.24 | 0.22 | 0.28 |
| **Canal System 02** | | | | | | | | |
| **Parameter** | **No. of layers** | **Neurons** | **Activation function** | **Learning rate** | **PDE weight** | **Data weight** | **IC weight** | **BC weight** |
| **Rate of Change of NSE** | 0.32 | 0.67 | 0.27 | 0.01 | 0.02 | 0.02 | 0.01 | 0.01 |
| **Rate of Change of RMSE** | 0.45 | 0.92 | 0.69 | 0.28 | 0.26 | 0.22 | 0.21 | 0.25 |
| **Canal System 03** | | | | | | | | |
| **Parameter** | **No. of layers** | **Neurons** | **Activation function** | **Learning rate** | **PDE weight** | **Data weight** | **IC weight** | **BC weight** |
| **Rate of Change of NSE** | 0.03 | 0.54 | 0.21 | 0.04 | 0.05 | 0.03 | 0.03 | 0.06 |
| **Rate of Change of RMSE** | 0.56 | 0.77 | 0.62 | 0.32 | 0.32 | 0.21 | 0.26 | 0.29 |

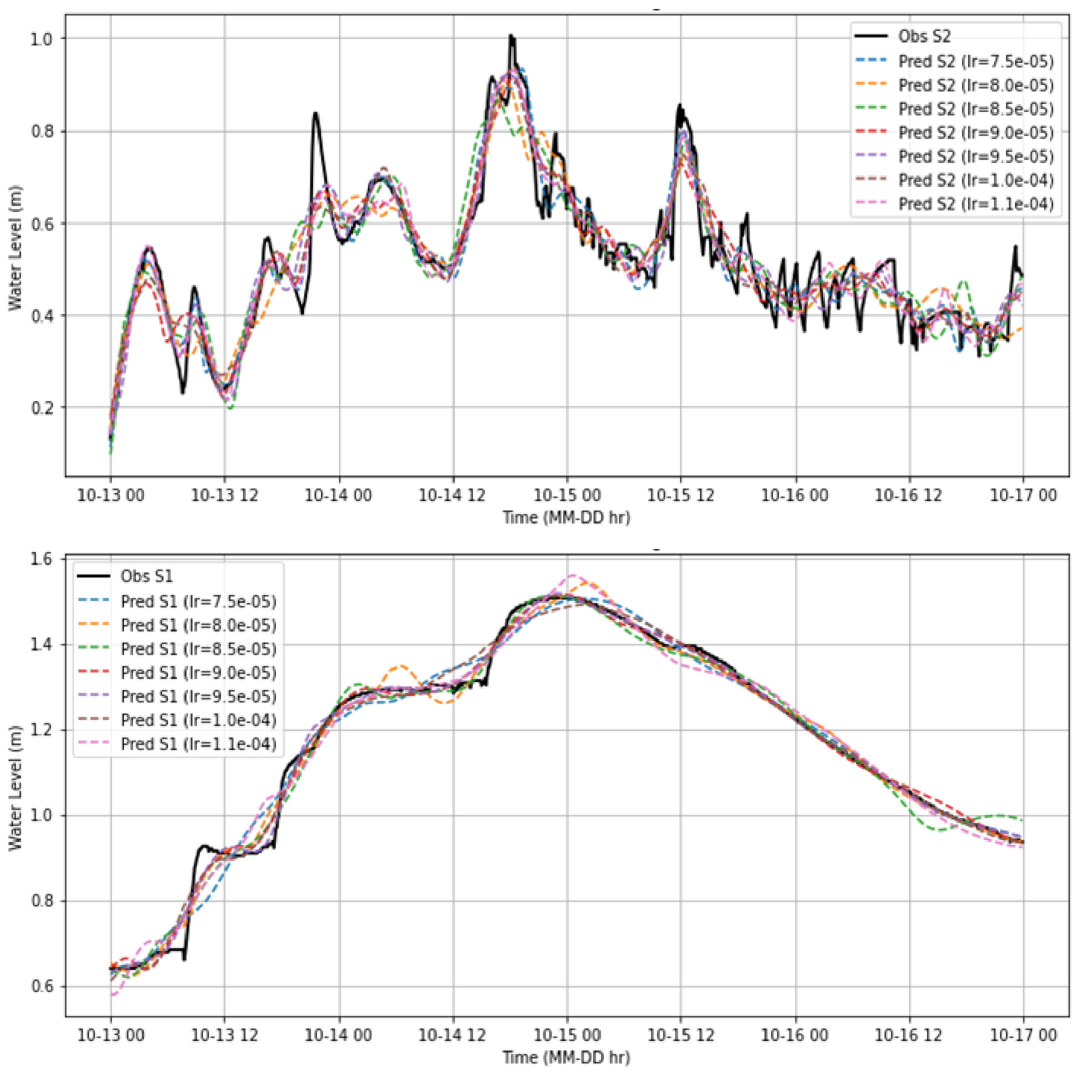


*Figure 79: Variation of model performances with changing learning rates for intermediate stations at Canal System 02*

## 4.6 Summary

This chapter presents a comprehensive comparison of PINN and HEC-RAS 1D hydraulic models for flood wave simulation and water level prediction across three key urban canal systems in Colombo, Sri Lanka. The evaluation focused on model performance during a selected extreme flood event, using observed water level data from multiple monitoring stations for training, testing, and spatial validation. Statistical metrics such as NSE and RMSE were used to quantify accuracy.

The PINN models demonstrated consistently superior performance across all three canal systems, Madiwela East Diversion, Dehiwala-Wellawatta-Kirulapone, and Parliament Lake-Kiththampahuwa-Kinda-Dematagoda. Testing results showed NSE values exceeding 0.975 and RMSE values generally below 3.5 cm, indicating high reliability in simulating both water level peaks and baseflows. Notably, the PINN model achieved NSE values above 0.99 during training, reflecting strong model fitting without significant overfitting when compared to validation performance (Table 17).

*Table 17: Summary of training, testing NSE and RMSE values of PINN code and HEC-RAS results*

| Canal Name | Station | PINN Training | | PINN Testing | | HEC-RAS | |
|---|---|---|---|---|---|---|---|
| | | NSE | RMSE | NSE | RMSE | NSE | RMSE |
| Canal System 01 | 01 | 0.9932 | 0.0301 | 0.9741 | 0.0345 | 0.9851 | 0.1000 |
| | 02 | 0.9984 | 0.0227 | 0.9951 | 0.0254 | | |
| Canal System 02 | 01 | 0.9982 | 0.0191 | 0.984 | 0.0216 | 0.9487 | 0.0306 |
| | 02 | 0.9964 | 0.0151 | 0.9776 | 0.0176 | | |
| Canal System 03 | 01 | 0.9923 | 0.0211 | 0.9941 | 0.0271 | 0.7932 | 0.1316 |
| | 02 | 0.9338 | 0.0394 | 0.9755 | 0.0335 | | |

In contrast, the HEC-RAS 1D model, while still providing reasonable accuracy, showed comparatively lower NSE values and higher RMSE values across the same locations. The NSE for HEC-RAS remained mostly in the range of 0.79 to 0.95, with RMSE values rising to 1 to 13 cm in some stations, especially in data-sparse or hydrologically complex areas like Station 02 of the Madiwela East Diversion and Yakbedda Bridge.

Intermediate station analysis at collocation points not used for training, such as Rajasinghe MW, Near Lanka Hospital, Diyatha Bridge, Yakbedda Bridge, and Orugodawatta Bridge, as in Table 18, further validated the PINN model's spatial generalization capability. At these points, PINN testing still yielded NSE values between 0.945 and 0.998 and RMSE values under 7.3 cm, while HEC-RAS performance was lower, particularly at Yakbedda (NSE = 0.7932, RMSE = 13.16 cm), indicating PINN's robustness even under high flow variability.

*Table 18: NSE and RMSE values for collocation points within the canals*

| Canal Name | Collocation Point Name | PINN Testing | | HEC-RAS | |
|---|---|---|---|---|---|
| | | NSE | RMSE | NSE | RMSE |
| Canal System 01 | Rajasinghe MW | 0.9987 | 0.0300 | 0.9851 | 0.0100 |
| Canal System 02 | Near Lanka Hospital | 0.9825 | 0.0179 | 0.9487 | 0.0306 |
| Canal System 03 | Diyatha Bridge | 0.9788 | 0.0436 | 0.9457 | 0.0691 |
| | Yakbedda Bridge | 0.9458 | 0.0726 | 0.7932 | 0.1316 |
| | Orugodawatta Bridge | 0.9730 | 0.0410 | 0.8456 | 0.0763 |

These results confirm that PINN models offer a highly accurate and computationally efficient alternative to traditional hydrodynamic models like HEC-RAS, particularly in data-scarce, urbanized flood-prone environments. The ability of PINNs to leverage physical laws through embedded differential equations while requiring fewer input parameters makes them suitable for rapid deployment in real-time flood forecasting systems.

# CHAPTER 5

# CONCLUSIONS, RECOMMENDATIONS AND FUTURE WORK

## 5.1 Conclusions

This research study successfully demonstrated the application of PINN for one-dimensional flood modeling across three urban canal systems in Colombo, Sri Lanka, under the constraints of limited data availability and complex canal connectivity. The primary objective was to develop a flood simulation framework that integrates physical hydrodynamic laws with machine learning to improve predictive accuracy, generalizability, and computational efficiency in urban flood routing.

The PINN model exhibited exceptional predictive accuracy across all three canal systems, Madiwela East Diversion, Wellewatta-Dehiwala-Kirulopone, and Parliament Lake-Kiththampahuwa-Dematagoda, achieving NSE values above 0.98 and RMSE values below 3 cm at both upstream and downstream monitoring stations during training. In validation, using intermediate stations such as Rajasinghe MW, Lanka Hospital, and Diyatha Bridge confirmed that the model could generalize 1D spatiotemporal flood dynamics with high confidence, maintaining NSE > 0.95 and RMSE typically < 5 cm. This indicates the model's capability to accurately simulate intermediate ungauged stations with high accuracy, which can be effectively used in giving flood warnings and in checking near-real-time flood wave variations.

In direct comparison with the industry-standard HEC-RAS 1D hydraulic model, the PINN model consistently outperformed HEC-RAS in all validation scenarios. While HEC-RAS achieved acceptable performance (NSE > 0.87), it often overestimated flood peaks, resulting in higher RMSE values up to 13.16 cm, especially at complex locations like Yakbedda Bridge. In contrast, the PINN model offered better hydrograph alignment, capturing flood peaks more accurately with significantly lower errors, thus proving its reliability in simulating flood behavior under both low and high flow conditions.

Beyond accuracy, the PINN framework proved to be more computationally efficient and adaptable for rapid deployment. It required fewer input parameters, avoided the need for complex geometric and hydraulic calibration, and could simulate water level variations across entire canal networks with reduced simulation time compared to HEC-RAS models, making it suitable for real-time flood forecasting in data-scarce environments. The PINN model was able to predict water level changes at every collocation point, making it highly useful for flood warning systems in densely populated urban areas. Further, with these advantages, introducing PINN to a new urban canal system, under flood routing, is an easy and fast approach compared to HEC-RAS models.

Despite being trained on a limited dataset of fewer than 800 water level observations per model, the PINN framework consistently achieved high predictive accuracy, with NSE values exceeding 0.95 and RMSE values remaining below 5 cm across all canal systems. This highlights the data efficiency of the PINN approach, demonstrating its strong generalization capability even under low data availability.

The sensitivity analysis further revealed that neural architecture (number of layers and neurons) and loss function weighting were the most influential factors affecting model performance, especially in hydrodynamically complex networks. Careful tuning of these hyperparameters was essential to maintain both accuracy and generalization capacity.

In conclusion, the study validates the application of PINN as a reliable, efficient, and physically consistent alternative to traditional hydraulic models for real-time flood simulation in data-scarce, highly urbanized settings. The ability to integrate hydrodynamic laws, simulate continuous water levels across spatial domains, and adapt quickly to new catchments makes the PINN approach a transformative advancement in flood risk modeling and early warning systems.

## 5.2 Limitations

Despite its strong performance, several limitations of the PINN model were also identified:

- The PINN model cannot predict water levels beyond the training time domain, as it is trained on specific spatiotemporal intervals ($\partial t$ and $\partial x$). This restricts its use for long-term forecasting unless retrained with updated data.
- As the model internally computes wetted perimeter and submerged areas for each water level and station, canal systems with irregular cross-sections increase computational time and complexity.
- Training a single PDE over a shared domain may allow variations at one input location to influence predictions at others, especially in closely spaced monitoring points.
- Kinematic wave approximation:

  One of the major assumptions that was taken for generating the guiding PDE for the PINN model is the usage of the kinematic wave form of the SVE, instead of the full dynamic or diffusion wave formulations. It was selected in this study primarily due to its computational simplicity and compatibility with PINNs for data-scarce urban flood contexts. The kinematic equation is mainly valid under contexts like mild slopes, slowly varying flows, with no backwater effects, and no tidal influence. But in the selected urban canal system, which has a close proximity to the sea, both the backwater effects and tidal influence can be major influential parameters. Even though the kinematic PINN provided high predictive performance under observed conditions, more complex flood scenarios may require an extension to include the full dynamic wave terms to improve generalizability and physical representativeness.

- Lack of usage of pumping stations in PINN models:

  The PINN model, trained on historical stage hydrographs, captured the effects of pumping stations in the observed datasets, as the stage hydrographs are changed along with the pumping phenomena. However, this approach does not explicitly model the operational behavior of pumping stations, which will reduce the model's generalizing ability. This limits the model’s ability to generalize to future scenarios where pump schedules, capacities, or operating conditions change. The current PINN learns the observed pump operations during the training period with use of water level variations. Without the direct incorporation of pump details, any deviation from historical operations, such as system upgrades, altered schedules, or pump failures, may cause the model’s predictions to diverge from actual conditions. Future work should consider the integration of the PINN with the influence of pumping infrastructure under variable conditions. But if the pumping scenarios are changed model can be re-trained for the respective time domain, and predictions can be conducted.

- The HEC-RAS model does not explicitly simulate the operation of pumping stations. Instead, it assumes that the effects of pumping are indirectly represented through the prescribed upstream and downstream boundary conditions derived from observed water level data.

## 5.3 Recommendations

Based on the findings of this research, the following recommendations are proposed for future implementations and operational applications:

- Adopt PINN-based models for near-real-time flood forecasting in urban areas, particularly where detailed hydraulic survey data for HEC-RAS calibration are unavailable.
- Integrate PINN outputs with early warning systems to enable dynamic flood level alerts along critical canal segments.
- Use PINNs as a complement to traditional models, especially in ungauged or partially gauged urban locations, where developing a HEC-RAS model will be time-consuming or complex.
- Train the PINN model on rainfall inputs without normalization to accurately detect peaks.

The partments related to water resource management can derive significant practical benefits from the outcomes of this research, particularly in the areas of flood forecasting and disaster preparedness. Traditional hydrodynamic models like HEC-RAS require detailed channel geometries, upstream and downstream boundary conditions, and extensive calibration, all of which increase computational time, expertise, and high-resolution datasets. In contrast, the PINN model offers a data-efficient alternative that significantly reduces model preparation time while maintaining high predictive accuracy. Thus, this PINN model can be introduced easily for a new urban or rural catchment in 1D flood routing compared to HEC-RAS models.

Further, the PINN model can simulate water levels at intermediate, ungauged locations within canal networks, areas that are typically overlooked in conventional modeling due to sensor limitations. This feature allows agencies such as the Sri Lanka Land Development Corporation (SLLDC), the Urban Development Authority (UDA), or the Disaster Management Centre (DMC) to gain situational awareness in locations where direct monitoring is unavailable.

Moreover, the research proposes a hybrid approach LSTM-PINN model, to predict water levels at canal boundaries based on rainfall inputs. This framework can be used for near-real-time flood forecasting across the entire canal system, making it highly adaptable for early warning systems. Since the model requires fewer inputs and delivers fast predictions, it can be used in other urban or rural catchments with minimal customization, enabling a more rapid response and planning during flood events.

## 5.4 Future Work

To build upon this study, the following future directions are proposed:

- Experiment with hybrid models, combining PINN with LSTM or attention-based architectures, to capture long-term dependencies and enhance prediction under extreme weather conditions.
- Couple PINN models with rainfall-runoff generation models to simulate full catchment response from rainfall to inundation.
- Investigate uncertainty quantification in PINN predictions, using Bayesian PINNs or ensemble modeling approaches to provide confidence intervals for predicted flood levels.
- Develop a dynamic PINN model retraining system, where real-time water level and rainfall data can be used to continuously update the trained model without full retraining from the beginning.

# REFERENCES


Abbot, J., & Marohasy, J. (2014). Input selection and optimisation for monthly rainfall forecasting in Queensland, Australia, using artificial neural networks. *Atmospheric Research*, *138*, 166–178. https://doi.org/10.1016/j.atmosres.2013.11.002

Bai, J., Alzubaidi, L., Wang, Q., Kuhl, E., Bennamoun, M., & Gu, Y. (n.d.). *Utilising physics-guided deep learning to overcome data scarcity*.

Bikše, J., Retike, I., Haaf, E., & Kalvāns, A. (2023). Assessing automated gap imputation of regional-scale groundwater level data sets with typical gap patterns. *Journal of Hydrology*, *620*, 129424. https://doi.org/10.1016/j.jhydrol.2023.129424

Chen, Y., Xu, Y., Wang, L., & Li, T. (2023). Modeling water flow in unsaturated soils through physics-informed neural network with principled loss function. *Computers and Geotechnics*, *161*, 105546. https://doi.org/10.1016/j.compgeo.2023.105546

Choubin, B., Khalighi-Sigaroodi, S., Malekian, A., & Kişi, Ö. (2016). Multiple linear regression, multi-layer perceptron network and adaptive neuro-fuzzy inference system for forecasting precipitation based on large-scale climate signals. *Hydrological Sciences Journal*, *61*(6), 1001–1009. https://doi.org/10.1080/02626667.2014.966721

Cuomo, S., De Rosa, M., Giampaolo, F., Izzo, S., & Schiano Di Cola, V. (2023). Solving groundwater flow equation using physics-informed neural networks. *Computers & Mathematics with Applications*, *145*, 106–123. https://doi.org/10.1016/j.camwa.2023.05.036

Dehghani, M., Saghafian, B., Nasiri Saleh, F., Farokhnia, A., & Noori, R. (2014). Uncertainty analysis of streamflow drought forecast using artificial neural networks and Monte-Carlo simulation. *International Journal of Climatology*, *34*(4), 1169–1180. https://doi.org/10.1002/joc.3754

Devia, G. K., Ganasri, B. P., & Dwarakish, G. S. (2015). A Review on Hydrological Models. *Aquatic Procedia*, *4*, 1001–1007. https://doi.org/10.1016/j.aqpro.2015.02.126

Ghobadi, F., & Kang, D. (2023). Application of Machine Learning in Water Resources Management: A Systematic Literature Review. *Water*, *15*(4), 620. https://doi.org/10.3390/w15040620

Idrees, M. O., Yusuf, A., Mokhtar, E. S., & Yao, K. (2022). Urban flood susceptibility mapping in Ilorin, Nigeria, using GIS and multi-criteria decision analysis. *Modeling Earth Systems and Environment*, *8*(4), 5779–5791. https://doi.org/10.1007/s40808-022-01479-3

Jackson, E. K., Roberts, W., Nelsen, B., Williams, G. P., Nelson, E. J., & Ames, D. P. (2019). Introductory overview: Error metrics for hydrologic modelling – A review of common practices and an open source library to facilitate use and adoption. *Environmental Modelling & Software*, *119*, 32–48. https://doi.org/10.1016/j.envsoft.2019.05.001

Jepkoech, J., Mugo, D. M., Kenduiywo, B. K., & Too, E. C. (2021). The Effect of Adaptive Learning Rate on the Accuracy of Neural Networks. *International Journal of Advanced Computer Science and Applications*, *12*(8). https://doi.org/10.14569/IJACSA.2021.0120885

Kohanpur, A. H., Saksena, S., Dey, S., Johnson, J. M., Riasi, M. S., Yeghiazarian, L., & Tartakovsky, A. M. (2023). Urban Flood Modeling: Uncertainty Quantification and Physics-Informed Gaussian Processes Regression Forecasting. *Water Resources Research*, *59*(3), e2022WR033939. https://doi.org/10.1029/2022WR033939

Luo, X., Yuan, S., Tang, H., Xu, D., Ran, Q., Cen, Y., & Liang, D. (2024a). Enhanced physics-informed neural networks for efficient modelling of hydrodynamics in river networks. *Hydrological Processes*, *38*(4), e15143. https://doi.org/10.1002/hyp.15143

Luo, X., Yuan, S., Tang, H., Xu, D., Ran, Q., Cen, Y., & Liang, D. (2024b). Enhanced physics-informed neural networks for efficient modelling of hydrodynamics in river networks. *Hydrological Processes*, *38*(4), e15143. https://doi.org/10.1002/hyp.15143

Luo, X., Yuan, S., Tang, H., Xu, D., Ran, Q., Cen, Y., & Liang, D. (2024c). Enhanced physics-informed neural networks for efficient modelling of hydrodynamics in river networks. *Hydrological Processes*, *38*(4), e15143. https://doi.org/10.1002/hyp.15143

Markidis, S. (2021a). The Old and the New: Can Physics-Informed Deep-Learning Replace Traditional Linear Solvers? *Frontiers in Big Data*, *4*, 669097. https://doi.org/10.3389/fdata.2021.669097

Markidis, S. (2021b). The Old and the New: Can Physics-Informed Deep-Learning Replace Traditional Linear Solvers? *Frontiers in Big Data*, *4*, 669097. https://doi.org/10.3389/fdata.2021.669097

Monfared, A. F., Ahmadi, M., Derafshi, K., Khodadadi, M., & Najafi, E. (2024). Urban development assessment in flood hazard areas using integrated HEC-RAS, SCS, and FAHP models: A case study of Pardisan Settlement, Qom. *Modeling Earth Systems and Environment*, *10*(4), 5103–5120. https://doi.org/10.1007/s40808-024-02053-9

Mosavi, A., Ozturk, P., & Chau, K. (2018). Flood Prediction Using Machine Learning Models: Literature Review. *Water*, *10*(11), 1536. https://doi.org/10.3390/w10111536

Niedzielski, T., & Halicki, M. (2023). Improving Linear Interpolation of Missing Hydrological Data by Applying Integrated Autoregressive Models. *Water Resources Management*, *37*(14), 5707–5724. https://doi.org/10.1007/s11269-023-03625-7

Nifa, K., Boudhar, A., Ouatiki, H., Elyoussfi, H., Bargam, B., & Chehbouni, A. (2023). Deep Learning Approach with LSTM for Daily Streamflow Prediction in a Semi-Arid Area: A Case Study of Oum Er-Rbia River Basin, Morocco. *Water*, *15*(2), 262. https://doi.org/10.3390/w15020262

Niu, J., Xu, W., Qiu, H., Li, S., & Dong, F. (2023a). 1-D coupled surface flow and transport equations revisited via the physics-informed neural network approach. *Journal of Hydrology*, *625*, 130048. https://doi.org/10.1016/j.jhydrol.2023.130048

Niu, J., Xu, W., Qiu, H., Li, S., & Dong, F. (2023b). 1-D coupled surface flow and transport equations revisited via the physics-informed neural network approach. *Journal of Hydrology*, *625*, 130048. https://doi.org/10.1016/j.jhydrol.2023.130048

Nourani, V., Hosseini Baghanam, A., Adamowski, J., & Kisi, O. (2014). Applications of hybrid wavelet–Artificial Intelligence models in hydrology: A review. *Journal of Hydrology*, *514*, 358–377. https://doi.org/10.1016/j.jhydrol.2014.03.057

Peel, M. C., & Blöschl, G. (2011). Hydrological modelling in a changing world. *Progress in Physical Geography: Earth and Environment*, *35*(2), 249–261. https://doi.org/10.1177/0309133311402550

Raczyński, K., & Dyer, J. (2022). Development of an Objective Low Flow Identification Method Using Breakpoint Analysis. *Water*, *14*(14), 2212. https://doi.org/10.3390/w14142212

Raissi, M., Perdikaris, P., & Karniadakis, G. E. (2017). *Physics Informed Deep Learning (Part I): Data-driven Solutions of Nonlinear Partial Differential Equations* (Version 1). arXiv. https://doi.org/10.48550/ARXIV.1711.10561

Reddy, B. S. N., Pramada, S. K., & Roshni, T. (2021). Monthly surface runoff prediction using artificial intelligence: A study from a tropical climate river basin. *Journal of Earth System Science*, *130*(1), 35. https://doi.org/10.1007/s12040-020-01508-8

Sajedi-Hosseini, F., Malekian, A., Choubin, B., Rahmati, O., Cipullo, S., Coulon, F., & Pradhan, B. (2018). A novel machine learning-based approach for the risk assessment of nitrate groundwater contamination. *Science of The Total Environment*, *644*, 954–962. https://doi.org/10.1016/j.scitotenv.2018.07.054

Schiano Di Cola, V., Bauduin, V., Berardi, M., Notarnicola, F., & Cuomo, S. (2025). Investigating neural networks with groundwater flow equation loss.

*Mathematics and Computers in Simulation*, *230*, 80–93. https://doi.org/10.1016/j.matcom.2024.10.039

Senthil Kumar, A. R., Sudheer, K. P., Jain, S. K., & Agarwal, P. K. (2005). Rainfall-runoff modelling using artificial neural networks: Comparison of network types. *Hydrological Processes*, *19*(6), 1277–1291. https://doi.org/10.1002/hyp.5581

Shekar, P. R., Mathew, A., Pandey, A., & Bhosale, A. (2023). A comparison of the performance of SWAT and artificial intelligence models for monthly rainfall–runoff analysis in the Peddavagu River Basin, India. *AQUA — Water Infrastructure, Ecosystems and Society*, *72*(9), 1707–1730. https://doi.org/10.2166/aqua.2023.048

Shekar, P. R., Mathew, A., Yeswanth, P. V., & Deivalakshmi, S. (2024). A combined deep CNN-RNN network for rainfall-runoff modelling in Bardha Watershed, India. *Artificial Intelligence in Geosciences*, *5*, 100073. https://doi.org/10.1016/j.aiig.2024.100073

Shu, C., & Ouarda, T. B. M. J. (2008). Regional flood frequency analysis at ungauged sites using the adaptive neuro-fuzzy inference system. *Journal of Hydrology*, *349*(1–2), 31–43. https://doi.org/10.1016/j.jhydrol.2007.10.050

Singh, V. P. (2018). Hydrologic modeling: Progress and future directions. *Geoscience Letters*, *5*(1), 15. https://doi.org/10.1186/s40562-018-0113-z

Sorooshian, S. (Ed.). (2008). *Hydrological modelling and the water cycle: Coupling the atmospheric and hydrological models*. Springer.

Sudheer, K. P., Gosain, A. K., Mohana Rangan, D., & Saheb, S. M. (2002). Modelling evaporation using an artificial neural network algorithm. *Hydrological Processes*, *16*(16), 3189–3202. https://doi.org/10.1002/hyp.1096

Szandała, T. (2021). Review and Comparison of Commonly Used Activation Functions for Deep Neural Networks. In A. K. Bhoi, P. K. Mallick, C.-M. Liu, & V. E. Balas (Eds.), *Bio-inspired Neurocomputing* (Vol. 903, pp. 203–224). Springer Singapore. https://doi.org/10.1007/978-981-15-5495-7_11

Vapnik, V., & Mukherjee, S. (n.d.). *Support Vector Method for Multivariate Density Estimation*.

Wagener, T., Boyle, D. P., Lees, M. J., Wheater, H. S., Gupta, H. V., & Sorooshian, S. (2001). A framework for development and application of hydrological models. *Hydrology and Earth System Sciences*, *5*(1), 13–26. https://doi.org/10.5194/hess-5-13-2001

Waqas, M., Shoaib, M., Saifullah, M., Naseem, A., Hashim, S., Ehsan, F., Ali, I., & Khan, A. (2021). Assessment of Advanced Artificial Intelligence Techniques for Streamflow Forecasting in Jhelum River Basin. *Pakistan Journal of Agricultural Research*, *34*(3). https://doi.org/10.17582/journal.pjar/2021/34.3.580.598

Wheater, H., Sorooshian, S., & Sharma, K. D. (2007). *Hydrological Modelling in Arid and Semi-Arid Areas*. Cambridge University Press.

Wu, C. L., & Chau, K. W. (2010). Data-driven models for monthly streamflow time series prediction. *Engineering Applications of Artificial Intelligence*, *23*(8), 1350–1367. https://doi.org/10.1016/j.engappai.2010.04.003

Xiang, Z., Yan, J., & Demir, I. (2020). A Rainfall-Runoff Model With LSTM-Based Sequence-to-Sequence Learning. *Water Resources Research*, *56*(1), e2019WR025326. https://doi.org/10.1029/2019WR025326

Yang, F., Ding, W., Zhao, J., Song, L., Yang, D., & Li, X. (2024). Rapid urban flood inundation forecasting using a physics-informed deep learning approach. *Journal of Hydrology*, *643*, 131998. https://doi.org/10.1016/j.jhydrol.2024.131998

Yang, S., Yang, D., Chen, J., Santisirisomboon, J., Lu, W., & Zhao, B. (2020). A physical process and machine learning combined hydrological model for daily streamflow simulations of large watersheds with limited observation data. *Journal of Hydrology*, *590*, 125206. https://doi.org/10.1016/j.jhydrol.2020.125206

Yu, P.-S., Yang, T.-C., Chen, S.-Y., Kuo, C.-M., & Tseng, H.-W. (2017). Comparison of random forests and support vector machine for real-time radar-derived rainfall forecasting. *Journal of Hydrology*, *552*, 92–104. https://doi.org/10.1016/j.jhydrol.2017.06.020

Zhang, J., Chen, Z., Ji, Y., Sun, X., & Bai, Y. (2023). A Multi-branch Feature Fusion Model Based on Convolutional Neural Network for Hyperspectral Remote Sensing Image Classification. *International Journal of Advanced Computer Science and Applications*, *14*(6). https://doi.org/10.14569/IJACSA.2023.0140617

Zhong, L., Lei, H., & Gao, B. (2023). Developing a Physics-Informed Deep Learning Model to Simulate Runoff Response to Climate Change in Alpine Catchments. *Water Resources Research*, *59*(6), e2022WR034118. https://doi.org/10.1029/2022WR034118